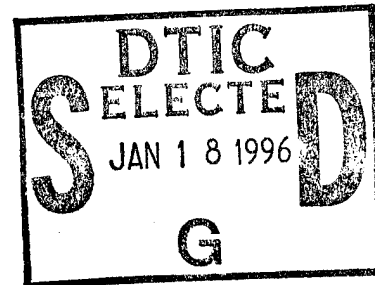


NAVAL POSTGRADUATE SCHOOL MONTEREY, CALIFORNIA



THESIS

ON THE USE OF TWO-DIMENSIONAL
ORTHOGONAL FUNCTION EXPANSIONS TO
MODEL OCEAN BATHYMETRIC AND SOUND-
SPEED DATA IN THE RECURSIVE RAY
ACOUSTICS ALGORITHM

by

Rodney K. Luck

June, 1995

Thesis Advisor:

Lawrence J. Ziomek

Approved for public release; distribution is unlimited.

19960116 059

REPORT DOCUMENTATION PAGE

Form Approved OMB No. 0704-0188

Public reporting burden for this collection of information is estimated to average 1 hour per response, including the time for reviewing instruction, searching existing data sources, gathering and maintaining the data needed, and completing and reviewing the collection of information. Send comments regarding this burden estimate or any other aspect of this collection of information, including suggestions for reducing this burden, to Washington Headquarters Services, Directorate for Information Operations and Reports, 1215 Jefferson Davis Highway, Suite 1204, Arlington, VA 22202-4302, and to the Office of Management and Budget, Paperwork Reduction Project (0704-0188) Washington DC 20503.

1. AGENCY USE ONLY <i>(Leave blank)</i>	2. REPORT DATE June 1995.	3. REPORT TYPE AND DATES COVERED Master's Thesis	
4. TITLE AND SUBTITLE ON THE USE OF TWO-DIMENSIONAL ORTHOGONAL FUNCTION EXPANSIONS TO MODEL OCEAN BATHYMETRIC AND SOUND-SPEED DATA IN THE RECURSIVE RAY ACOUSTICS ALGORITHM		5. FUNDING NUMBERS	
6. AUTHOR(S) Luck, Rodney K.			
7. PERFORMING ORGANIZATION NAME(S) AND ADDRESS(ES) Naval Postgraduate School Monterey CA 93943-5000		8. PERFORMING ORGANIZATION REPORT NUMBER	
9. SPONSORING/MONITORING AGENCY NAME(S) AND ADDRESS(ES)		10. SPONSORING/MONITORING AGENCY REPORT NUMBER	
11. SUPPLEMENTARY NOTES The views expressed in this thesis are those of the author and do not reflect the official policy or position of the Department of Defense or the U.S. Government.			
12a. DISTRIBUTION/AVAILABILITY STATEMENT Approved for public release; distribution is unlimited.		12b. DISTRIBUTION CODE	
<p>13. ABSTRACT <i>(maximum 200 words)</i></p> <p>The two-dimensional orthogonal function expansion technique was used to model discrete ocean bathymetric data as a function of cross-range and down-range, and to model discrete sound-speed data as a function of depth and down-range. The technique was tested and validated via computer simulation. It was shown to have many positive features, but the approach is flawed by the set of generating functions that were selected.</p> <p>A reflection angle algorithm for arbitrary two-dimensional ocean bottom models was tested and validated, and was found to be accurate. Computer simulations of acoustic ray interaction with various two-dimensional ocean bottoms modeled with the orthogonal function expansion and using the reflection angle algorithm were also conducted.</p>			
14. SUBJECT TERMS Two-dimensional Orthogonal Function Expansion based upon the Gram-Schmidt Procedure, and the Recursive Ray Acoustics Algorithm		15. NUMBER OF PAGES 112	16. PRICE CODE
17. SECURITY CLASSIFICATION OF REPORT Unclassified	18. SECURITY CLASSIFICATION OF THIS PAGE Unclassified	19. SECURITY CLASSIFICATION OF ABSTRACT Unclassified	20. LIMITATION OF ABSTRACT UL

NSN 7540-01-280-5500

Standard Form 298 (Rev. 2-89)
Prescribed by ANSI Std. Z39-18 298-102

Approved for public release; distribution is unlimited.

**ON THE USE OF TWO-DIMENSIONAL ORTHOGONAL FUNCTION
EXPANSIONS TO MODEL OCEAN BATHYMETRIC AND SOUND-SPEED
DATA IN THE RECURSIVE RAY ACOUSTICS ALGORITHM**

Rodney K. Luck
Lieutenant, United States Navy
B.S., United States Naval Academy, 1988

Submitted in partial fulfillment
of the requirements for the degree of

MASTER OF SCIENCE IN ELECTRICAL ENGINEERING

from the

NAVAL POSTGRADUATE SCHOOL

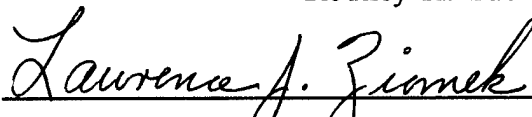
June 1995

Author:

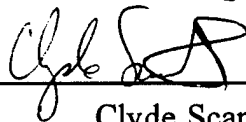


Rodney K. Luck

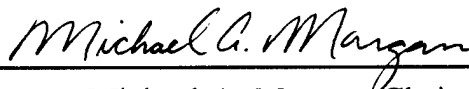
Approved by:



Lawrence J. Ziomek, Thesis Advisor



Clyde Scandrett, Second Reader



Michael A. Morgan, Chairman,
Department of Electrical and Computer Engineering

ABSTRACT

The two-dimensional orthogonal function expansion technique was used to model discrete ocean bathymetric data as a function of cross-range and down-range, and to model discrete sound speed-data that is a function of depth and down-range. The technique was tested and validated via computer simulation. It was shown to have many positive features, but the approach is flawed by the set of generating functions that were selected.

A reflection angle algorithm for arbitrary two-dimensional ocean bottom models was tested and validated, and was found to be accurate. Computer simulations of acoustic ray interaction with various two-dimensional ocean bottoms modeled with the orthogonal function expansion and using the reflection angle algorithm were also conducted.

Accession For	
NTIS CRA&I	<input checked="" type="checkbox"/>
DTIC TAB	<input type="checkbox"/>
Unannounced	<input type="checkbox"/>
Justification	
By	
Distribution /	
Availability Codes	
Dist	Avail and/or Special
A-1	

TABLE OF CONTENTS

I. INTRODUCTION	1
II. TWO-DIMENSIONAL ORTHOGONAL FUNCTION EXPANSIONS OF BATHYMETRIC DATA	5
A. ORTHOGONAL FUNCTION EXPANSION AND THE BASIS FUNCTIONS	5
1. Definition of the Two-Dimensional Orthogonal Function Expansion	5
2. Derivation of the Basis Functions from the Generating Functions	7
3. The Generating Functions and the Minimum Mean-Squared Error Criterion	11
B. COMPUTER SIMULATION RESULTS OF BATHYMETRIC FITS	13
1. Exact Fit Test Cases	14
2. Complicated Test Cases	34
3. Summary	51
III. THE BATHYMETRIC MODEL APPLIED TO RAY TRACING IN THE RRA ALGORITHM	53
A. REFLECTION ANGLES OFF THE TWO-DIMENSIONAL OCEAN BOTTOM MODEL	53
B. COMPUTER SIMULATION RESULTS	58
IV. TWO-DIMENSIONAL ORTHOGONAL FUNCTION EXPANSIONS OF SOUND-SPEED DATA	75
A. ORTHOGONAL FUNCTION EXPANSION AND THE BASIS FUNCTIONS	75
1. Definition of the Two-Dimensional Orthogonal Function Expansion	77
2. The Basis Functions from the Generating Functions	77
B. COMPUTER SIMULATION RESULTS OF SOUND SPEED FITS	79
V. CONCLUSIONS AND RECOMMENDATIONS	97
LIST OF REFERENCES	101
INITIAL DISTRIBUTION LIST	103

I. INTRODUCTION

In the area of underwater acoustics, the development of an accurate, fast, and simple computer model to calculate ray paths and sound-pressure levels is an important first step for modeling and studying sound propagation in the ocean. The RRA (recursive ray acoustics) algorithm developed by Professor L. Ziomek [Ref.1,2] provides these features. It requires only discrete input data of the bottom depth and the sound speed for the ocean being modeled, and uses orthogonal function expansions to fit the data in a minimum mean-squared error (MMSE) sense using orthogonal polynomials. However, until now, the concept of orthogonal function expansions had only been implemented and tested for one-dimensional data in the RRA algorithm, that is, bottom depth as a function of down-range and the speed of sound as a function of depth.

The intent of this thesis is to show that two-dimensional orthogonal function expansions can be used to fit discrete data as a function of two independent variables, that is, bottom depth as a function of cross-range and down-range, and the speed of sound as a function of depth and down-range. This technique is implemented in the RRA algorithm to provide more realistic models of the ocean bottom and the speed of sound.

The direction of propagation of a sound ray reflected off the ocean bottom is calculated based on the unit normal vector to the ocean bottom at the point of incidence. The unit normal vector is calculated based on the derivatives of the ocean bottom with respect to down-range and cross-range.

For a one-dimensional model of ocean bottom depth (as a function of down-range) the angle of reflection is computed only from the derivative of bottom depth with respect to down-range. The one-dimensional model provides no cross-range information; the derivative of bottom depth with respect to cross-range is zero. A two-dimensional model of ocean bottom depth (as a function of cross-range and down-range) would provide derivatives of the ocean bottom with respect to both cross-range and down-range. A two-dimensional math model will provide components in the down-range and the cross-range direction, and the reflected ray will travel down-range and cross-range. By

modeling the ocean bottom with a two-dimensional orthogonal function expansion, an accurate model of the ocean bottom will be incorporated into the RRA algorithm.

The sound-speed model currently implemented uses only one-dimensional data to produce a sound-speed vs. depth profile that is used in a zone (a particular area of the ocean). A two-dimensional orthogonal function expansion results in a model of the sound-speed as a function of depth and down-range that could be used to fit multiple sound-speed profiles (SSP) that are taken at different down-range locations.

Chapter II discusses the two-dimensional orthogonal function expansion used to fit bathymetric data as a function of down-range and cross-range. The generating function that was chosen, and the algorithm used to orthogonalize the set of generating functions using the Gram-Schmidt procedure is detailed. Computer simulation results are shown that demonstrate the accuracy and the applicability of this method. The result is a smooth surface fit of the ocean bottom obtained from discrete data.

A shortcoming of the generating functions chosen is that cross-range and down-range values have an equal effect on the estimated value of the ocean bottom depth. In some cases, ocean bottom depth may have little or no dependence on one of the parameters. Independent weighting of the parameters will correct this shortcoming for all planar ocean bottom cases. This thesis will demonstrate the need to weight parameters independently in these cases, and show some examples where weighting is applied. For more complicated ocean bottom geometries, a simple weighting scheme will not correct the problem created by the choice of generating functions. Alternative choices for the set of generating functions used in the orthogonal function expansion is discussed in Chapter V, and is offered as an area for future research.

Chapter III presents the implementation of the ocean bottom models developed in Chapter II into the RRA Algorithm FORTRAN ray tracing program. The orthogonal function expansion technique allows accurate calculations of ray reflections off the ocean bottom. The algorithm used to calculate accurate reflection angles for sound rays will be presented. Using the unit normal vector to the ocean bottom at the point of incidence, the

direction of propagation of a reflected ray is obtained using vector calculus. Computer simulation results showing incident and reflected rays propagated with the RRA algorithm are presented.

Chapter IV discusses the application of the two-dimensional orthogonal function expansion technique to fit sound-speed data as a function of both depth *and down-range*. The procedure is the same to fit both bathymetric and sound-speed data. Computer simulation results are shown that demonstrate the smooth fit of the discrete data. The results show that one math model can fit more than one sound-speed profile (SSP) taken at different down range locations.

Chapter V discusses the problems encountered with the two-dimensional orthogonal function expansion technique used to model bathymetric and sound-speed data, states conclusions as well as recommendations for future research.

II. TWO-DIMENSIONAL ORTHOGONAL FUNCTION EXPANSIONS OF BATHYMETRIC DATA

A. ORTHOGONAL FUNCTION EXPANSION AND THE BASIS FUNCTIONS

Ocean bathymetry data is commonly measured and stored as a set of discrete measurements of ocean bottom depth at distinct, sampled locations. Matrices of data have been generated by the U.S. Navy to chart ocean bottom depth, and provide bottom contour navigation. This type of data is ideal for developing a model of the ocean bottom that can be used in the RRA (Recursive Ray Acoustics) algorithm. In ray acoustics, the model of the ocean bottom is used to calculate ray reflections at the point of incidence to the ocean bottom. The model of the ocean bottom must provide a smooth fit to the discrete data, and it must be capable of providing first and second order derivatives of the ocean bottom at the point of incidence. The orthogonal function expansion technique provides these features, and it has been demonstrated as an effective method when ocean bottom depth is a function of one variable, that is, down-range [Ref. 2].

1. Definition of the Two-Dimensional Orthogonal Function Expansion

The two-dimensional orthogonal function expansion used to fit a smooth surface to a rectangular matrix of ocean bathymetric data as a function of cross-range and down-range is given by

$$\hat{y}_b(x, z) = \sum_{n=0}^{N_b} b_n \varphi_{b_n}(x, z), \quad (2.1)$$

where the coefficient

$$\begin{aligned} b_n &= \left\langle y_{b_n}(x_{ij}, z_{ij}), \varphi_{b_n}(x_{ij}, z_{ij}) \right\rangle, \\ &= \sum_{i=1}^{M_{b_x}} \sum_{j=1}^{M_{b_z}} y_{b_n}(x_{ij}, z_{ij}) \varphi_{b_n}^*(x_{ij}, z_{ij}), \quad n = 0, 1, \dots, N_b, \end{aligned} \quad (2.2)$$

represents the inner product of the measured discrete ocean bathymetric data $y_{b_m}(x_{ij}, z_{ij})$, for $i = 1, 2, \dots, M_{b_x}$ and $j = 1, 2, \dots, M_{b_z}$, with the set of orthonormal basis functions $\varphi_{b_n}(x, z)$, $n = 0, 1, \dots, N_b$, evaluated at the discrete cross-range (x_{ij}) and down-range (z_{ij}) values corresponding to the discrete ocean bathymetric data. The order of the expansion is represented by N_b . The discrete data must be entered in a matrix, where M_{b_x} is the total number of cross-range rows and M_{b_z} is the total number of down-range columns. It is important to note that although the data is entered in a matrix, the matrix is, in general, rectangular, not square, and the data is, in general, *unevenly spaced* in both the x and z directions. Figure 1 shows an example of unevenly spaced data entered in a rectangular matrix. Each data point of the matrix (i, j) has a cross-range (x_{ij}), down-range (z_{ij}), and depth $y_{b_m}(x_{ij}, z_{ij})$ value associated with it.

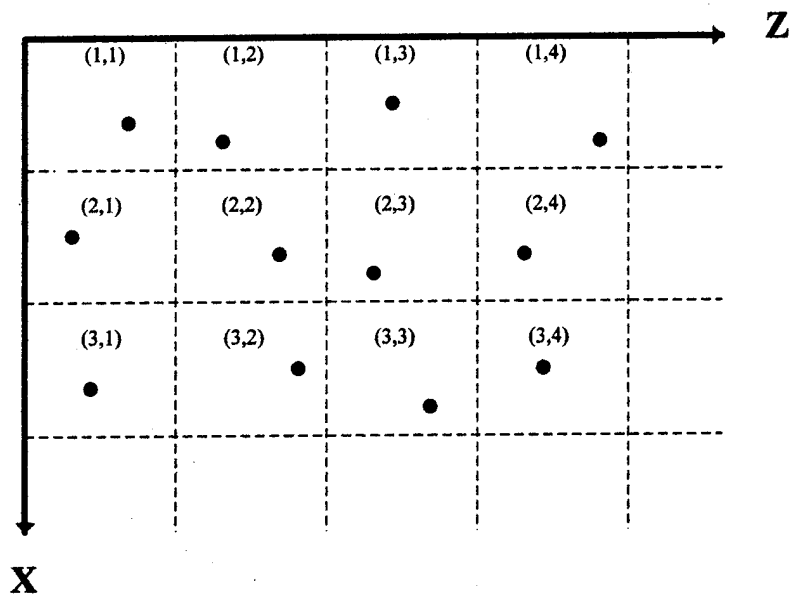


Figure 1. Discrete bathymetric data, unevenly spaced, entered in a rectangular matrix.

2. Derivation of the Basis Functions from the Generating Functions

The set of orthonormal basis functions $\varphi_{b_n}(x, z)$, $n = 0, 1, \dots, N_b$, were determined by using the Gram-Schmidt procedure [Ref. 3] on the set of generating functions $f_n(x, z) = (x + z)^n$, $n = 0, 1, \dots, N_b$. The choice of this particular set of generating functions will be discussed later. The general equation of the *Gram-Schmidt Orthogonalization Procedure* is given by

$$\begin{aligned} \varphi_{b_n}(x, z) = f_n(x, z) - \frac{\langle f_n(x, z), \varphi_{b_0}(x, z) \rangle}{\langle \varphi_{b_0}(x, z), \varphi_{b_0}(x, z) \rangle} \varphi_{b_0}(x, z) - \dots \\ \dots - \frac{\langle f_n(x, z), \varphi_{b_{n-1}}(x, z) \rangle}{\langle \varphi_{b_{n-1}}(x, z), \varphi_{b_{n-1}}(x, z) \rangle} \varphi_{b_{n-1}}(x, z), \quad n = 0, 1, 2, \dots \quad (2.3) \end{aligned}$$

The Gram-Schmidt procedure to find φ_{b_0} , φ_{b_1} , and φ_{b_2} is shown in Equations (2.4) to (2.16). The development of the higher order basis functions, for $n = 3, 4, \dots, N_b$, is not shown since the procedure to expand Equation (2.3) is similar to that demonstrated with the first three basis functions.

The *0th*-order basis function is given by

$$\varphi_{b_0}(x, z) = f_0(x, z) = (x + z)^0 = 1. \quad (2.4)$$

The *1st*-order basis function is given by

$$\varphi_{b_1}(x, z) = f_1(x, z) - \frac{\langle f_1(x, z), \varphi_{b_0}(x, z) \rangle}{\langle \varphi_{b_0}(x, z), \varphi_{b_0}(x, z) \rangle} \varphi_{b_0}(x, z), \quad (2.5)$$

where the inner products on the right-hand side of Equation (2.5) are given by

$$\begin{aligned}
\langle f_1(x, z), \varphi_{b_0}(x, z) \rangle &= \sum_{i=1}^{M_{b_x}} \sum_{j=1}^{M_{b_z}} f_1(x_{ij}, z_{ij}) \varphi_{b_0}^*(x_{ij}, z_{ij}), \\
&= \sum_{i=1}^{M_{b_x}} \sum_{j=1}^{M_{b_z}} (x_{ij} + z_{ij})^1, \\
&= \sum_{i=1}^{M_{b_x}} \sum_{j=1}^{M_{b_z}} x_{ij} + z_{ij}, \tag{2.6}
\end{aligned}$$

and

$$\begin{aligned}
E_{\varphi_{b_0}} = \langle \varphi_{b_0}(x, z), \varphi_{b_0}(x, z) \rangle &= \sum_{i=1}^{M_{b_x}} \sum_{j=1}^{M_{b_z}} \varphi_{b_0}(x_{ij}, z_{ij}) \varphi_{b_0}^*(x_{ij}, z_{ij}), \\
&= \sum_{i=1}^{M_{b_x}} \sum_{j=1}^{M_{b_z}} 1 \cdot 1 = M_{b_x} M_{b_z}, \tag{2.7}
\end{aligned}$$

is the *energy* contained in $\varphi_{b_0}(x, z)$. Note that the ratio of inner products that appears on the right-hand side of Equation (2.5) will show up in later equations. It needs to be evaluated during the computation of the *1st-order* basis function and is saved as

$$W_{10} = \frac{\langle f_1(x, z), \varphi_{b_0}(x, z) \rangle}{\langle \varphi_{b_0}(x, z), \varphi_{b_0}(x, z) \rangle} = \frac{\langle f_1(x, z), \varphi_{b_0}(x, z) \rangle}{E_{\varphi_{b_0}}}. \tag{2.8}$$

Finally, the *1st-order* basis function becomes

$$\varphi_{b_1}(x, z) = x + z - W_{10}. \tag{2.9}$$

Similarly, the 2nd-order basis function is given by [see Equation (2.3)]

$$\begin{aligned} \varphi_{b_2}(x, z) = f_2(x, z) - \frac{\langle f_2(x, z), \varphi_{b_0}(x, z) \rangle}{\langle \varphi_{b_0}(x, z), \varphi_{b_0}(x, z) \rangle} \varphi_{b_0}(x, z) \\ - \frac{\langle f_2(x, z), \varphi_{b_1}(x, z) \rangle}{\langle \varphi_{b_1}(x, z), \varphi_{b_1}(x, z) \rangle} \varphi_{b_1}(x, z), \end{aligned} \quad (2.10)$$

where the inner products in the numerators on the right-hand side of Equation (2.10) are given by

$$\begin{aligned} \langle f_2(x, z), \varphi_{b_0}(x, z) \rangle &= \sum_{i=1}^{M_{b_x}} \sum_{j=1}^{M_{b_z}} f_2(x_{ij}, z_{ij}) \varphi_{b_0}^*(x_{ij}, z_{ij}), \\ &= \sum_{i=1}^{M_{b_x}} \sum_{j=1}^{M_{b_z}} (x_{ij} + z_{ij})^2, \end{aligned} \quad (2.11)$$

and

$$\begin{aligned} \langle f_2(x, z), \varphi_{b_1}(x, z) \rangle &= \sum_{i=1}^{M_{b_x}} \sum_{j=1}^{M_{b_z}} f_2(x_{ij}, z_{ij}) \varphi_{b_1}^*(x_{ij}, z_{ij}), \\ &= \sum_{i=1}^{M_{b_x}} \sum_{j=1}^{M_{b_z}} (x_{ij} + z_{ij})^3 - W_{10} \sum_{i=1}^{M_{b_x}} \sum_{j=1}^{M_{b_z}} (x_{ij} + z_{ij})^2. \end{aligned} \quad (2.12)$$

The *energy* contained in $\varphi_{b_0}(x, z)$ is given by Equation (2.7) and the energy contained

in $\varphi_{b_1}(x,z)$ is given by

$$\begin{aligned} E_{\varphi_{b_1}} &= \langle \varphi_{b_1}(x,z), \varphi_{b_1}(x,z) \rangle = \sum_{i=1}^{M_{b_x}} \sum_{j=1}^{M_{b_z}} \varphi_{b_1}(x_{ij}, z_{ij}) \varphi_{b_1}^*(x_{ij}, z_{ij}) , \\ &= \sum_{i=1}^{M_{b_x}} \sum_{j=1}^{M_{b_z}} |\varphi_{b_1}(x_{ij}, z_{ij})|^2 . \end{aligned} \quad (2.13)$$

Equation (2.13) is evaluated by using Equation (2.9) for the *1st*-order basis function, $\varphi_{b_1}(x,z)$. The ratios of inner products that appear on the right-hand side of Equation (2.10) are saved for use in later equations as

$$W_{20} = \frac{\langle f_2(x,z), \varphi_{b_0}(x,z) \rangle}{\langle \varphi_{b_0}(x,z), \varphi_{b_0}(x,z) \rangle} = \frac{\langle f_2(x,z), \varphi_{b_0}(x,z) \rangle}{E_{\varphi_{b_0}}} , \quad (2.14)$$

and

$$W_{21} = \frac{\langle f_2(x,z), \varphi_{b_1}(x,z) \rangle}{\langle \varphi_{b_1}(x,z), \varphi_{b_1}(x,z) \rangle} = \frac{\langle f_2(x,z), \varphi_{b_1}(x,z) \rangle}{E_{\varphi_{b_1}}} . \quad (2.15)$$

Finally, the *2nd*-order basis function is given by

$$\varphi_{b_2}(x,z) = (x+z)^2 - W_{20} - W_{21}[x+z - W_{10}] . \quad (2.16)$$

As mentioned earlier, the equations for the higher-order basis functions, for $n = 3, 4, \dots, N_b$, are found by expanding Equation (2.3) in the same manner. It is important to note from Equations (2.4) to (2.16) that all the input needed to determine the basis functions comes from the discrete data points of the ocean bathymetry. This

technique is ideally suited for implementation by a computer program. Additionally, the order of the orthogonal function expansion, N_b , can be increased by simply computing the next higher order coefficient b_n and orthonormal basis function ϕ_{b_n} ; all previous coefficients and basis functions do not have to be recomputed. In fact, many of the computations needed for the lower order coefficients and basis functions can be saved and used in the computation of the higher order coefficients and basis functions. The choice of N_b will be discussed in the next section concerning the minimum mean-squared error (MMSE) criterion for the best fit of the data.

Finally, the data for this technique do not have to be evenly spaced. The ability to use unevenly spaced data allows for data sets with slight perturbations in the down-range or cross-range values. Real data will contain randomness. For example, set and drift of a ship collecting bathymetric data could introduce such perturbations in down-range and cross-range of measured data, but there would be no effect on the estimated value of ocean depth.

3. The Generating Functions and the Minimum Mean-Squared Error Criterion

Theoretically, any finite set of functions may be transformed into a set of orthonormal basis functions by using the Gram-Schmidt procedure, and a MMSE fit to a finite set of data can be obtained using Equation (2.1) [Ref. 3]. Basis functions that are based on sinusoidal functions are frequently used in signal processing to model natural occurring phenomena with a finite Fourier series expansion. A previous effort to model the ocean bottom using a finite Spatial Fourier Series (SFS) expansion was attempted in 1991 [Ref. 4]. The SFS technique encountered difficulty due to the oscillations that are inherent in using a finite set of sinusoids to fit the ocean bottom. Additionally, the estimation of the first and second order derivatives at the point of incidence of a ray reflecting off the ocean bottom proved to be inaccurate due to the oscillatory fit. The use of a set of generating functions with increasing powers of the independent variable,

$f_n(z) = z^n$, $n = 0, 1, \dots, N_b$, was used successfully for one-dimensional orthogonal function expansions of ocean bathymetric data [Ref. 2].

The choice of using increasing powers of the sum of the cross-range and down-range variables as the set of generating functions was used in this thesis research, that is, $f_n(x, z) = (x + z)^n$, $n = 0, 1, \dots, N_b$. The lower order functions, for $n = 0, 1$, and 2, fit the most common trends in the ocean bathymetry without introducing oscillations. For $n = 0$, the orthogonal function expansion fits a constant depth ocean bottom. For $n = 1$, the orthogonal function expansion fits an up-sloping or down-sloping ocean bottom in both the x and z directions. For $n = 2$, the orthogonal function expansion fits a slope with increased curvature. The higher orders tend to fit ocean bottoms with many and various contour changes. In computer simulation, the highest order fit used is the designer's choice. Section B of Chapter II will present results with the highest order fit being 7th-order, that is, $N_b = 7$. The choice of the highest order fit is a trade-off between exactly fitting data (interpolation) versus providing a smooth fit to the trend of the data. Higher order, or a higher value of N_b , will fit contour changes more exactly. That is, the estimated fit will more closely match the input data. A lower order fits the discrete data by smoothing through contour changes in the bathymetric data that could be due to a rough bottom or measurement error. Data is corrupted by measurement noise and by a lack of precision in the measurement equipment. Limiting the highest order to $N_b = 7$ provides a smooth fit when the number of data points is greater than eight points.

If the discrete data is fit as accurately with $N_b < 7$ as with $N_b = 7$, then the use of the higher order terms is unnecessary. Lower order fits are used based on a minimum mean-squared error criterion [Ref. 2,3]. The order of the fit is determined by computing the mean-squared error (MSE) for each order fit, $N_b = 0, 1, \dots, 7$, as follows:

$$MSE_{y_b} = E_{y_{b_m}} - E_{\hat{y}_b} \quad , \quad (2.17)$$

where

$$E_{y_{b_m}} = \langle y_{b_m}(x_{ij}, z_{ij}), y_{b_m}(x_{ij}, z_{ij}) \rangle = \sum_{i=1}^{M_{b_x}} \sum_{j=1}^{M_{b_z}} |y_{b_m}(x_{ij}, z_{ij})|^2 \quad (2.18)$$

is the energy contained in the measured bathymetric data, and

$$E_{\hat{y}_b} = \langle \hat{y}_b(x_{ij}, z_{ij}), \hat{y}_b(x_{ij}, z_{ij}) \rangle = \sum_{i=1}^{M_{b_x}} \sum_{j=1}^{M_{b_z}} |\hat{y}_b(x_{ij}, z_{ij})|^2 \quad (2.19)$$

is the energy contained in the bathymetric estimate. The value of N_b that produces the lowest *MSE* becomes the order of expansion used to reconstruct the bathymetric data.

B. COMPUTER SIMULATION RESULTS OF BATHYMETRIC FITS

The technique of orthogonal function expansion to model ocean bathymetry that was derived in Section A of Chapter II was implemented in the RRA Algorithm FORTRAN ray tracing program. The results of various test cases are presented graphically to demonstrate both the successes and the shortcomings of this method of ocean bathymetry modeling. The graphs, presented in Figures 2 to 23, show the discrete bathymetric data points as large black dots (\bullet). The estimated fit to the discrete data computed by the orthogonal function expansion is presented as a mesh of lines to represent the two-dimensional, continuous surface. As can be seen from these figures, the surfaces, in general, do not pass through all of the data points. Instead, the curves fit the trend of the data. Computer simulation of this technique did reveal shortcomings. The test cases presented will show examples of the problems encountered, discuss the reasons for the problems, and suggest areas of future research to explore methods to correct these shortcomings.

Each plot contains a legend with the following information:

- (1) 'CASE:', a description of the test case
- (2) 'SIGMAYB:', the value of the standard deviation, (σ_{y_b}) , of a randomly generated zero-mean gaussian noise added to each data point
- (3) the order of the fit, (N_b) , based on the minimum mean-squared error criterion
- (4) 'MSE0:' to 'MSE7:', the mean-squared error for $N_b = 0,1,2,\dots,7$, computed using Equation (2.17)

The test cases are grouped in two categories. *0th*-order and *1st*-order fits are presented to show that exact fits are obtained in simple cases. The ability to handle unevenly spaced data is presented. Also, a problem with the choice of the generating function is discussed. Then, ocean bottoms with a more complicated or arbitrary shape are presented to demonstrate fitting the trend of the data. The shortcomings of the generating function that was chosen is discussed further.

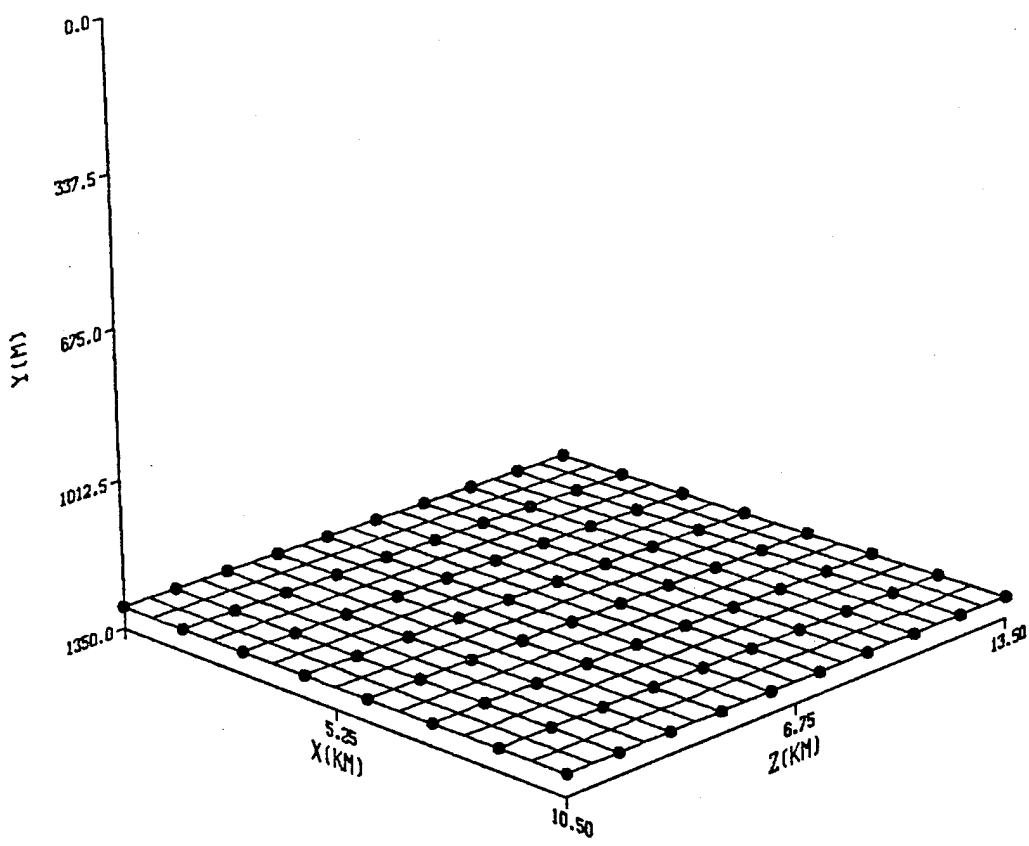
1. Exact Fit Test Cases

Figures 2 and 3 demonstrate the fit of the most basic test case, a flat ocean bottom with a constant depth. The exact equation used to generate the 8×10 rectangular matrices of data for Figures 2 and 3 is given by

$$y_b(x,z) = 1300. \quad (2.20)$$

Figure 2 shows the discrete data points entered at evenly spaced cross-range and down-range locations. Figure 3 shows that the data may be entered at unevenly spaced coordinates without affecting the fit. In both cases the fit is an exact *0th*-order fit with the orthogonal function expansion returning a value of 1300 meters for any combination of cross range and down range. The *0th*-order mean-squared error, MSE0, is 9.09×10^{-7} and not exactly equal to zero due to round-off error in the computer simulation which

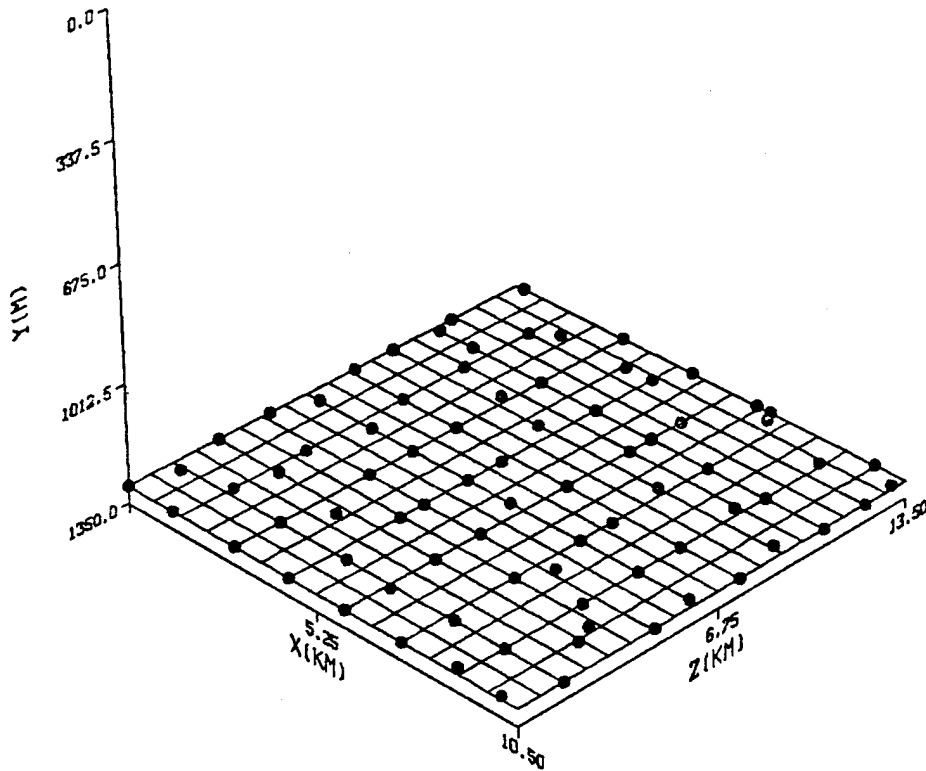
OCEAN BOTTOM BATHYMETRY



CASE: 8X10 FLAT OCEAN BOTTOM
SIGMAYB: 0.0M OTH-ORDER MMSE SURFACE FIT
MSE0: 9.090×10^{-7} MSE2: 9.090×10^{-7} MSE4: 9.090×10^{-7} MSE6: 9.090×10^{-7}
MSE1: 9.090×10^{-7} MSE3: 9.090×10^{-7} MSE5: 9.090×10^{-7} MSE7: 9.090×10^{-7}

Figure 2. Flat ocean bottom with evenly spaced data.

OCEAN BOTTOM BATHYMETRY



CASE: 8X10 FLAT BOTTOM IN X AND Z, UNEVENLY SPACED DATA
SIGMAYB: 0.0M 0TH-ORDER MMSE SURFACE FIT
MSE0: 9.090×10^{-7} MSE2: 9.090×10^{-7} MSE4: 9.090×10^{-7} MSE6: 9.090×10^{-7}
MSE1: 9.090×10^{-7} MSE3: 9.090×10^{-7} MSE5: 9.090×10^{-7} MSE7: 9.090×10^{-7}

Figure 3. Flat ocean bottom with unevenly spaced data.

uses double precision numbers. The values of the higher order mean-squared errors, MSE1 to MSE7, are equal to MSE0. This shows that no additional accuracy is obtained for $N_b > 0$.

Figures 4, 5, and 6 demonstrate exact 1st-order fits. The exact equation used to generate the 7×8 rectangular matrices of data for Figures 4 and 5 is given by

$$y_b(x,z) = 1500 - \frac{1}{160}(x+z), \quad (2.21)$$

which represents a planar ocean bottom that slopes upward at the same rate with respect to cross-range and down-range. The exact equation used to generate the 8×8 rectangular matrix of data for Figure 6 is given by

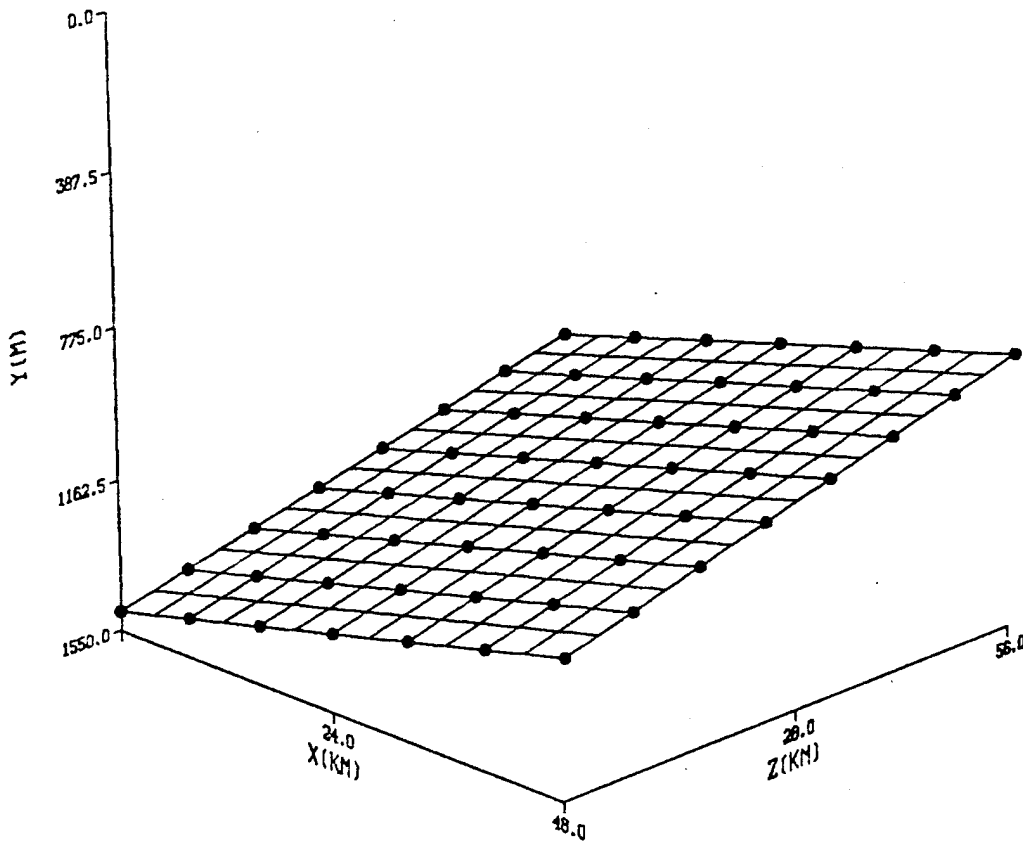
$$y_b(x,z) = 1350 + \frac{1}{30}(x+z), \quad (2.22)$$

which represents a planar ocean bottom that slopes downward at the same rate with respect to cross-range and down-range. In Figures 4 and 6, the orthogonal function expansion fits the data with an exact first order fit. For $N_b = 1$, the orthogonal function expansion is given by

$$\hat{y}_b(x,z) = b_0 + b_1(x+z - W_{10}) = (b_0 - b_1 W_{10}) + b_1(x+z), \quad (2.23)$$

which exactly matches the form of Equations (2.21) and (2.22). Note that the choice of generating functions used for this technique, $f_n(x,z) = (x+z)^n$, for $n = 0,1,\dots,7$, will result in an orthogonal function expansion based upon the sum of x and z . Since x and z are multiplied by the constant b_1 , the same slope with respect to cross range and down range will result.

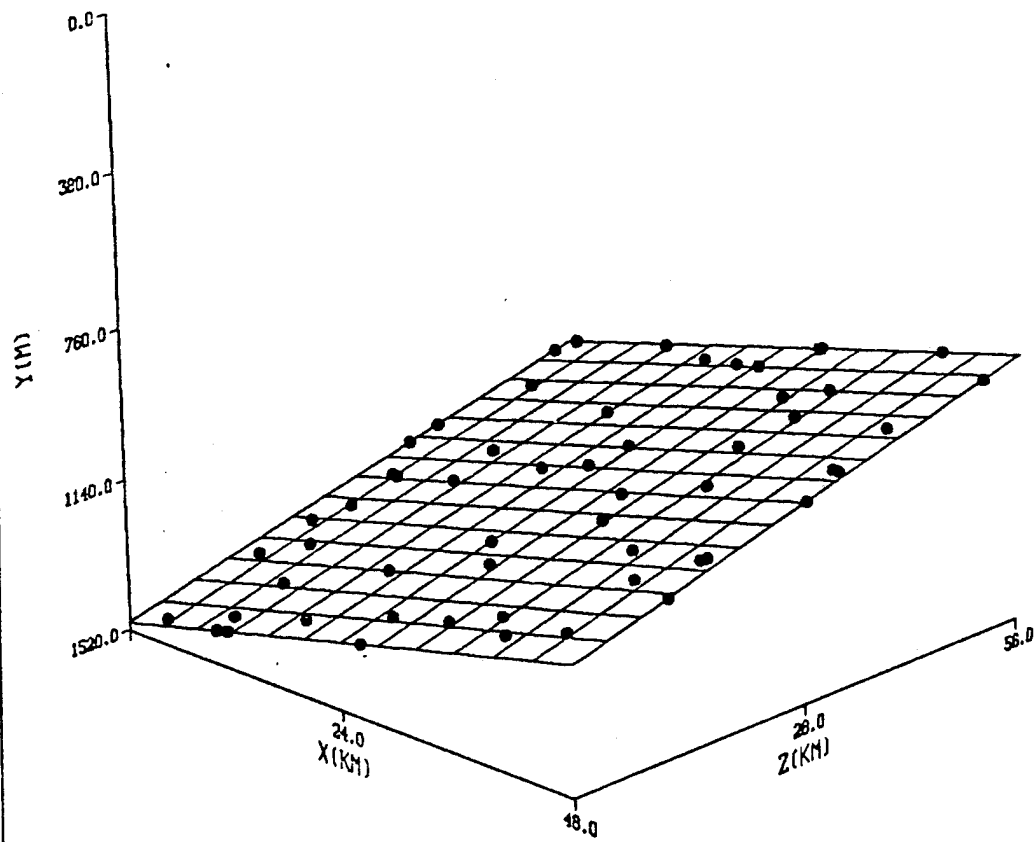
OCEAN BOTTOM BATHYMETRY



CASE: 7X8 UP-SLOPE IN BOTH X AND Z DIRECTIONS
SIGMAYB: 0.0M 1ST-ORDER MMSE SURFACE FIT
MSE0: 1.295×10^6 MSE2: 2.645×10^{-7} MSE4: 2.645×10^{-7} MSE6: 2.645×10^{-7}
MSE1: 2.645×10^{-7} MSE3: 2.645×10^{-7} MSE5: 2.645×10^{-7} MSE7: 2.645×10^{-7}

Figure 4. Planar ocean bottom sloping upward in both the x and z directions with evenly spaced data.

OCEAN BOTTOM BATHYMETRY



CASE: 7X8 UP-SLOPE IN BOTH X AND Z, UNEVENLY SPACED DATA
SIGMAYB: 0.0M 7TH-ORDER MMSE SURFACE FIT
MSE0: 1.237×10^6 MSE2: 4.415×10^{-2} MSE4: 4.334×10^{-2} MSE6: 4.294×10^{-2}
MSE1: 4.805×10^{-2} MSE3: 4.341×10^{-2} MSE5: 4.303×10^{-2} MSE7: 4.238×10^{-2}

Figure 5. Planar ocean bottom sloping upward in both the x and z directions with unevenly spaced data.

OCEAN BOTTOM BATHYMETRY

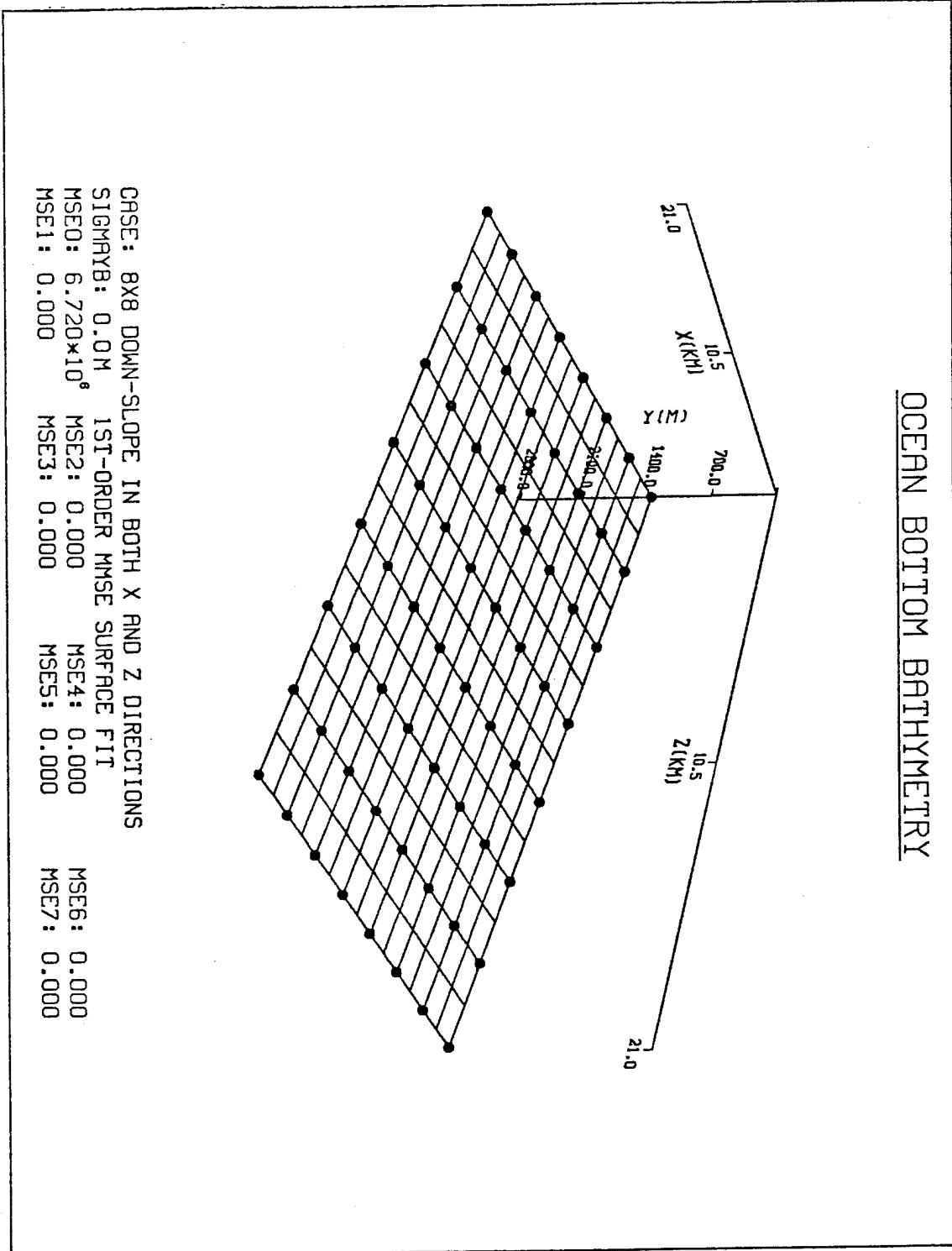


Figure 6. Planar ocean bottom sloping downward in both the x and z directions with evenly spaced data.

Figure 5 demonstrates that the data may be unevenly spaced. Note that the fit indicated in Figure 5 is *7th*-order and not *1st*-order. Equation (2.21) was used to generate the discrete data entered for the computer simulation shown in Figure 5, however, only five significant digits were entered. Round-off error results from having only five significant digits in the discrete bathymetric data. For the orthogonal function expansion, the double-precision computations that evaluate the best fit of the data based on the mean-squared error criterion found that the *7th*-order fit was slightly more accurate. The *1st*-order mean-squared error is of the same order of magnitude as the *7th*-order mean-squared error. The orthogonal function expansion coefficients,

$$\begin{aligned}
 b_0 &= 8.82963 \times 10^3, & b_1 &= -1.11226 \times 10^3, \\
 b_2 &= -6.24349 \times 10^{-2}, & b_3 &= -2.73240 \times 10^{-2}, \\
 b_4 &= 8.38137 \times 10^{-3}, & b_5 &= -1.74958 \times 10^{-2}, \\
 b_6 &= -9.30174 \times 10^{-3}, & b_7 &= 2.38320 \times 10^{-2},
 \end{aligned}$$

show that the fit is essentially *1st*-order. The *0th*- and *1st*-order coefficients, b_0 and b_1 , are five orders of magnitude larger than the higher order coefficients, b_2, b_3, \dots, b_7 . In this test case, the higher order terms of the orthogonal function expansion will affect only the fourth or fifth significant digit of the ocean bathymetry evaluated using the orthogonal function expansion.

Figures 7, 8, and 9 show the results of fitting discrete bathymetric data that shoals, or has an upward slope, in only the down-range (z) direction. The data is constant with respect to variations in the cross-range (x) direction. The exact equation used to generate the discrete data for Figures 7, 8, and 9 is given by

$$y_b(x, z) = 550 - \frac{1}{6}z. \quad (2.24)$$

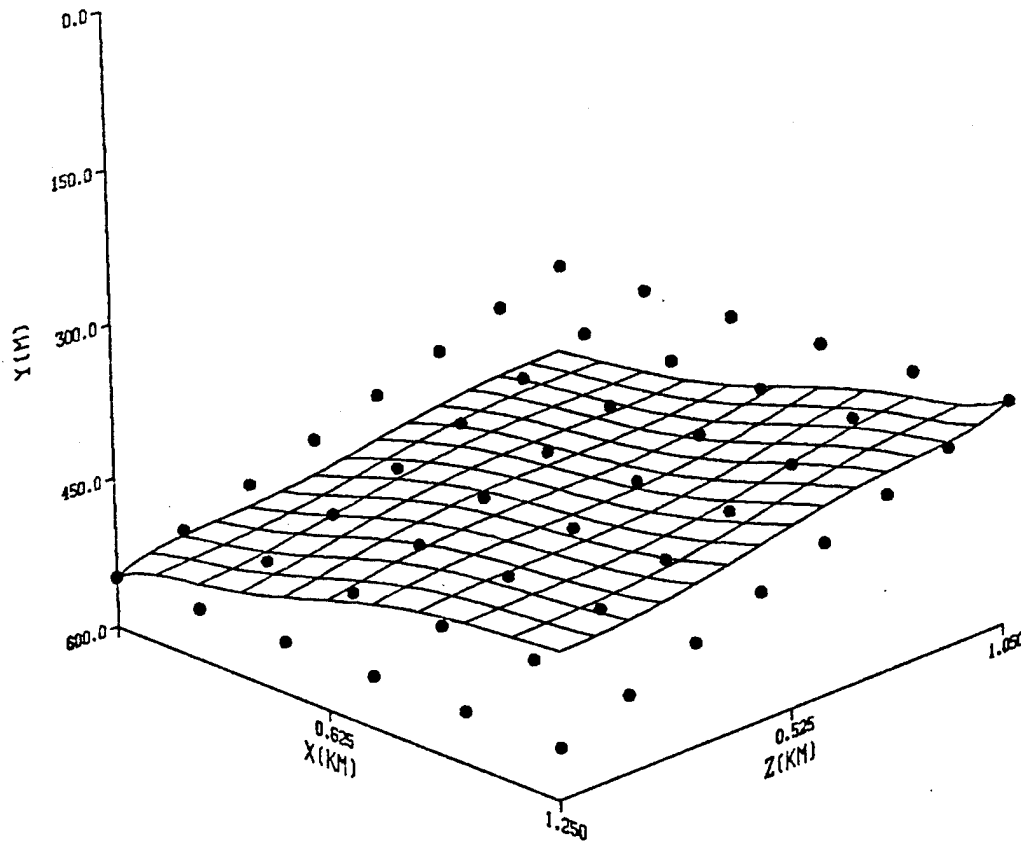
Figure 7 shows the results of the orthogonal function expansion as detailed in Section A of Chapter II. The fit that is presented in Figure 7 is the best fit to the data when using the generating function given in Section A of Chapter II. The corner of the surface fit at the maximum cross-range and minimum down-range location ($x = 1.250$ km, $z = 0.0$ km) is above the discrete bathymetric data points; the corner of the surface fit at the minimum cross-range and maximum down-range location ($x = 0.0$ km, $z = 1.050$ km) is below the discrete bathymetric data points. The fitted surface approximates a *1st*-order planar ocean bottom model that slopes upward equally in both the x and z directions. Therefore, the fitted plane is above half of the discrete bathymetric data points in the lower half of Figure 7, and it is below half of the discrete bathymetric data points in the upper half of Figure 7. The best fit is limited in its accuracy due to the fact that x and z are summed in every term of the orthogonal function expansion. The orthogonal function expansion does not treat the x and z dependence separately, and this is the major shortcoming of this technique.

In order to correct this shortcoming, an independent weighting with respect to x and an independent weighting with respect to z need to be added to the orthogonal function expansion. With the addition of weighting factors to Equation (2.1), the orthogonal function expansion becomes

$$\hat{y}_b(x, z) = \sum_{n=0}^{N_b} b_n \varphi_{b_n}(W_x x, W_z z), \quad (2.25)$$

where W_x and W_z are weighting factors to introduce independence in x and in z . For the exact *1st*-order cases presented in Figures 7 through 15, the weighting factors are constants in order to independently match the rate of change of the ocean bottom depth with respect to x and to z . In the following section, for more complicated ocean bottom geometries, the weighting factors would need to be functions of the independent

OCEAN BOTTOM BATHYMETRY



CASE: 6X8 UP-SLOPE IN Z DIRECTION ONLY, NO WEIGHTING
SIGMAYB: 0.0M 7TH-ORDER MMSE SURFACE FIT
MSE0: 1.575×10^5 MSE2: 9.557×10^4 MSE4: 9.452×10^4 MSE6: 9.419×10^4
MSE1: 9.557×10^4 MSE3: 9.452×10^4 MSE5: 9.419×10^4 MSE7: 9.384×10^4

Figure 7. Planar ocean bottom sloping upward in the z direction only with no variation in the x direction, modeled without weighting x and z separately, with evenly spaced data.

variables. The development of an algorithm to determine the weighting factors, W_x and W_z , from the discrete data is not presented as part of this thesis and is left as an area of future research. The choices of W_x and W_z in Figures 7 through 15 are based on *a priori* knowledge of the signs (positive or negative) of the slopes of the data with respect to cross-range (x) and down-range (z).

Figure 8 presents the same test case presented in Figure 7, except that weighting factors, W_x and W_z , were added as shown in Equation (2.25) with $W_x = 0$ and $W_z = 1$. The result is an exact *1st*-order fit. Figure 9 presents the same test case with the discrete bathymetric data entered at unevenly spaced locations. As discussed concerning Figure 5, the fit determined by the orthogonal function expansion is *7th*-order due to using only five significant digits for the discrete bathymetric data. The overall fit is *1st*-order; the higher order terms of the orthogonal function expansion only affect the lower significant digits of the estimated value of the ocean bottom.

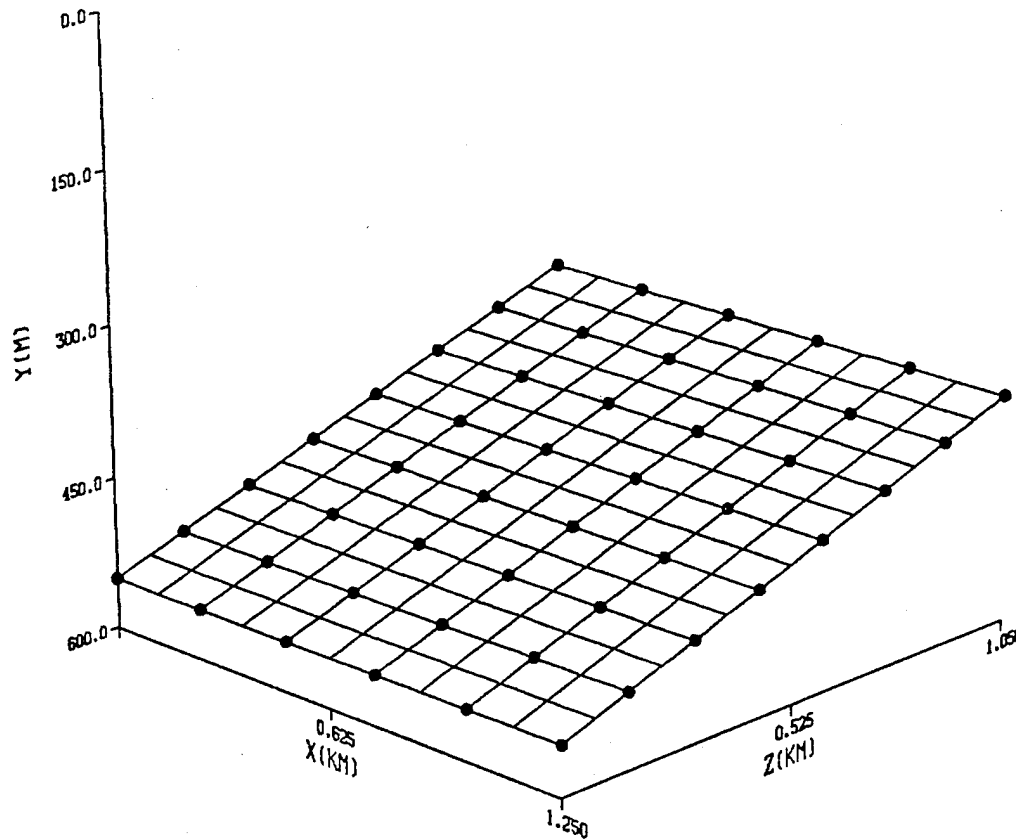
Figures 10 and 11 show the fit to discrete bathymetric data that has a downward slope in only the down-range (z) direction. The data is constant with respect to variations in the cross-range (x) direction. The exact equation used to generate the discrete data for Figures 10 and 11 is given by

$$y_b(x,z) = 1700 + \frac{1}{20}z. \quad (2.26)$$

Figure 10 shows the result of the orthogonal function expansion as detailed in Section A of Chapter II. Figure 11 presents the same test case presented in Figure 10, except that weighting factors, W_x and W_z , were added as shown in Equation (2.25) with $W_x = 0$ and $W_z = 1$.

Figures 12 and 13 show the results of fitting discrete bathymetric data that has opposite slopes with respect to cross-range and down-range, that is, an upward slope in the down-range (z) direction and a downward slope in the cross-range (x) direction. The

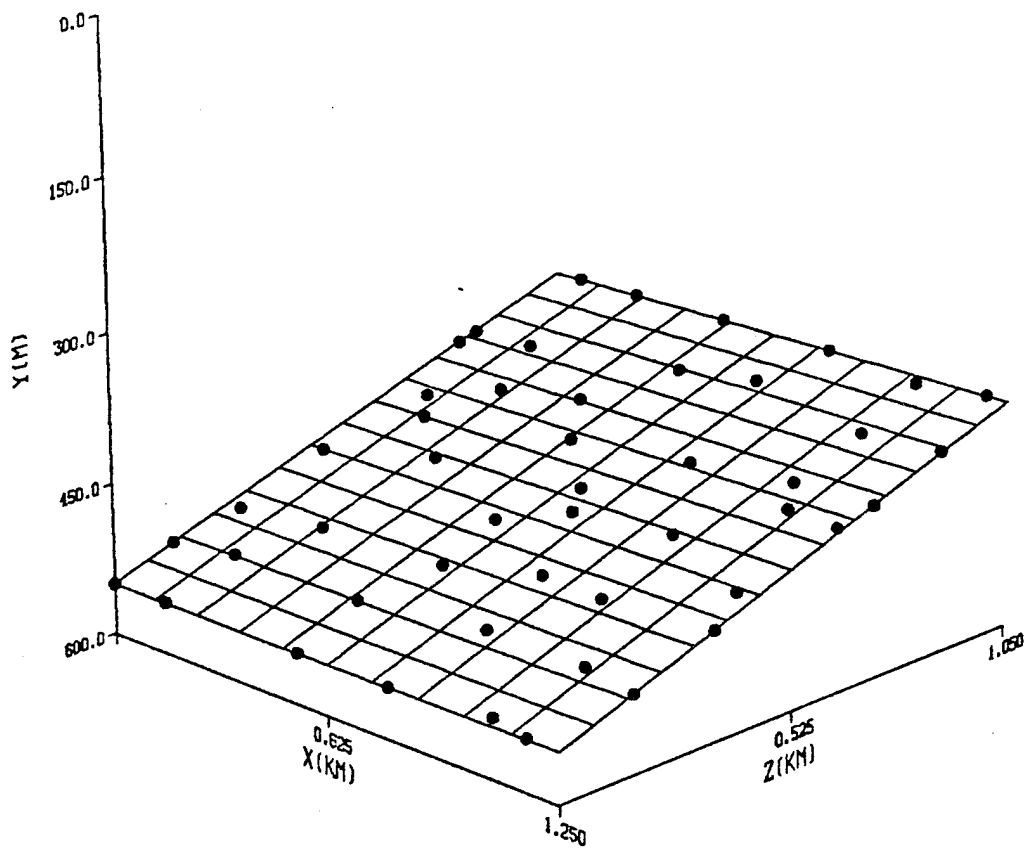
OCEAN BOTTOM BATHYMETRY



CASE: 6X8 UP-SLOPE IN Z DIRECTION ONLY, WITH WEIGHTING
SIGMAYB: 0.0M 1ST-ORDER MMSE SURFACE FIT
MSE0: 1.575×10^5 MSE2: 1.094×10^{-8} MSE4: 1.094×10^{-8} MSE6: 1.094×10^{-8}
MSE1: 1.094×10^{-8} MSE3: 1.094×10^{-8} MSE5: 1.094×10^{-8} MSE7: 1.094×10^{-8}

Figure 8. Planar ocean bottom sloping upward in the z direction only with no variation in the x direction, using $W_x = 0$ and $W_z = 1$, with evenly spaced data.

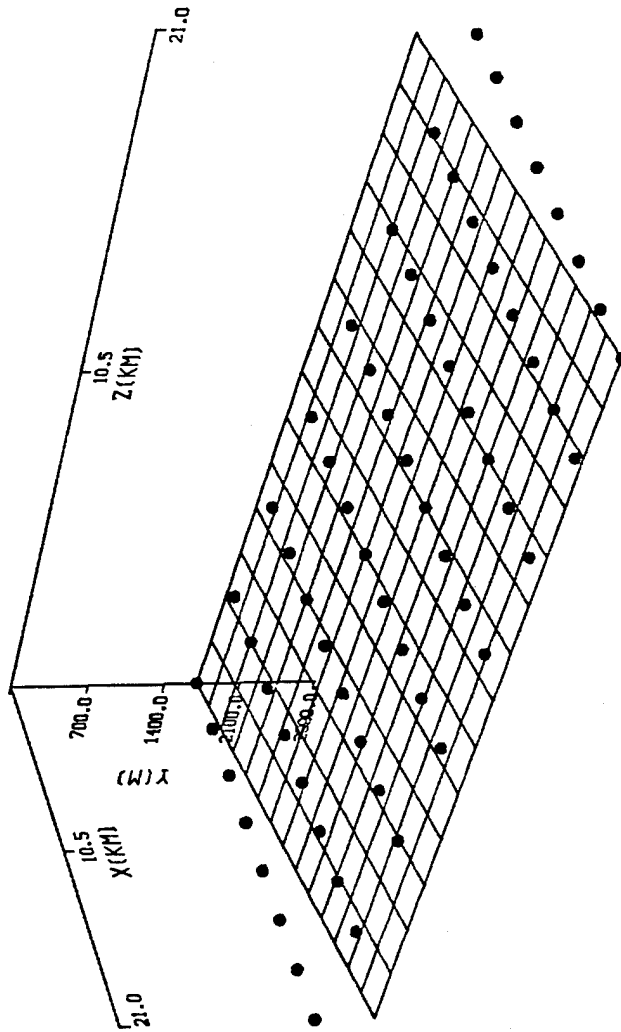
OCEAN BOTTOM BATHYMETRY



CASE: 6X8 UP-SLOPE IN Z ONLY, WITH UNEVENLY SPACED DATA
SIGMAYB: 0.0M 7TH-ORDER MMSE SURFACE FIT
MSE0: 1.523×10^5 MSE2: 3.621×10^{-2} MSE4: 3.522×10^{-2} MSE6: 2.803×10^{-2}
MSE1: 3.740×10^{-2} MSE3: 3.523×10^{-2} MSE5: 3.149×10^{-2} MSE7: 2.803×10^{-2}

Figure 9. Planar ocean bottom sloping upward in the z direction only with no variation in the x direction, using $W_x = 0$ and $W_z = 1$, with unevenly spaced data.

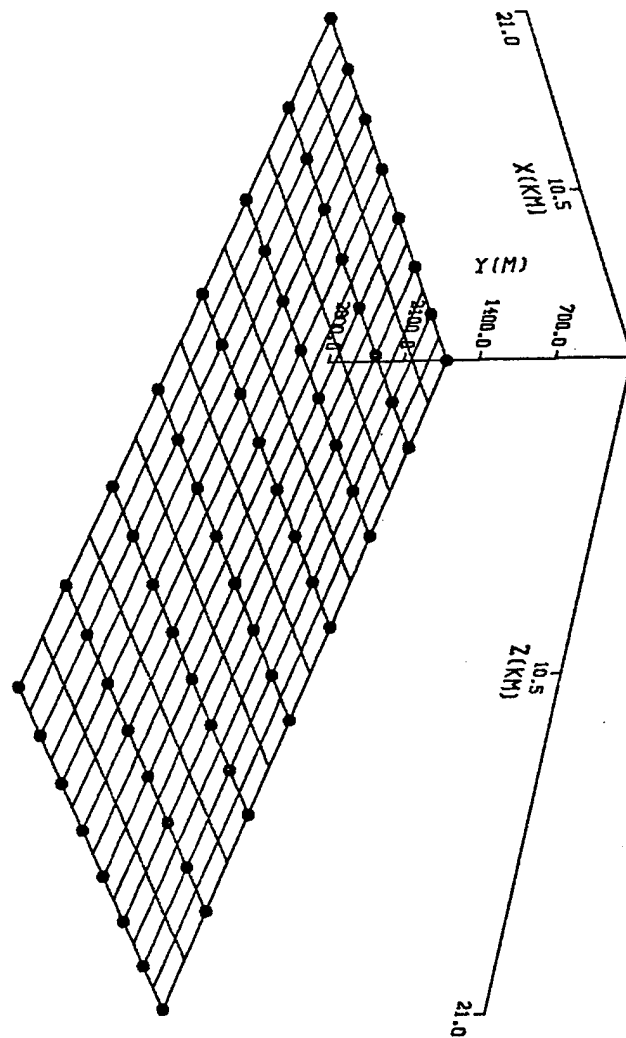
OCEAN BOTTOM BATHYMETRY



CASE: 8X8 DOWN-SLOPE IN Z DIRECTION ONLY, NO WEIGHTING
 SIGMAYB: 0.0M 1ST-ORDER MMSE SURFACE FIT
 MSE0: 7.560×10^6 MSE2: 3.780×10^6 MSE4: 3.780×10^6 MSE6: 3.780×10^6
 MSE1: 3.780×10^6 MSE3: 3.780×10^6 MSE5: 3.780×10^6 MSE7: 3.780×10^6

Figure 10. Planar ocean bottom sloping downward in the z direction only with no variation in the x direction, modeled without weighting x and z separately, with evenly spaced data.

OCEAN BOTTOM BATHYMETRY



CASE: 8X8 DOWN-SLOPE IN Z DIRECTION ONLY
 SIGMAYB: 0.0M 1ST-ORDER MMSE SURFACE FIT
 MSE0: 7.560×10^{-8} MSE2: 5.960×10^{-9} MSE4: 5.960×10^{-9} MSE6: 5.960×10^{-9}
 MSE1: 5.960×10^{-9} MSE3: 5.960×10^{-9} MSE5: 5.960×10^{-9} MSE7: 5.960×10^{-9}

Figure 11. Planar ocean bottom sloping downward in the z direction only with no variation in the x direction, using $W_x = 0$ and $W_z = 1$, with evenly spaced data.

slopes are equal in magnitude, but opposite in sign. The exact equation used to generate the discrete data for Figures 12 and 13 is given by

$$y_b(x,z) = 1500 + \frac{3}{160}(x-z). \quad (2.27)$$

Figure 12 shows the result of using the orthogonal function expansion as detailed in Section A of Chapter II. Figure 13 presents the same test case presented in Figure 12, except that weighting factors, W_x and W_z , were added as shown in Equation (2.25) with $W_x = -1$ and $W_z = 1$.

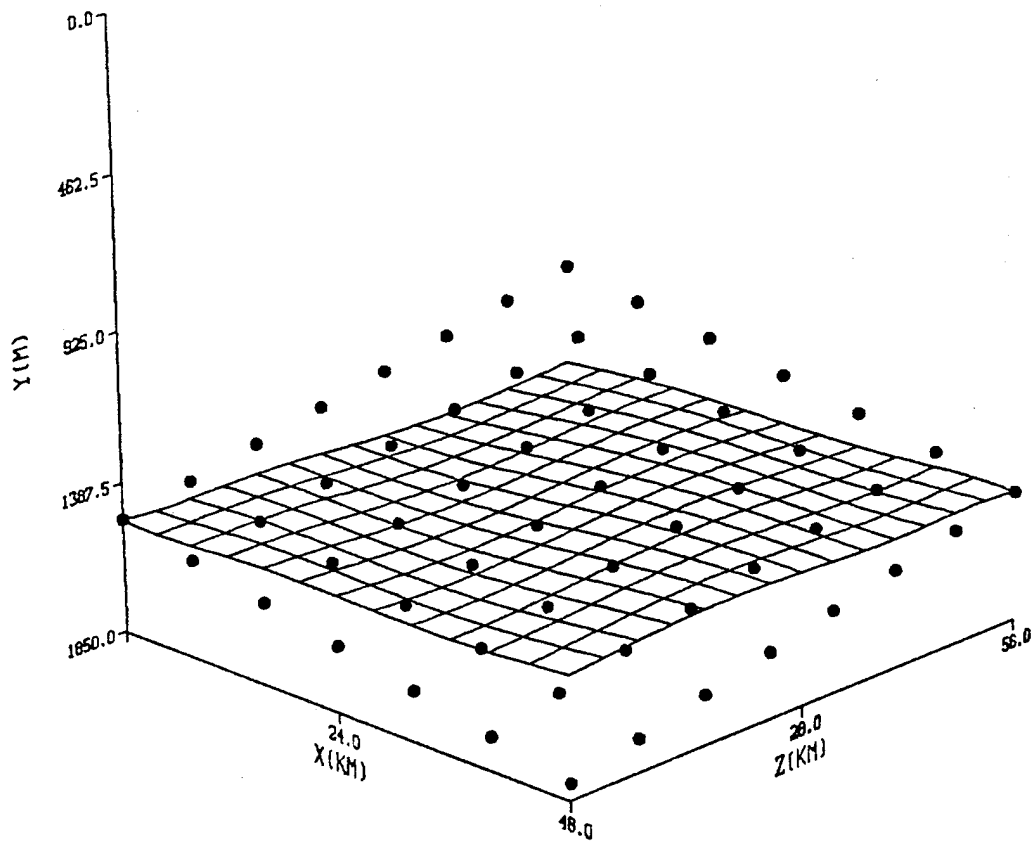
Figures 14 and 15 show the results of fitting a rectangular matrix of discrete bathymetric data that has opposite slopes with respect to cross-range and down-range, that is, a downward slope in the down-range (z) direction and an upward slope in the cross-range (x) direction. The slopes are equal in magnitude, but opposite in sign. The exact equation used to generate the discrete bathymetric data for Figures 14 and 15 is given by

$$y_b(x,z) = 1300 - \frac{1}{20}(x-z). \quad (2.28)$$

Figure 14 shows the result of using the orthogonal function expansion as detailed in Section A of Chapter II. Figure 15 presents the same test case presented in Figure 14, except that weighting factors, W_x and W_z , were added as shown in Equation (2.25) with $W_x = -1$ and $W_z = 1$.

Figures 2 through 15 have shown that the method of orthogonal function expansion accurately models discrete bathymetric data in the most basic test cases of planar ocean bottoms. From discrete bathymetric data, a continuous model is produced. The discrete bathymetric data does not need to be evenly spaced. Errors in the discrete

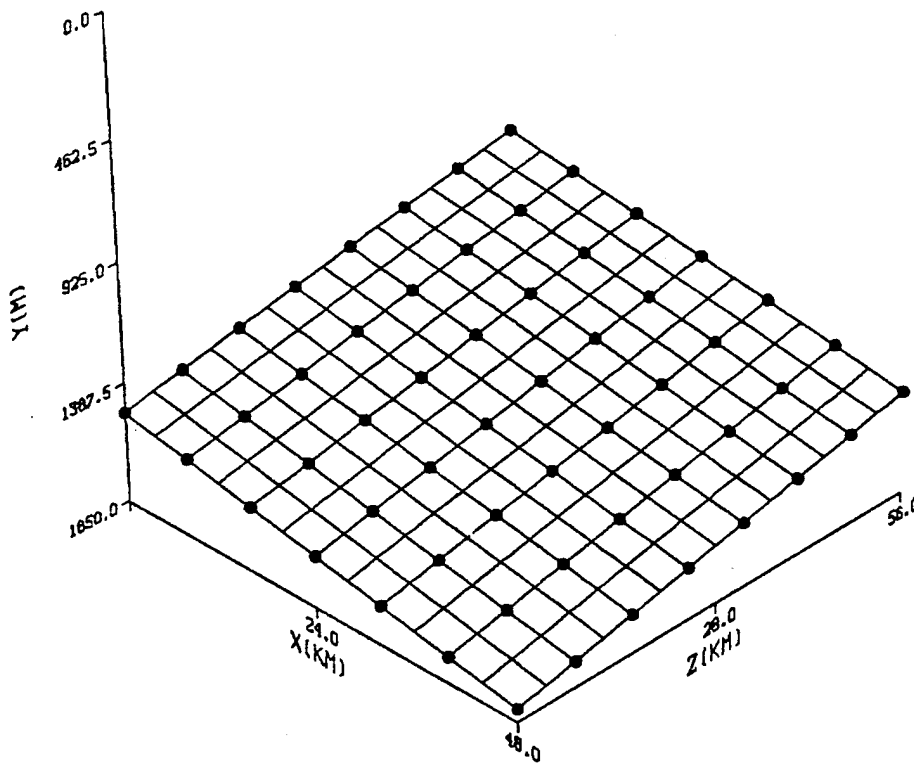
OCEAN BOTTOM BATHYMETRY



CASE: 7X8 DOWN-SLOPE IN X, UP-SLOPE IN Z, NO WEIGHTING
SIGMAYB: 0.0M 7TH-ORDER MMSE SURFACE FIT
MSE0: 1.295×10^6 MSE2: 1.271×10^6 MSE4: 1.267×10^6 MSE6: 1.265×10^6
MSE1: 1.271×10^6 MSE3: 1.267×10^6 MSE5: 1.265×10^6 MSE7: 1.263×10^6

Figure 12. Planar ocean bottom sloping upward in the z direction and downward in the x direction, modeled without weighting x and z separately, with evenly spaced data.

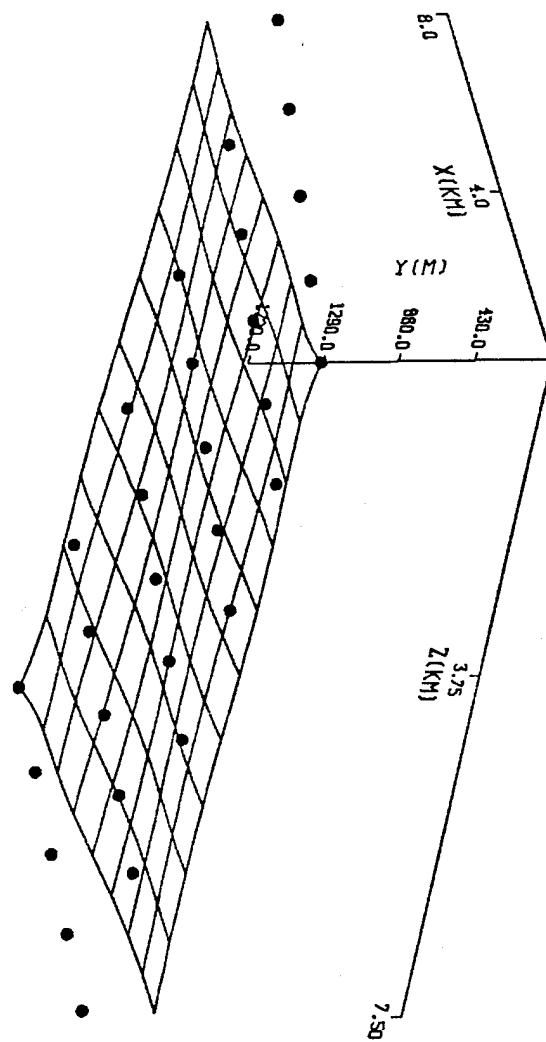
OCEAN BOTTOM BATHYMETRY



CASE: 7X8 DOWN-SLOPE IN X, UP-SLOPE IN Z, WITH WEIGHTING
 SIGMAYB: 0.0M 1ST-ORDER MMSE SURFACE FIT
 MSE0: 1.295×10^8 MSE2: 3.353×10^{-7} MSE4: 3.353×10^{-7} MSE6: 3.353×10^{-7}
 MSE1: 3.353×10^{-7} MSE3: 3.353×10^{-7} MSE5: 3.353×10^{-7} MSE7: 3.353×10^{-7}

Figure 13. Planar ocean bottom sloping upward in the z direction and downward in the x direction, using $W_x = -1$ and $W_z = 1$, with evenly spaced data.

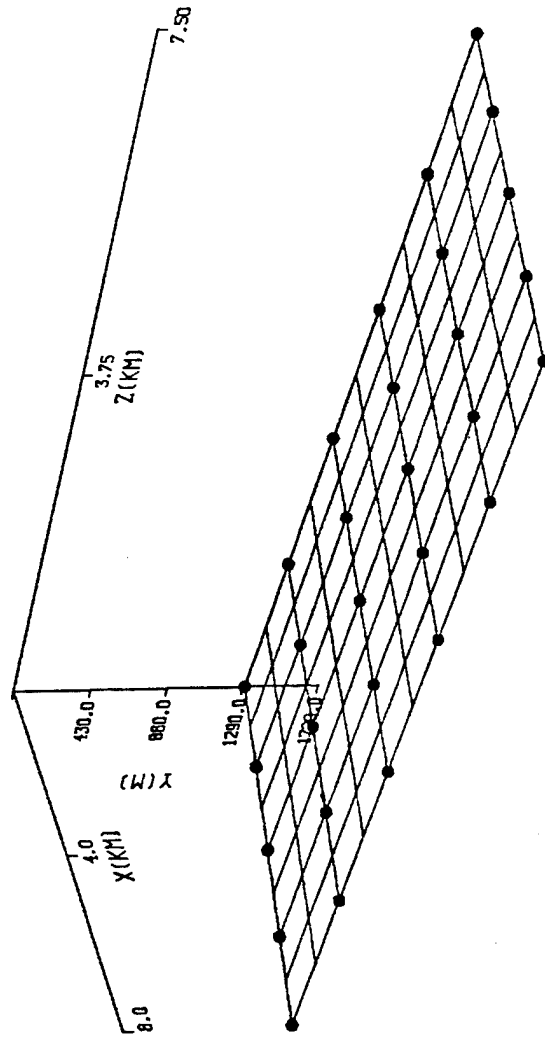
OCEAN BOTTOM BATHYMETRY



CASE: 5X6 DOWN-SLOPE IN Z, UP-SLOPE IN X, NO WEIGHTING
 SIGMAYB: 0.0M 7TH-ORDER MMSE SURFACE FIT
 MSE0: 1.092×10^8 MSE2: 1.082×10^8 MSE4: 1.078×10^8 MSE6: 1.077×10^8
 MSE1: 1.082×10^8 MSE3: 1.078×10^8 MSE5: 1.077×10^8 MSE7: 1.075×10^8

Figure 14. Planar ocean bottom sloping downward in the z direction and upward in the x direction, modeled without weighting x and z separately, with evenly spaced data.

OCEAN BOTTOM BATHYMETRY



CASE: 5X6 DOWN-SLOPE IN Z, UP-SLOPE IN X, WITH WEIGHTING
 SIGMAYB: 0.0M 1ST-ORDER MMSE SURFACE FIT
 MSE0: 1.092×10⁶ MSE2: 8.196×10⁶ MSE4: 8.196×10⁶ MSE6: 8.196×10⁶
 MSE1: 8.196×10⁶ MSE3: 8.196×10⁶ MSE5: 8.196×10⁶ MSE7: 8.196×10⁶

Figure 15. Planar ocean bottom sloping downward in the z direction and upward in the x direction, using $W_x = -1$ and $W_z = 1$, with evenly spaced data.

bathymetric data, such as round-off error, do not affect the dominant results of a 1st-order fit. The only major shortcoming is the need of an algorithm to weight x and z independently.

2. Complicated Test Cases

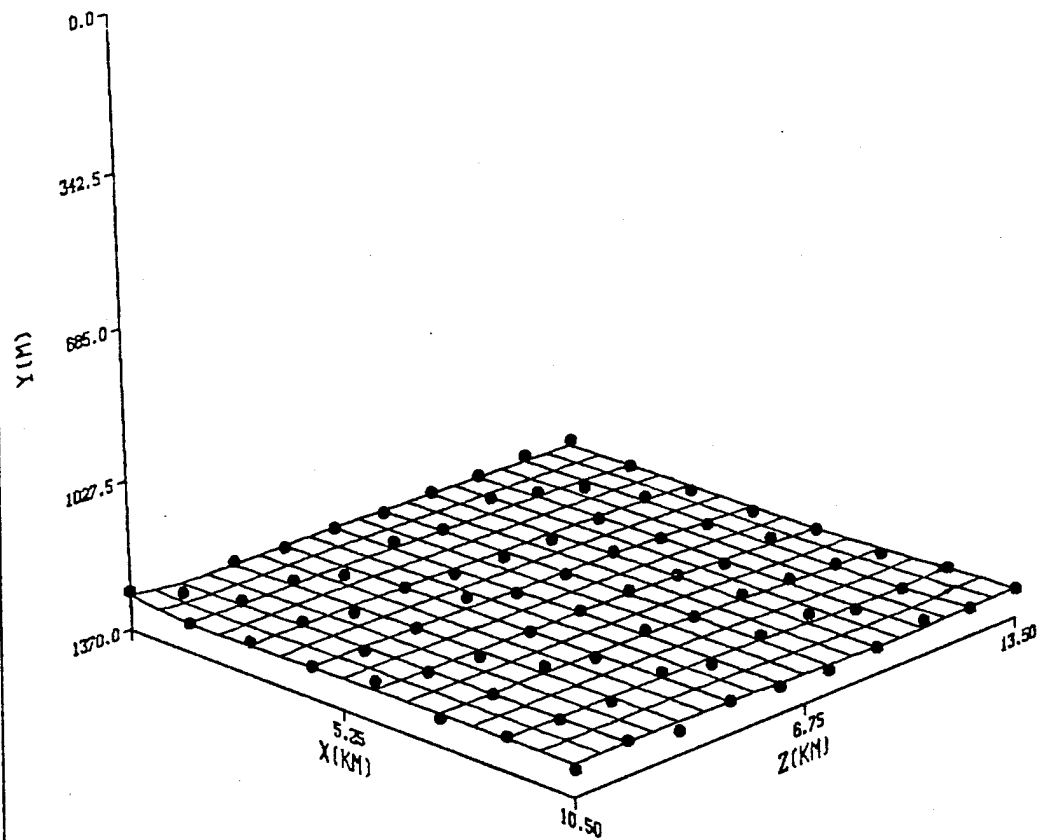
Figures 16(a), 16(b), and 17 show test cases that were presented in the previous section, except that now the discrete ocean bathymetric data has been corrupted by a zero-mean random gaussian noise with standard deviation, σ_{y_b} , that has been added to each point. Note that the plots refer to the value of σ_{y_b} as 'SIGMAYB:' in the legend of the plot. Only the value of the depth of each point has been corrupted. The cross-range and down-range values have been left at evenly spaced coordinates so that the (x,z) coordinate of each discrete data point corresponds to the intersection of the lines in the mesh of the estimated ocean bottom.

Figures 16(a) and 16(b) show the flat ocean bottom that was presented in Figure 2. Equation (2.20) has been modified as follows:

$$y_b(x,z) = 1300 + \sigma_{y_b} N(0,1), \quad (2.29)$$

where $N(0,1)$ represents a zero-mean gaussian (normal) random variable with a unit standard deviation obtained from a gaussian random number generator. For Figure 16(a), σ_{y_b} is 13 meters, a standard deviation that is 1% of the value of the uncorrupted ocean bottom data. For Figure 16(b), σ_{y_b} is 130 meters, a standard deviation that is 10% of the value of the uncorrupted ocean bottom data. In both cases, the overall trend of the discrete bathymetric data is fit by the orthogonal function expansion. Note in Figures 16(a) and 16(b) that the 7th-order mean-squared error and the 0th-order mean-squared error are of the same order of magnitude. Although a 7th-order fit is produced, the 0th-order, flat ocean bottom, predominates.

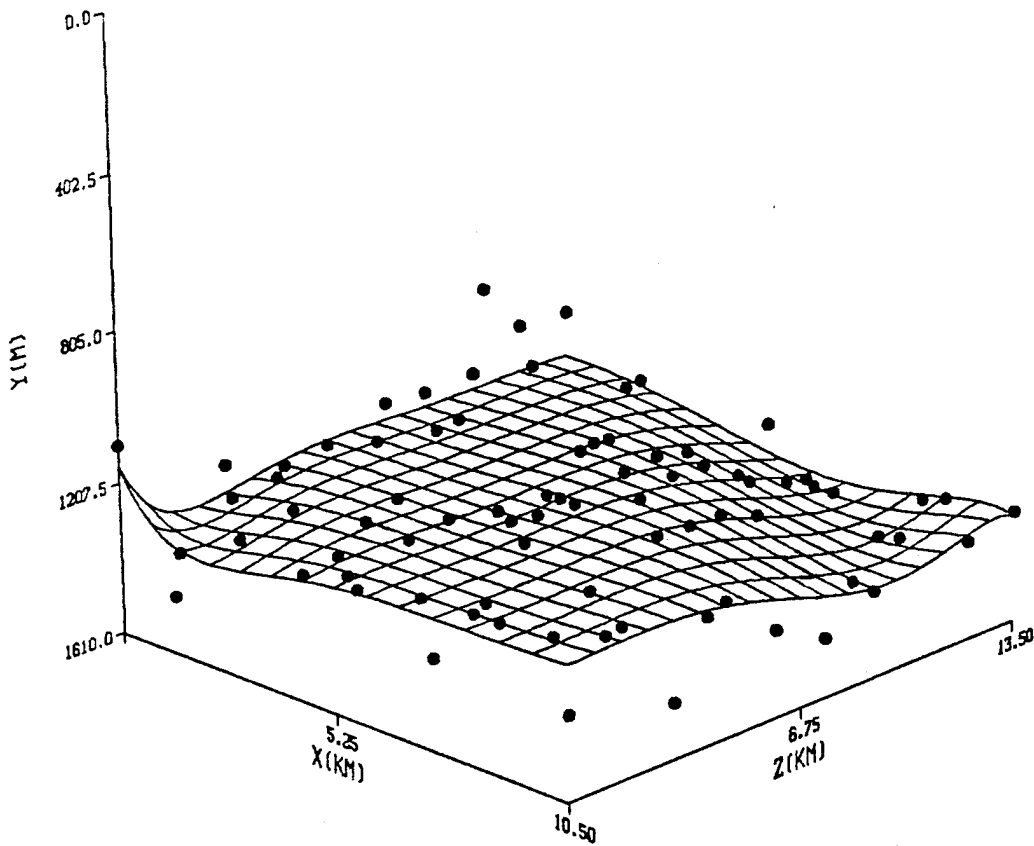
OCEAN BOTTOM BATHYMETRY



CASE: 8X10 FLAT BOTTOM WITH 1% DEVIATION IN DEPTHS
SIGMAYB: 13.0M 7TH-ORDER MMSE SURFACE FIT
MSE0: 1.128×10^4 MSE2: 1.068×10^4 MSE4: 1.028×10^4 MSE6: 1.025×10^4
MSE1: 1.100×10^4 MSE3: 1.068×10^4 MSE5: 1.028×10^4 MSE7: 1.009×10^4

Figure 16(a). Flat ocean bottom with evenly spaced data corrupted by a zero-mean random gaussian noise added to the depth of each data point.

OCEAN BOTTOM BATHYMETRY



CASE: 8X10 FLAT BOTTOM WITH 10% DEVIATION IN DEPTHS
SIGMAYB: 130.0M 7TH-ORDER MMSE SURFACE FIT
MSE0: 1.128×10^6 MSE2: 1.068×10^6 MSE4: 1.028×10^6 MSE6: 1.025×10^6
MSE1: 1.100×10^6 MSE3: 1.068×10^6 MSE5: 1.028×10^6 MSE7: 1.009×10^6

Figure 16(b). Flat ocean bottom with evenly spaced data corrupted by a zero-mean random gaussian noise added to the depth of each data point.

Figure 17 shows the shoaling ocean bottom presented in Figure 8 with Equation (2.24) modified to

$$y_b(x, z) = 1350 - \frac{1}{3}z + \sigma_{y_b} N(0,1), \quad (2.30)$$

where $\sigma_{y_b} = 20$ meters. Again, the orthogonal function expansion fits the trend of the discrete bathymetric data. The values of the mean-squared errors in the legend of Figure 17 indicate that a *1st*-order fit dominates, demonstrating that the orthogonal function expansion smoothes through noise in the discrete bathymetric data.

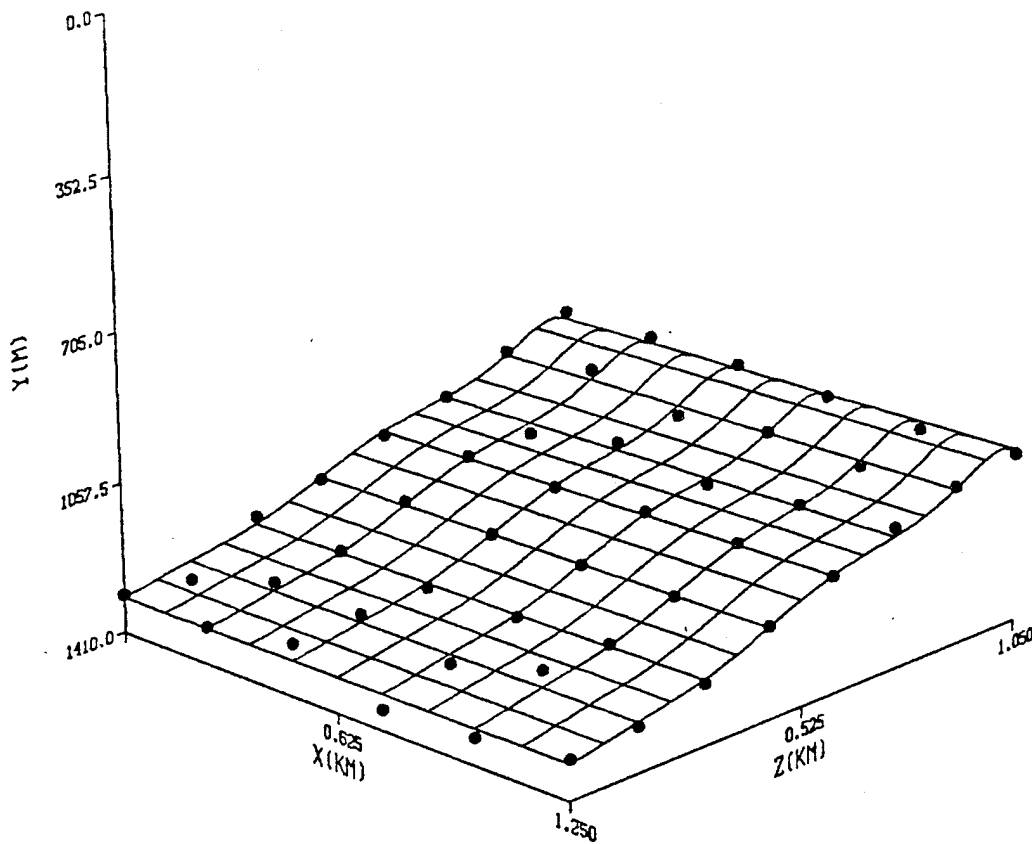
More complicated ocean bottom geometries are presented in Figures 18 through 23. The models presented in each case continue to fit the trend of the discrete bathymetric data and provide a smooth, continuous model of the ocean bathymetry from discrete data. However, the poor performance illustrated in Figure 23 demonstrates serious shortcomings with the two-dimensional orthogonal function expansion based on the current choice of generating functions.

Figure 18 shows a shoaling ocean bottom with a non-constant slope that increases as x and z increase. The exact equation used to generate the 5×6 rectangular matrix of discrete data for this test case is given by

$$y_b(x, z) = 2000 - 3(x + z)^2. \quad (2.31)$$

Equation (2.31) is of the same form as the orthogonal function expansion with $N_b = 2$. The mean-squared errors shown in the legend of Figure 18 show that the resulting fit is predominantly a *2nd*-order fit. The small value of the *2nd*-order mean-squared error shows close agreement between the discrete bathymetric data and the *2nd*-order estimated fit. Again, the algorithm computes higher order terms, but these terms have little effect on the overall fit.

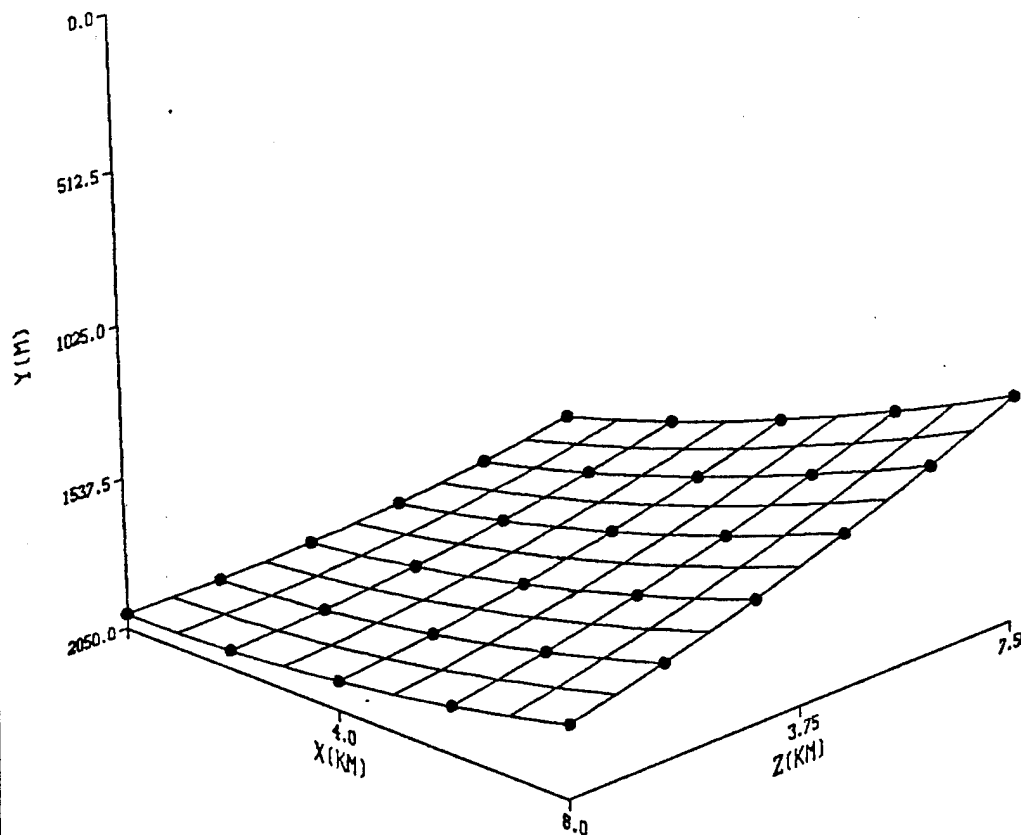
OCEAN BOTTOM BATHYMETRY



CASE: 6X8 UP-SLOPE IN Z DIRECTION ONLY, WITH WEIGHTING
SIGMAYB: 20.0M 7TH-ORDER MMSE SURFACE FIT
MSE0: 5.955×10^5 MSE2: 1.629×10^4 MSE4: 1.445×10^4 MSE6: 1.344×10^4
MSE1: 1.683×10^4 MSE3: 1.476×10^4 MSE5: 1.440×10^4 MSE7: 1.331×10^4

Figure 17. Planar ocean bottom sloping upward in the z direction only with no variation in the x direction, using $W_x = 0$ and $W_z = 1$, with evenly spaced data corrupted by a zero-mean random gaussian noise added to the depth of each data point.

OCEAN BOTTOM BATHYMETRY



CASE: 5X6 QUADRATIC UPWARD SLOPING OCEAN BOTTOM
SIGMAYB: 0.0M 7TH-ORDER MMSE SURFACE FIT
MSE0: 1.022×10^5 MSE2: 1.803×10^{-2} MSE4: 1.789×10^{-2} MSE6: 1.754×10^{-2}
MSE1: 7.730×10^4 MSE3: 1.789×10^{-2} MSE5: 1.754×10^{-2} MSE7: 1.720×10^{-2}

Figure 18. Shoaling ocean bottom in both the x and z directions with evenly spaced data.

Figures 19 and 20 show a rolling or oscillating ocean bottom. The exact equation used to generate the data for Figure 19 is given by

$$y_b(x, z) = 1500 - 180(x + z) + 30(x + z)^2 - 1.3(x + z)^3, \quad (2.32)$$

and

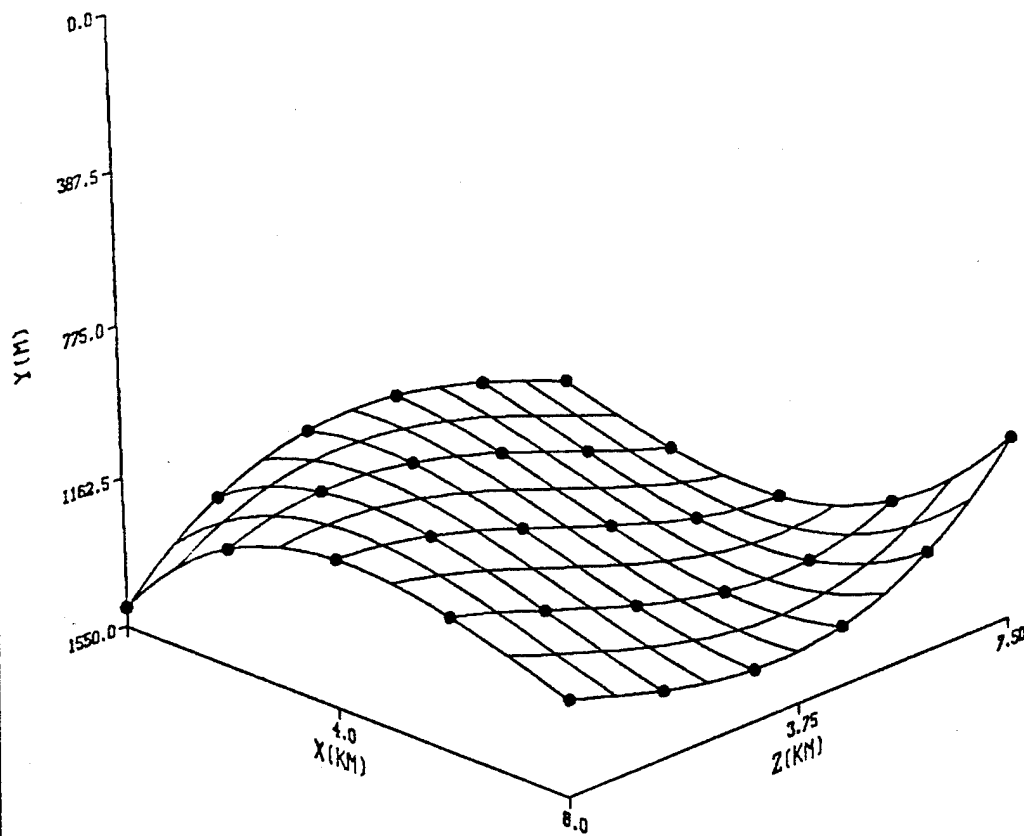
$$y_b(x, z) = 1500 - 180(x + z) + 30(x + z)^2 - 1.3(x + z)^3 + \sigma_{y_b} N(0,1), \quad (2.33)$$

is used to generate the data for Figure 20. In Equation (2.33), a standard deviation of $\sigma_{y_b} = 40$ meters is used to add zero-mean random gaussian noise for the test case shown in Figure 20. Equations (2.32) and (2.33) are of the same form as the orthogonal function expansion with $N_b = 3$. The mean-squared errors shown in the legend of Figures 19 and 20 show that the resulting fits are predominantly 3rd-order. The small value of the 3rd-order mean-squared error shows close agreement between the bathymetric data and the 3rd-order estimated fit. Figure 20 demonstrates the ability of the orthogonal function expansion to fit the trend of discrete bathymetric data in the presence of noise, even for complex ocean bottom geometries.

Figures 21(a) and 21(b) present results from the same test case, but shown graphically from two different points of view. The test case presented shows a flat ocean bottom with a gaussian shaped mound centered at the origin. The exact equation used to generate the 8×10 rectangular matrix of data is given by

$$y_b(x, z) = c_1 - c_2 \frac{1}{\sqrt{2\pi}\sigma} e^{-\frac{x^2}{2\sigma^2}} e^{-\frac{z^2}{2\sigma^2}}. \quad (2.34)$$

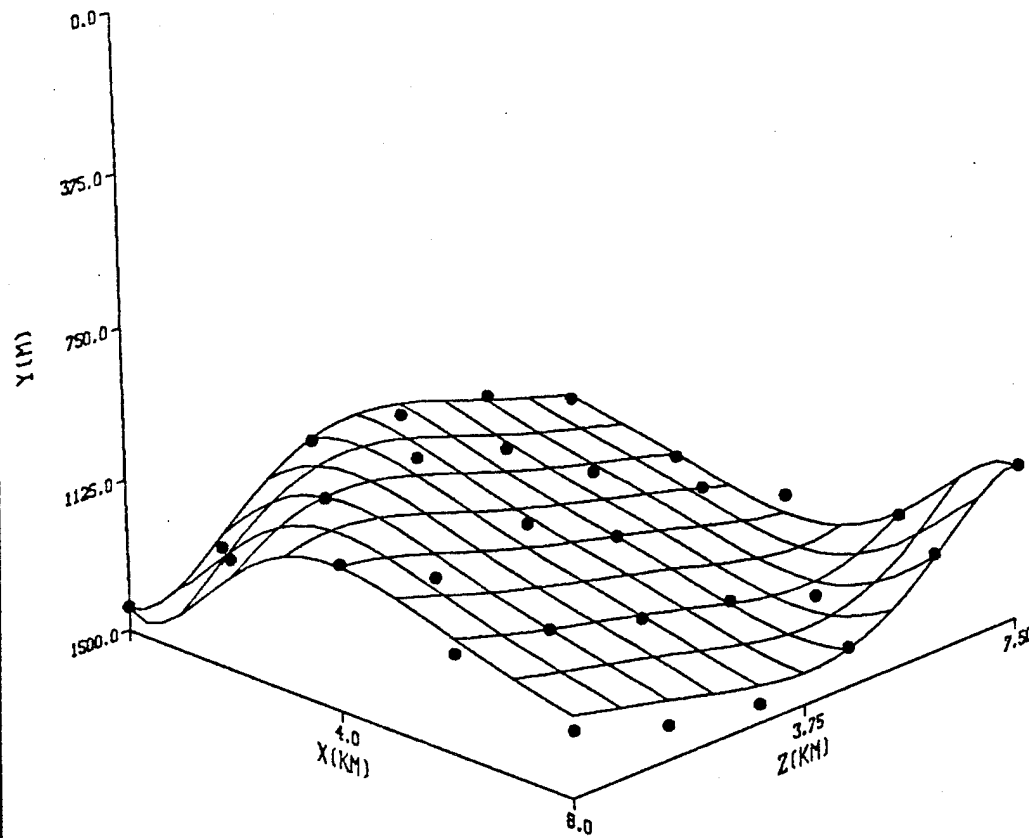
OCEAN BOTTOM BATHYMETRY



CASE: 5X6 OSCILLATING OCEAN BOTTOM
SIGMAYB: 0.0M 7TH-ORDER MMSE SURFACE FIT
MSE0: 2.831×10^5 MSE2: 2.655×10^5 MSE4: 1.104×10^{-2} MSE6: 1.062×10^{-2}
MSE1: 2.659×10^5 MSE3: 1.169×10^{-2} MSE5: 1.076×10^{-2} MSE7: 1.061×10^{-2}

Figure 19. Rolling or oscillating ocean bottom with evenly spaced data.

OCEAN BOTTOM BATHYMETRY



CASE: 5X6 OSCILLATING OCEAN BOTTOM
SIGMAYB: 40.0M 7TH-ORDER MMSE SURFACE FIT
MSE0: 2.880×10^5 MSE2: 2.683×10^5 MSE4: 4.883×10^4 MSE6: 4.649×10^4
MSE1: 2.683×10^5 MSE3: 4.889×10^4 MSE5: 4.749×10^4 MSE7: 3.831×10^4

Figure 20. Rolling or oscillating ocean bottom with evenly spaced data corrupted by a zero-mean random gaussian noise added to the depth of each data point.

With the constants set to $c_1 = 1300$, $c_2 = 10^5$, and $\sigma = 4$, Equation (2.34) becomes

$$y_b(x,z) = 1300 - 994.72e^{-\frac{x^2+z^2}{32}}. \quad (2.35)$$

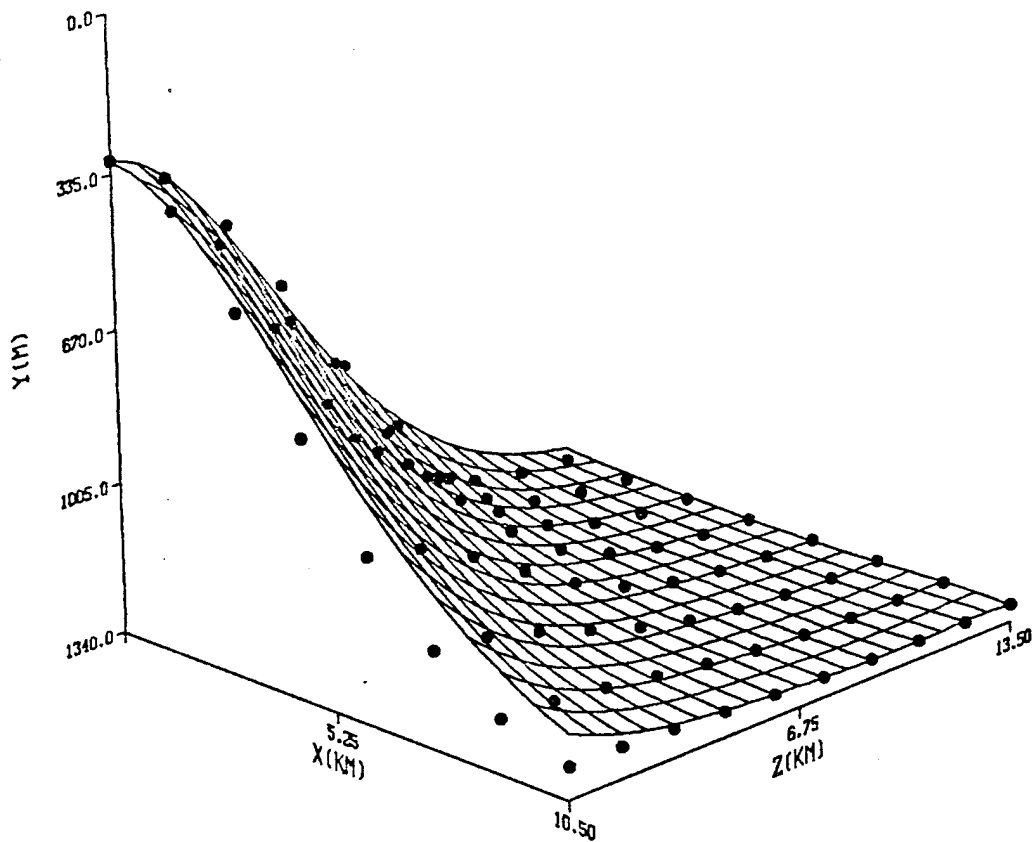
Equation (2.35) is modified by adding a zero-mean random gaussian noise with $\sigma_{y_b} = 50$ meters, for the test case presented in Figures 22(a) and 22(b).

Figures 21(a) and 21(b) present a test case that does not match the form of Equation (2.1) for the orthogonal function expansion. Although the orthogonal function expansion does not exactly fit the data, the model fits the trend of the data. The gaussian function given in Equation (2.34) is centered at the origin. Therefore, the orthogonal function expansion, which is derived from the generating functions, $f_n(x,z) = (x+z)^n$, for $n = 0,1,\dots,7$, can follow the data as it rolls away from the origin. In Figures 22(a) and 22(b), the addition of randomness to the data creates a more realistic test case of a downward sloping, complex ocean bottom. The model smoothly fits through the discrete bathymetric data with some data points above and some data below the fit.

Figures 23(a) and 23(b) demonstrate the major shortcoming of the algorithm being tested. This test case presents a gaussian shaped ocean bottom with the peak of the gaussian function centered within the rectangular matrix of data at $x = 5$ km, $z = 5$ km. The exact equation used to generate the 8×10 rectangular matrix of discrete bathymetric data is given by

$$y_b(x,z) = c_1 - c_2 \frac{1}{\sqrt{2\pi\sigma}} e^{-\frac{(x-5)^2}{2\sigma^2}} e^{-\frac{(z-5)^2}{2\sigma^2}}. \quad (2.36)$$

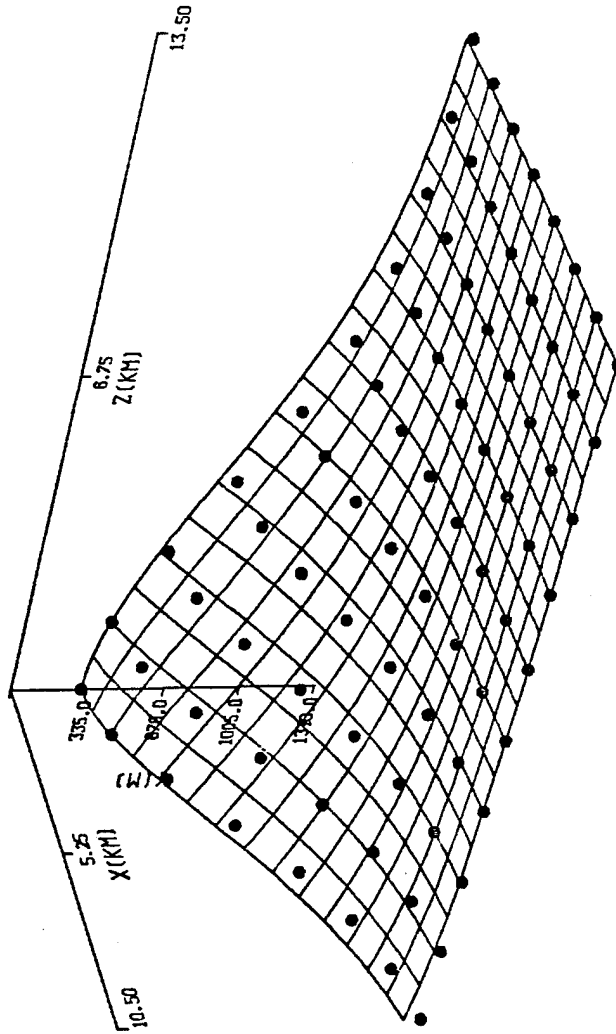
OCEAN BOTTOM BATHYMETRY



CASE: 8X10 FLAT BOTTOM WITH A GAUSSIAN MOUND
SIGMAYB: 0.0M 7TH-ORDER MMSE SURFACE FIT
MSE0: 5.440×10^6 MSE2: 3.245×10^5 MSE4: 2.428×10^5 MSE6: 2.131×10^5
MSE1: 1.658×10^6 MSE3: 2.819×10^5 MSE5: 2.147×10^5 MSE7: 2.128×10^5

Figure 21(a). Downward sloping ocean bottom with a gaussian shape in both the x and z directions with evenly spaced data.

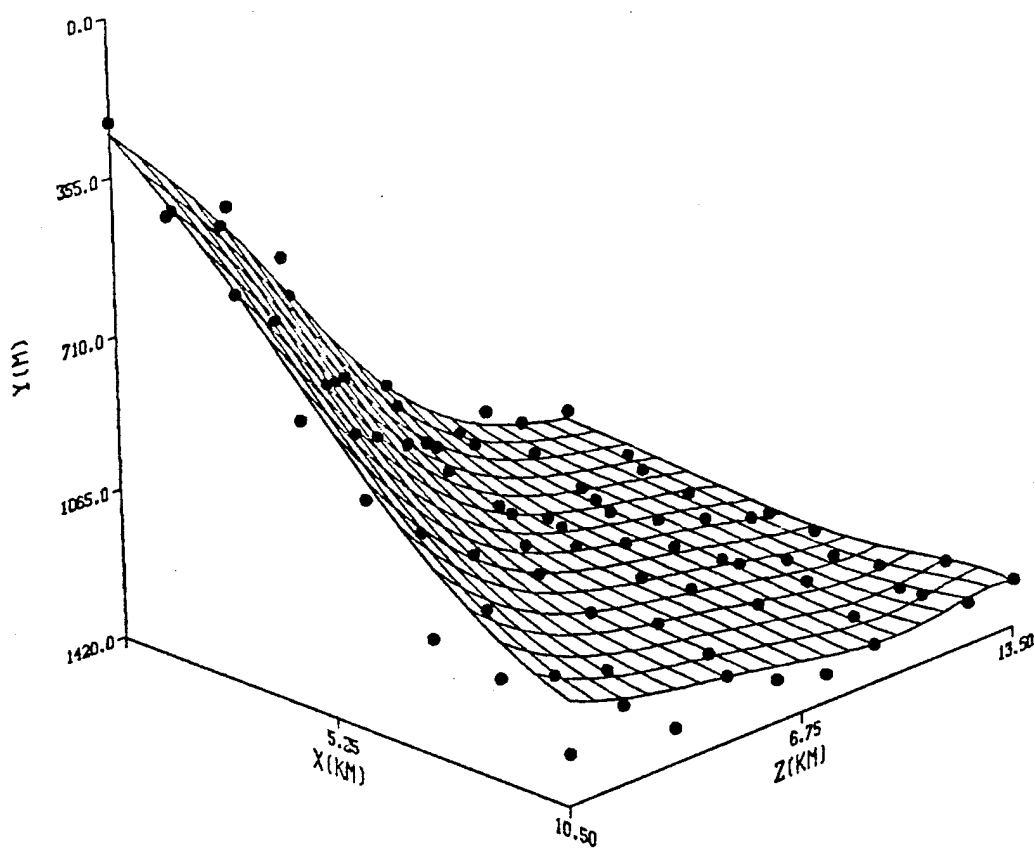
OCEAN BOTTOM BATHYMETRY



CASE: 8X10 FLAT BOTTOM WITH A GAUSSIAN MOUND
 SIGMAYB: 0.0M 7TH-ORDER MMSE SURFACE FIT
 MSE0: 5.440×10^6 MSE2: 3.245×10^5 MSE4: 2.428×10^5 MSE6: 2.131×10^5
 MSE1: 1.658×10^6 MSE3: 2.819×10^5 MSE5: 2.147×10^5 MSE7: 2.128×10^5

Figure 21(b). Downward sloping ocean bottom with a gaussian shape in both the x and z directions with evenly spaced data.

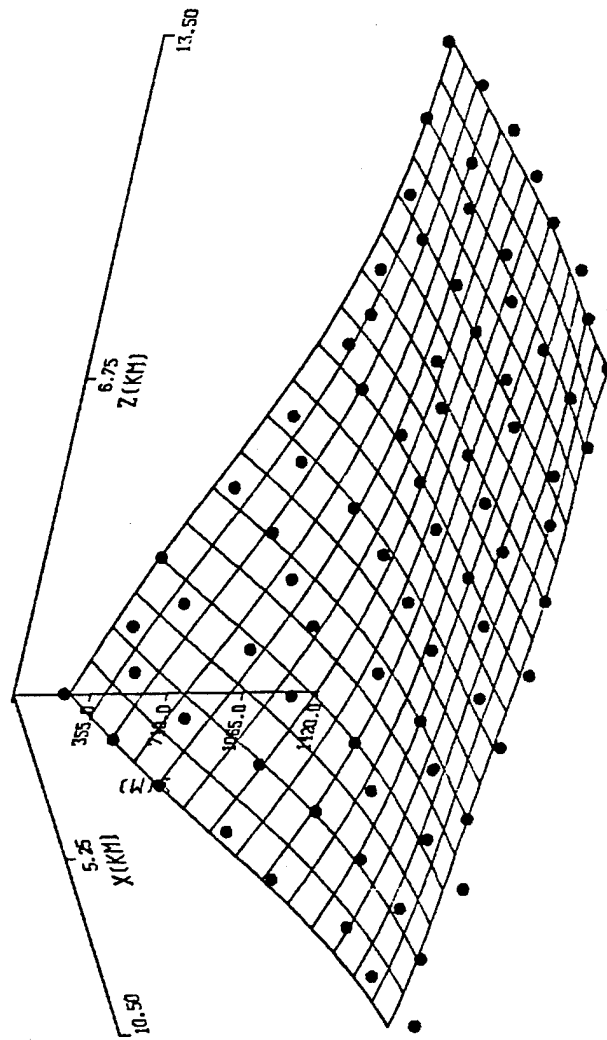
OCEAN BOTTOM BATHYMETRY



CASE: 8X10 FLAT BOTTOM WITH A GAUSSIAN MOUND
SIGMAYB: 50.0M 7TH-ORDER MMSE SURFACE FIT
MSE0: 5.640×10^6 MSE2: 4.226×10^5 MSE4: 3.660×10^5 MSE6: 3.395×10^5
MSE1: 1.602×10^5 MSE3: 3.806×10^5 MSE5: 3.399×10^5 MSE7: 3.353×10^5

Figure 22(a). Downward sloping ocean bottom with a gaussian shape in both the x and z directions with evenly spaced data corrupted by a zero-mean random gaussian noise added to the depth of each data point.

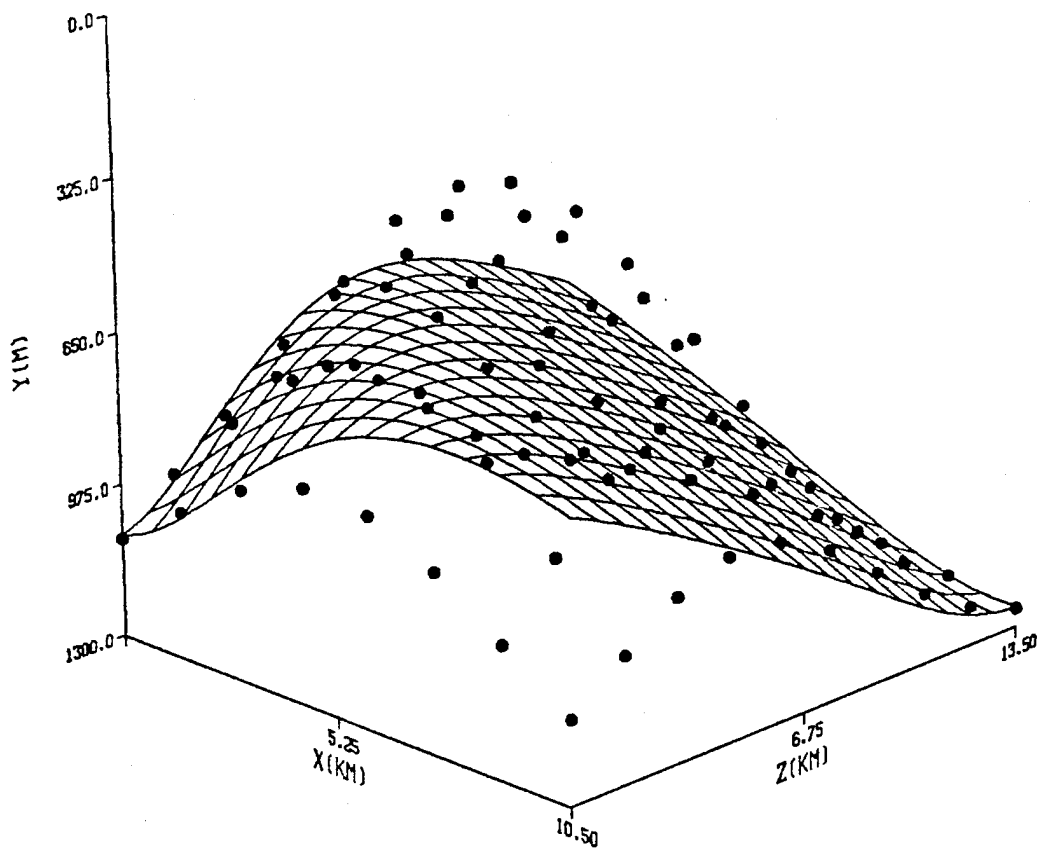
OCEAN BOTTOM BATHYMETRY



CASE: 8X10 FLAT BOTTOM WITH A GAUSSIAN MOUND
 SIGMAYB: 50.0M 7TH-ORDER MMSE SURFACE FIT
 MSE0: 5.640×10^6 MSE2: 4.226×10^5 MSE4: 3.660×10^5 MSE6: 3.395×10^5
 MSE1: 1.602×10^6 MSE3: 3.806×10^5 MSE5: 3.399×10^5 MSE7: 3.353×10^5

Figure 22(b). Downward sloping ocean bottom with a gaussian shape in both the x and z directions with evenly spaced data corrupted by a zero-mean random gaussian noise added to the depth of each data point.

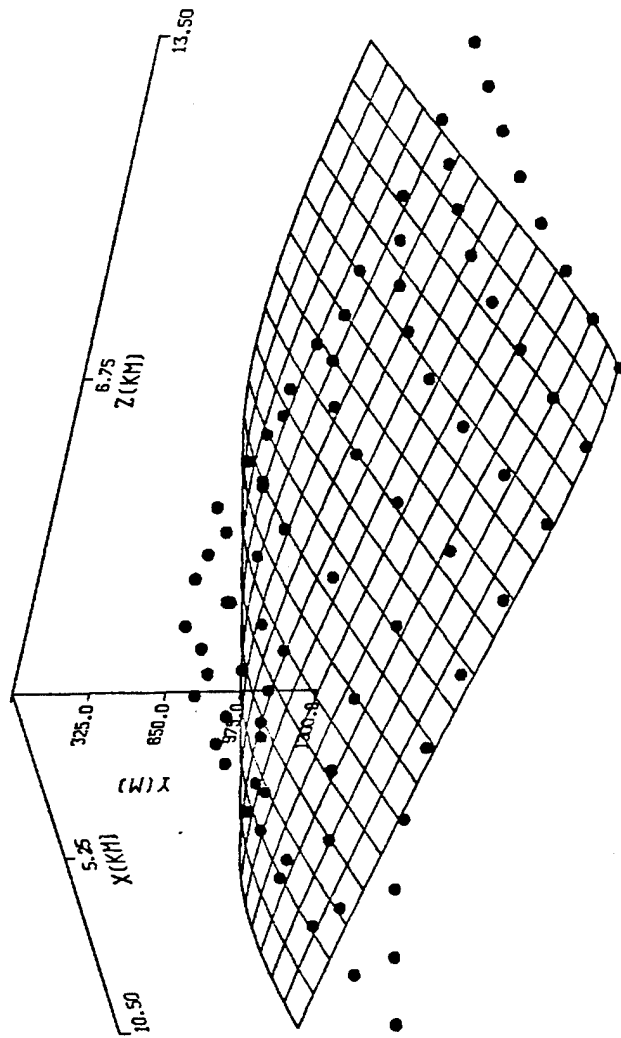
OCEAN BOTTOM BATHYMETRY



CASE: 8X10 GAUSSIAN SHAPED OCEAN BOTTOM
SIGMAYB: 0.0M 7TH-ORDER MMSE SURFACE FIT
MSE0: 5.350×10^5 MSE2: 3.442×10^5 MSE4: 3.254×10^6 MSE6: 3.243×10^6
MSE1: 4.359×10^6 MSE3: 3.255×10^5 MSE5: 3.251×10^6 MSE7: 3.243×10^6

Figure 23(a). Gaussian shaped ocean bottom with the peak of the gaussian function at $x = 5$ km, $z = 5$ km with evenly spaced data.

OCEAN BOTTOM BATHYMETRY



CASE: 8X10 GAUSSIAN SHAPED OCEAN BOTTOM
 SIGMAYB: 0.0M 7TH-ORDER MMSE SURFACE FIT
 MSE0: 5.350×10⁶ MSE2: 3.442×10⁶ MSE4: 3.254×10⁶ MSE6: 3.243×10⁶
 MSE1: 4.359×10⁶ MSE3: 3.255×10⁶ MSE5: 3.251×10⁶ MSE7: 3.243×10⁶

Figure 23(b). Gaussian shaped ocean bottom with the peak of the gaussian function at $x = 5$ km, $z = 5$ km with evenly spaced data.

With the constants set to $c_1 = 1300$, $c_2 = 10^5$, and $\sigma = 4$, Equation (2.36) becomes

$$y_b(x,z) = 1300 - 994.72e^{-\frac{[(x-5)^2+(z-5)^2]}{32}} \quad (2.37)$$

The fit produced by the orthogonal function expansion in Figures 23(a) and 23(b) smoothes through the peak of the gaussian shape and provides a poor fit to the discrete data. This shortcoming may be due to two reasons. First, if the orthogonal function expansion was computed to a higher order using $N_b > 7$, then the surface fit would more closely match the curvature of the gaussian shape of the discrete data. The maximum value of N_b is a designer's choice. The chosen value is a trade-off between exactly fitting rough or rapidly varying ocean bottoms versus smoothing through some of the roughness or rapid changes. A higher value of N_b may be more appropriate if this technique is used to model rough or rapidly varying ocean bottoms. Second, the set of generating functions used to derive the equations for the two-dimensional orthogonal function expansion was selected due to the success of the set of generating functions used in the one-dimensional orthogonal function expansion presented in [Ref. 2]. The set of generating functions used in this thesis research may not have been the best choice.

As can be seen in Figures 16 through 23, the surface fits have a constant value for the estimated ocean bottom depth across lines of contour given by

$$x + z = C, \quad (2.38)$$

where C is a positive constant. The set of generating functions, $f_n(x,z) = (x+z)^n$, for $n = 0,1,\dots,7$, result in the same estimated depth being computed for values of x and z that satisfy Equation (2.38). Therefore, the surface fits have no curvature along these contours. This effect can be seen in both Figures 21(a) and 23(a). The estimated surface fits fail to roll off in two corners, the corner given by the maximum cross-range and

minimum down-range location, and the corner given by the minimum cross-range and maximum down-range location. This shortcoming is not as noticeable in Figure 21(a) since the discrete data has much less curvature across these contours. In Figure 23(a), this shortcoming results in an unacceptable fit of the discrete bathymetric data. Correcting this shortcoming is offered as an area of future research and possible alternatives will be discussed in Chapter V.

3. Summary

The method of orthogonal function expansion to fit two-dimensional, discrete ocean bathymetric data performs well, but more research is needed to fit all arbitrarily shaped ocean bottom geometries. The orthogonal function expansion has many positive features. It needs only discrete bathymetric data that may be unevenly spaced. It is unaffected by noise in the discrete bathymetric data, and it smoothes through noisy or rapidly varying data to provide a smooth, continuous model of the ocean bottom. Chapter III will further demonstrate the utility of this method of ocean bottom modeling by using this technique in the RRA Algorithm to produce accurate three-dimensional ray traces with rays reflecting off of arbitrarily shaped two-dimensional ocean bottoms.

III. THE BATHYMETRIC MODEL APPLIED TO RAY TRACING IN THE RRA ALGORITHM

A. REFLECTION ANGLES OFF THE TWO-DIMENSIONAL OCEAN BOTTOM MODEL

In a ray acoustics ray tracing program, an important feature of a model of the ocean bathymetry is that it facilitates accurate ray reflection calculations. The ocean bottom model must provide accurate first order derivatives in order to calculate the propagation vector of a sound ray reflecting off the ocean bottom. Additionally, in order for the ray tracing program to allow for three-dimensional ray propagation, a two-dimensional ocean bottom model is needed which can be used to calculate, or accurately estimate, first order partial derivatives of the ocean bottom depth with respect to both cross-range and down-range at the point of incidence of a propagating ray. Given these partial derivatives, the reflected ray can be calculated using vector analysis.

The partial derivatives of the ocean bottom depth with respect to cross-range and down-range can be accurately estimated with a central differencing algorithm that was originally presented in [Ref. 7], and was tested for accuracy in estimating reflection angles off one-dimensional ocean bottom models in [Ref. 4]. The reflection angles calculated in [Ref. 4] were found to be accurate, and had an average percentage error of less than 0.1%. The equation for estimating the partial derivative of the ocean bottom depth with respect to down-range is given by

$$f_z = \frac{\partial y_b(x,z)}{\partial z} = \frac{-y_b(x,z+2h) + 8y_b(x,z+h) - 8y_b(x,z-h) + y_b(x,z-2h)}{12h}, \quad (3.1)$$

and the equation for estimating the partial derivative of the ocean bottom depth with

respect to cross-range is given by

$$f_x = \frac{\partial y_b(x,z)}{\partial x} = \frac{-y_b(x+2h,z) + 8y_b(x+h,z) - 8y_b(x-h,z) + y_b(x-2h,z)}{12h}, \quad (3.2)$$

where h is some arbitrarily small number, with value nominally between 0.01 and 1. For the computer simulation test cases performed in this thesis research, a value of $h = 0.1$ was used.

Although the partial derivatives with respect to cross-range and down-range could be found by algebraically differentiating the equations for the orthogonal function expansion, the central differencing algorithm has been maintained as the method for estimating the partial derivatives. This technique of estimating the partial derivatives given any mathematical model of the ocean bottom has allowed the mathematical modeling technique to be changed and improved during research without having to change the method of calculating the partial derivatives.

The problem geometry is illustrated in Figure 24. The angles of propagation shown in Figure 24(a) are taken from [Ref.1], where the direction of the unit vector along a ray path, \hat{n} , is determined by the angles ϕ and β . The angle β is measured from the positive Y axis to the unit vector, and the angle ϕ is measured from the positive X axis to the projection of the unit vector into the XZ plane. The unit vector \hat{n} can be expressed as

$$\hat{n} = u\hat{x} + v\hat{y} + w\hat{z}, \quad (3.3)$$

where

$$u = \sin\beta\cos\phi, \quad (3.4)$$

$$v = \cos\beta, \quad (3.5)$$

and

$$w = \sin \beta \sin \phi, \quad (3.6)$$

are the dimensionless direction cosines with respect to the X , Y , and Z axes.

Figures 24(b) and 24(c) illustrate a sound ray reflecting off the ocean bottom. Figure 24(b) shows the tangent plane to the ocean bottom at the point of incidence of a sound ray. The incident sound ray is denoted by the unit vector \hat{n}_i , and the reflected sound ray is denoted by the unit vector \hat{n}_r . The tangent plane is defined by the unit normal vector to the ocean bottom, denoted \hat{n}_b . Figure 24(c) presents a two-dimensional view of the three unit vectors shown in Figure 24(b).

With the partial derivatives of the ocean bottom depth with respect to cross-range and down-range at the point of incidence of a sound ray available, the normal vector to the ocean bottom, denoted \vec{N}_b , can be calculated as follows [Ref. 8]:

$$\vec{N}_b = -f_x \hat{x} + \hat{y} - f_z \hat{z}. \quad (3.7)$$

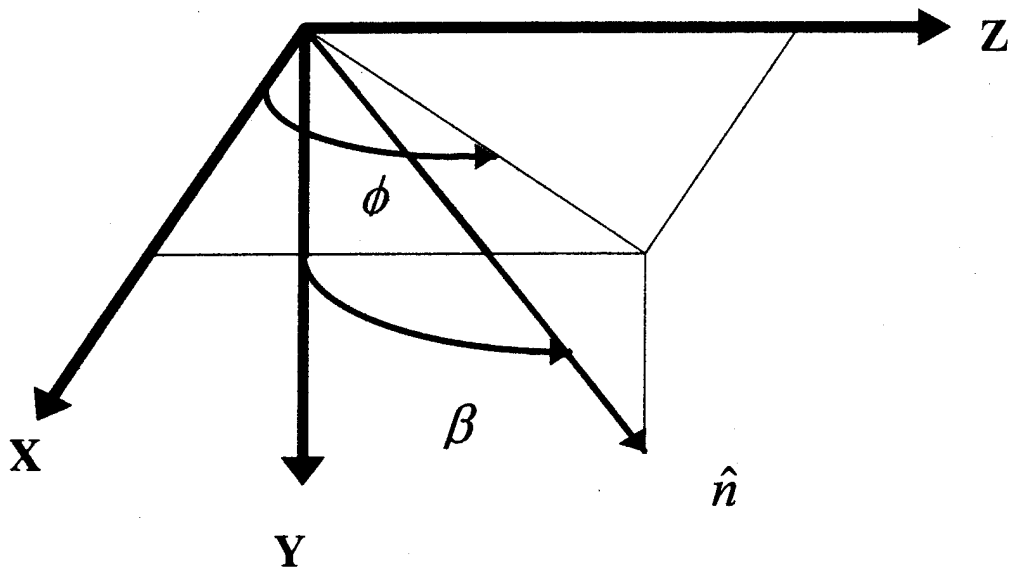
The unit normal to the ocean bottom is given by

$$\hat{n}_b = -\frac{f_x}{|\vec{N}_b|} \hat{x} + \frac{1}{|\vec{N}_b|} \hat{y} - \frac{f_z}{|\vec{N}_b|} \hat{z}, \quad (3.8)$$

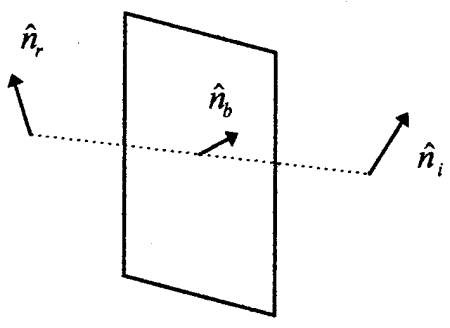
where the magnitude of the normal vector to the ocean bottom is

$$|\vec{N}_b| = \sqrt{f_x^2 + 1 + f_z^2}. \quad (3.9)$$

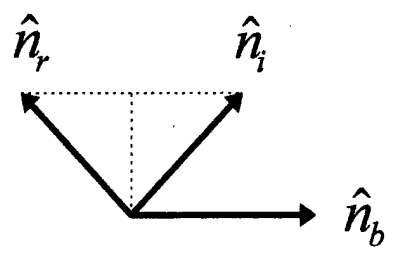
The unit vector along a sound ray at the point of incidence on the ocean bottom is denoted



(a)



(b)



(c)

Figure 24. (a) The unit vector along a ray path, (b) Three-dimensional view of a sound ray reflected off the ocean bottom in terms of the unit normal to the ocean bottom at the point of incidence, (c) Two-dimensional view of the vectors shown in (b).

by

$$\hat{n}_i = u_i \hat{x} + v_i \hat{y} + w_i \hat{z}. \quad (3.10)$$

The unit vector of the reflected ray at the point of incidence, \hat{n}_r , and the unit vector \hat{n}_i , have the same component perpendicular to the unit vector normal to the ocean bottom, \hat{n}_b , but the parallel components are opposite. To obtain \hat{n}_r from \hat{n}_i , this parallel component, denoted \vec{N}_\parallel , must be subtracted twice [Ref.6]. See Figures 24(b) and 24(c). The equation for \hat{n}_r is given by

$$\hat{n}_r = \hat{n}_i - 2\vec{N}_\parallel = \hat{n}_i - 2(\hat{n}_i \cdot \hat{n}_b)\hat{n}_b, \quad (3.11)$$

where the inner product, $(\hat{n}_i \cdot \hat{n}_b)$, is a scalar denoted $NINB$. Substituting Equations (3.8) and (3.10) into Equation (3.11) yields

$$\hat{n}_r = u_r \hat{x} + v_r \hat{y} + w_r \hat{z} = u_i \hat{x} + v_i \hat{y} + w_i \hat{z} - 2NINB \left[-\frac{f_x}{|\vec{N}_b|} \hat{x} + \frac{1}{|\vec{N}_b|} \hat{y} - \frac{f_z}{|\vec{N}_b|} \hat{z} \right], \quad (3.12)$$

where the dimensionless direction cosines associated with \hat{n}_r are

$$u_r = u_i + 2NINB \frac{f_x}{|\vec{N}_b|}, \quad (3.13)$$

$$v_r = v_i - 2NINB \frac{1}{|\vec{N}_b|}, \quad (3.14)$$

and

$$w_r = w_i + 2NINB \frac{f_z}{|\vec{N}_b|}. \quad (3.15)$$

In terms of the angles β and ϕ shown in Figure 24(a), angles of reflection are

$$\beta_r = \cos^{-1}(v_r), \quad (3.16)$$

and

$$\phi_r = \tan^{-1}\left(\frac{w_r}{u_r}\right). \quad (3.17)$$

B. COMPUTER SIMULATION RESULTS

The reflection angle algorithm presented in Section A was incorporated into the RRA Algorithm FORTRAN ray tracing program. Seven of the ocean bottom models presented in Section B of Chapter II were selected to test the accuracy of computing first order partial derivatives and reflection angles for propagating sound rays that reflect off the ocean bottom. The computer generated estimates of the partial derivatives and the reflection angles are compared with theoretical values. An isospeed ocean was assumed in each case in order to facilitate interpretation of the results.

The seven ocean bottom models employed were:

- (1) Flat ocean bottom with evenly spaced data, as presented in Figure 2
- (2) Planar ocean bottom sloping downward in the z direction only, with no variation in the x direction, using $W_x = 0$ and $W_z = 1$, with evenly spaced data, as presented in Figure 11
- (3) Planar ocean bottom sloping upward in both the x and z directions with evenly spaced data, as presented in Figure 4
- (4) Planar ocean bottom sloping upward in the z direction only, with no variation in the x direction, using $W_x = 0$ and $W_z = 1$, with evenly spaced data, as

presented in Figure 8

- (5) Planar ocean bottom sloping upward in the z direction only, with no variation in the x direction, using $W_x = 0$ and $W_z = 1$, with unevenly spaced data, as presented in Figure 9
- (6) Rolling bottom with evenly spaced data, as presented in Figure 19
- (7) Flat ocean bottom with evenly spaced data corrupted by a zero-mean random gaussian noise added to each data point, as presented in Figure 16(a)

In Figures 25 through 31, one ray is launched that propagates in the cross-range and down-range directions, with several reflections off the ocean bottom models. The ray is launched from an initial (x,y,z) coordinate of $(0,y_0,0)$, and initial launch angles β_0 and ϕ_0 . Each plot shows the propagating ray's path, a projection of the ray path onto the ocean bottom, and a projection of the ray path onto the ocean surface. Each plot contains a legend with the following information:

- (1) 'CASE:', a brief description of each test case
- (2) 'Y0:', the launch depth, y_0 , in meters
- (3) 'DLTS:', the arc length step size, Δs , in meters, used in the Recursive Ray Acoustics (RRA) algorithm
- (4) 'BETA0:', the initial launch angle, β_0 , in degrees
- (5) 'PHI0:', the initial launch angle, ϕ_0 , in degrees

For each of the seven test cases, a table of data accompanies each figure. The table compares computer simulation results and theoretical results for the bottom reflections. The theoretical values of the partial derivatives of the ocean bottom depth with respect to cross-range and down-range at the point of incidence, $\frac{\partial y_b(x,z)}{\partial x}$ and $\frac{\partial y_b(x,z)}{\partial z}$, are found by taking the partial derivatives of the exact equations that were used to generate the discrete data for each test case. The theoretical values for the angles of reflection off the ocean bottom are computed using $\frac{\partial y_b(x,z)}{\partial x}$, $\frac{\partial y_b(x,z)}{\partial z}$, and the angles of the incident

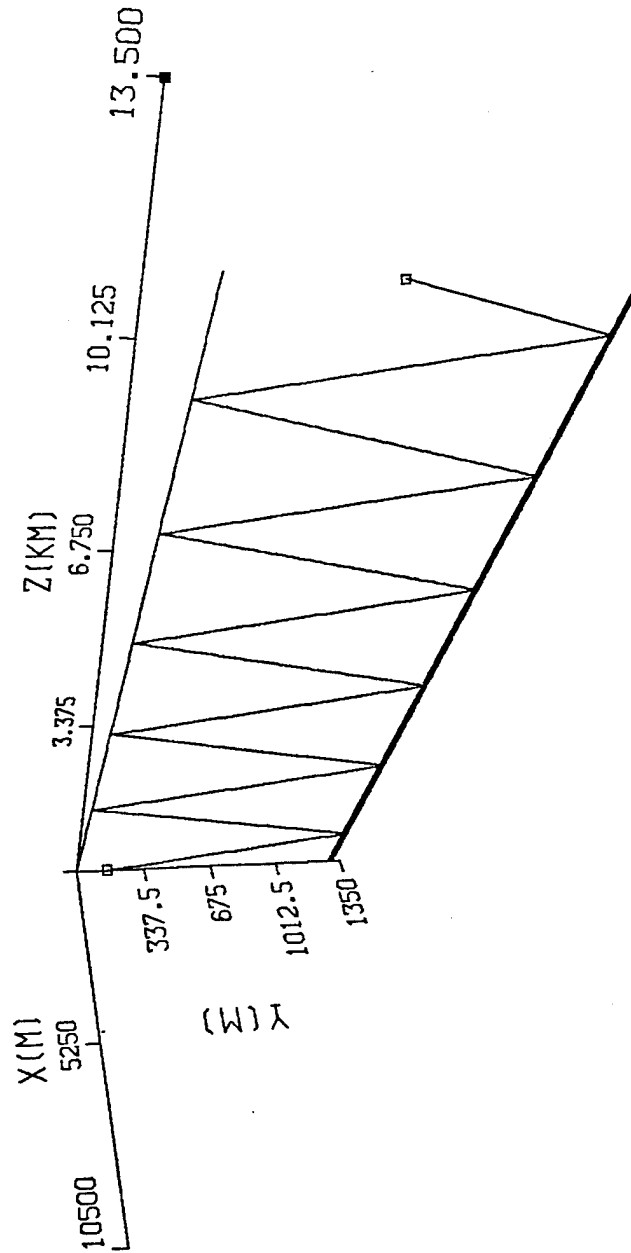
ray β_i and ϕ_i . These values are applied to Equations (3.7) to (3.17) to compute β_r and ϕ_r . The estimated partial derivatives of the ocean bottom depth with respect to cross-range and down-range at the point of incidence, $\frac{\partial y_b(x,z)}{\partial x}$ and $\frac{\partial y_b(x,z)}{\partial z}$, are computed in the RRA algorithm using the central differencing algorithm of Equations (3.1) and (3.2). The estimated angles of reflection for a ray reflected off the ocean bottom computed in the RRA algorithm are listed as $\hat{\beta}_r$ and $\hat{\phi}_r$.

Figure 25 shows a ray propagating and reflecting off the flat ocean bottom depicted in Figure 2. The exact fit of the ocean bottom model to the discrete bathymetric data results in accurate partial derivatives of the ocean bottom depth with respect to cross-range and down-range. For all six of the ocean bottom reflections shown in Figure 25, the central differencing algorithm of Equations (3.1) and (3.2) returns values of $\frac{\partial y_b(x,z)}{\partial x} = \frac{\partial y_b(x,z)}{\partial z} = -0.663172 \times 10^{-12}$ in the computer simulation. These values are a good double-precision computer approximation of the actual slope of zero, that is, $\frac{\partial y_b(x,z)}{\partial x} = \frac{\partial y_b(x,z)}{\partial z} = 0$. Table 1 shows that the computer simulation results for the angles of propagation (in degrees) of the reflected ray are extremely accurate.

BOUNCE	β_i	$\hat{\beta}_r$	% Error	ϕ_i	$\hat{\phi}_r$	% Error
1	135.000	135.000	0.00	65.000	65.000	0.00
2	135.000	135.000	0.00	65.000	65.000	0.00
3	135.000	135.000	0.00	65.000	65.000	0.00
4	135.000	135.000	0.00	65.000	65.000	0.00
5	135.000	135.000	0.00	65.000	65.000	0.00
6	135.000	135.000	0.00	65.000	65.000	0.00

Table 1. Angles of reflection off a flat ocean bottom with evenly spaced bathymetric data.

RECURSIVE RAY ACOUSTICS



CASE: 8X10 FLAT OCEAN BOTTOM
 YO: 150.0M DLTS: 4.0M
 BETAO: 45.0DEG PHIO: 65.0DEG

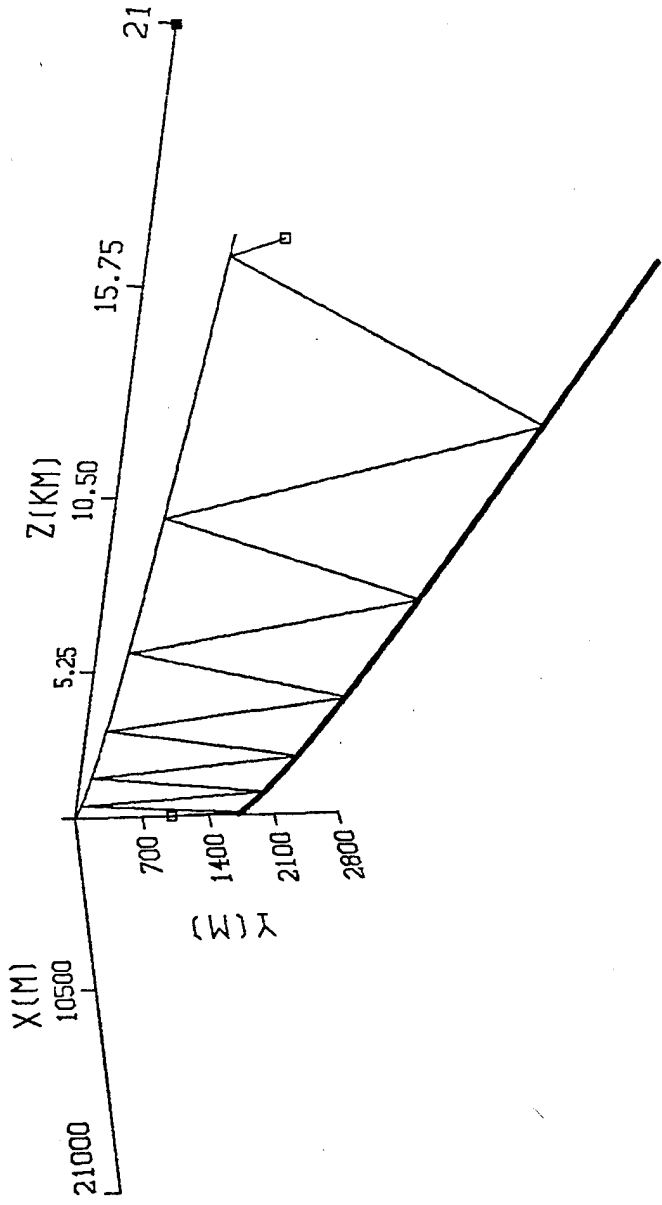
Figure 25. A sound ray propagating and reflecting off a flat ocean bottom with evenly spaced bathymetric data.

Figure 26 shows a ray propagating and reflecting off a planar ocean bottom sloping downward in the z direction only, with no variation in the x direction, as depicted in Figure 11. The value of the actual slope of the discrete bathymetric data with respect to down-range is $\frac{\partial y_b(x,z)}{\partial z} = \frac{1}{20} = 0.05$. The first order partial derivative calculated by the RRA algorithm for each bottom reflection is exactly equal to the slope of the discrete data, that is, $\frac{\partial \hat{y}_b(x,z)}{\partial z} = 0.05$. The value of the actual slope of the discrete bathymetric data with respect to cross-range is $\frac{\partial y_b(x,z)}{\partial x} = 0$. The first order partial derivative calculated by the RRA algorithm for each bottom reflection is exactly equal to the slope of the discrete data, that is, $\frac{\partial \hat{y}_b(x,z)}{\partial x} = 0$, due to the weighting term $W_x = 0$. Table 2 shows that the double-precision computer simulation results for the angles of propagation of the reflected ray are extremely accurate. Note that although the ray is launched with an initial launch angle ϕ_0 equal to 40 degrees, the ray reflections off the downward sloping plane cause the overall ray path to bend such that ϕ_r approaches 90 degrees.

BOUNCE	β_r	$\hat{\beta}_r$	% Error	ϕ_r	$\hat{\phi}_r$	% Error
1	146.062	146.062	0.00	46.681	46.681	0.00
2	141.720	141.720	0.00	51.810	51.810	0.00
3	137.097	137.097	0.00	55.761	55.761	0.00
4	132.277	132.277	0.00	58.824	58.824	0.00
5	127.316	127.316	0.00	61.210	61.210	0.00
6	122.253	122.253	0.00	63.070	63.070	0.00

Table 2. Angles of reflection off a planar ocean bottom sloping downward in the z direction only, with no variation in the x direction.

RECURSIVE RAY ACOUSTICS



CASE: 8X8 DOWN-SLOPE IN Z DIRECTION ONLY
 YO: 1000.0M DLTS: 5.0M
 BETAO: 30.0DEG PHIO: 40.0DEG

Figure 26. A sound ray propagating and reflecting off a planar ocean bottom sloping downward in the z direction, with no variation in the x direction, with evenly spaced bathymetric data.

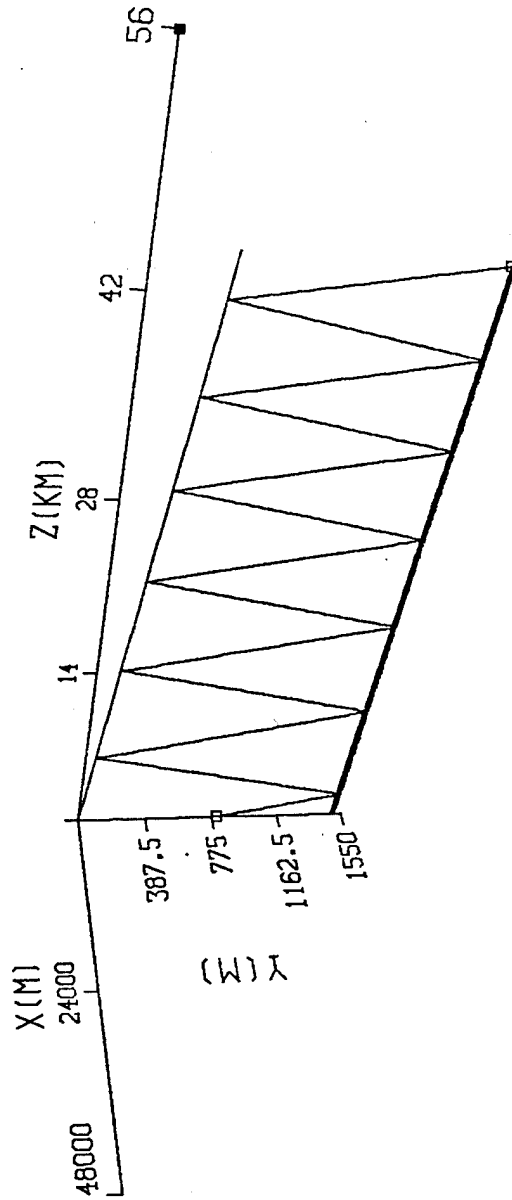
Figure 27 shows a ray propagating and reflecting off a planar ocean bottom sloping upward in both the x and z directions, as presented in Figure 4. The exact fit of the ocean bottom model to the discrete bathymetric data results in accurate partial derivatives of the ocean bottom depth with respect to cross-range and down-range. For all six of the ocean bottom reflections shown in Figure 27, the partial derivatives produced by the RRA algorithm are $\frac{\partial \hat{y}_b(x,z)}{\partial x} = \frac{\partial \hat{y}_b(x,z)}{\partial z} = -0.00625$, which are exactly equal to the partial derivatives of the discrete bathymetric data. Table 3 shows that the angles of propagation of the reflected rays produced by the RRA algorithm are equal to their theoretical values.

BOUNCE	β_i	$\hat{\beta}_i$	% Error	ϕ_i	$\hat{\phi}_i$	% Error
1	100.978	100.978	0.00	60.049	60.049	0.00
2	101.956	101.956	0.00	60.102	60.102	0.00
3	102.934	102.934	0.00	60.160	60.160	0.00
4	103.911	103.911	0.00	60.224	60.224	0.00
5	104.888	104.888	0.00	60.292	60.292	0.00
6	105.865	105.865	0.00	60.366	60.366	0.00

Table 3. Angles of reflection off a planar ocean bottom sloping upward in both the x and z directions.

Figure 28 shows a ray propagating and reflecting off a shoaling ocean bottom as depicted in Figure 8. The first order partial derivative of the ocean bottom depth with respect to down-range calculated by the RRA algorithm for each bottom reflection in double precision accuracy is $\frac{\partial \hat{y}_b(x,z)}{\partial z} = -0.166667$, which is equal to the exact slope of the discrete data, that is, $\frac{\partial y_b(x,z)}{\partial z} = -\frac{1}{6}$. Table 4 shows that the double-precision

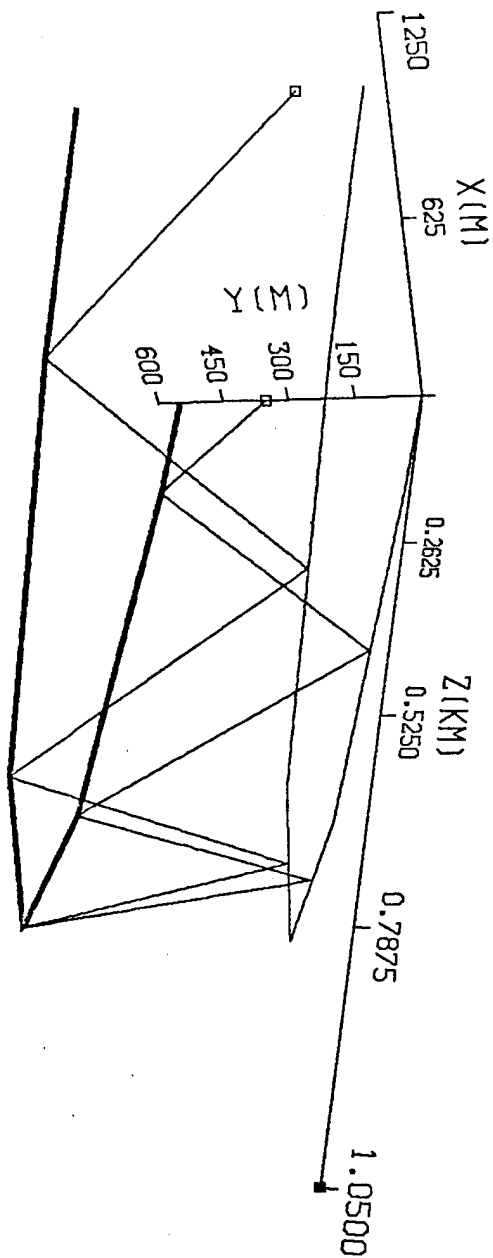
RECURSIVE RAY ACOUSTICS



CASE: 7X8 UP-SLOPE IN BOTH X AND Z DIRECTIONS
 YO: 800.0M DLTS: 10.0M
 BETA0: 80.0DEG PHIO: 60.0DEG

Figure 27. A sound ray propagating and reflecting off a planar ocean bottom sloping upward in both the x and z directions, with evenly spaced bathymetric data.

RECURSIVE RAY ACOUSTICS



CASE: 6X8 UP-SLOPE IN Z DIRECTION ONLY, WITH WEIGHTING
Y0: 350.0M DLTS: 1.0M
BETA0: 52.5DEG PHIO: 70.0DEG

Figure 28. A sound ray propagating and reflecting off a planar ocean bottom sloping upward in the z direction, with no variation in the x direction, with evenly spaced bathymetric data.

computer simulation results for the angles of propagation of the reflected ray are extremely accurate.

BOUNCE	β_i	$\hat{\beta}_i$	% Error	ϕ_i	$\hat{\phi}_i$	% Error
1	144.849	144.849	0.00	61.881	61.881	0.00
2	159.740	159.740	0.00	38.411	38.411	0.00
3	163.176	163.176	0.00	-20.368	-20.368	0.00
4	150.783	150.783	0.00	-56.227	-56.227	0.00
5	133.949	133.949	0.00	-67.859	-67.859	0.00

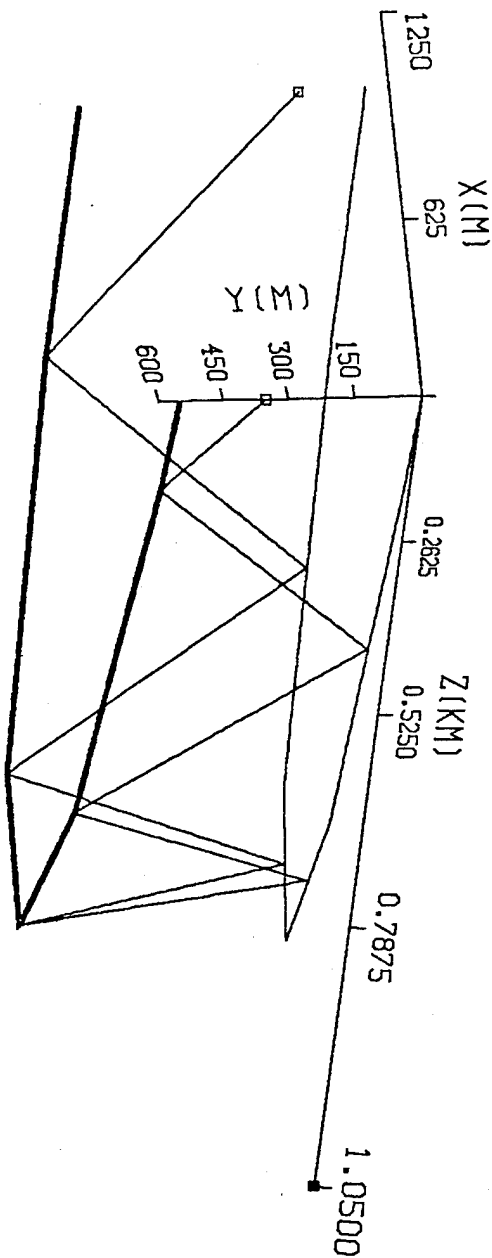
Table 4. Angles of reflection off a planar ocean bottom sloping upward in the z direction only, with no variation in the x direction, with evenly spaced bathymetric data.

Figure 29 shows a ray propagating and reflecting off a shoaling ocean bottom with the discrete bathymetric data entered at unevenly spaced intervals as depicted in Figure 9. Table 5 shows that small errors are introduced by rounding off the input bathymetric data to five significant digits. The ocean bottom surface fit produced for the test case shown in Figures 9 and 29 is 7th-order and not 1st-order due to the round off error introduced in the discrete bathymetric data. Overall, the effect on ray propagation is small. After propagating the sound ray for a path length of over 4 kilometers, the

BOUNCE	β_i	$\hat{\beta}_i$	% Error	ϕ_i	$\hat{\phi}_i$	% Error
1	144.849	144.855	0.004	61.881	61.877	0.006
2	159.740	159.730	0.006	38.411	38.442	0.081
3	163.176	163.187	0.007	-20.368	-20.270	0.481
4	150.783	150.858	0.050	-56.227	-56.137	0.160
5	133.949	134.026	0.057	-67.859	-67.829	0.044

Table 5. Angles of reflection off a planar ocean bottom sloping upward in the z direction only, with no variation in the x direction, with unevenly spaced bathymetric data.

RECURSIVE RAY ACOUSTICS



CASE: 6X8 UP-SLOPE IN Z ONLY, WITH UNEVENLY SPACED DATA
Y0: 350.0M DLTS: 1.0M
BETA0: 52.5DEG PHIO: 70.0DEG

Figure 29. A sound ray propagating and reflecting off a planar ocean bottom sloping upward in the z direction, with no variation in the x direction, with unevenly spaced bathymetric data.

coordinate (x,y,z) of the point of incidence of the fifth bounce in Figure 29 has been displaced 2.449 meters as compared to the coordinate (x,y,z) of the point of incidence of the fifth bounce of the sound ray propagated in Figure 28. Table 6 shows the theoretical partial derivatives of the ocean bottom depth with respect to down-range and cross-range, and the estimated partial derivatives computed using the central differencing algorithm at each bottom reflection location.

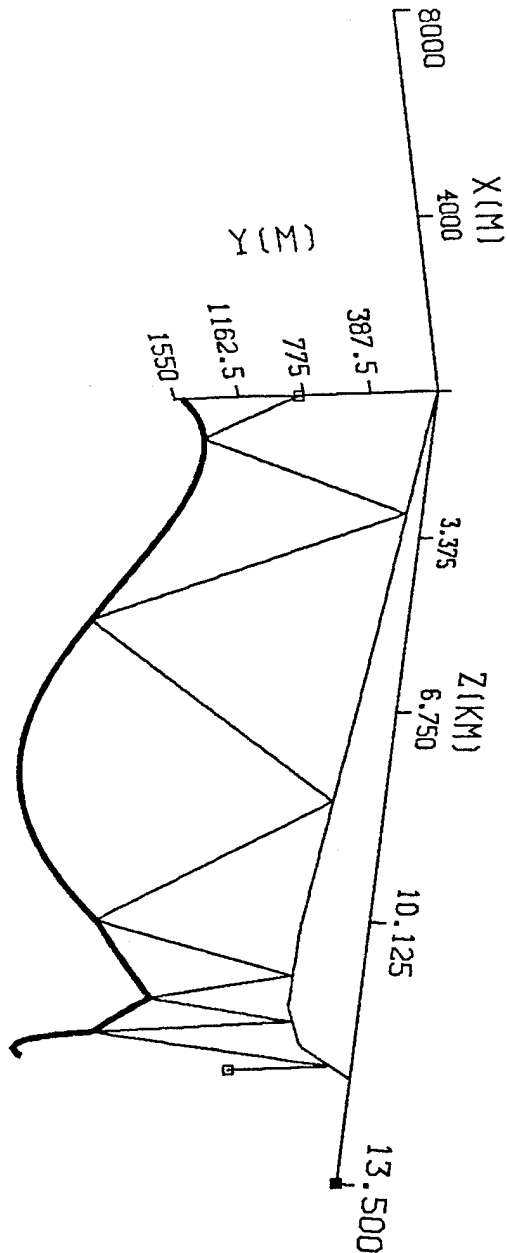
BOUNCE	$\frac{\partial b(x,z)}{\partial z}$	$\frac{\partial b(x,z)}{\partial z}$	% Error
1	-0.16666667	-0.16672578	0.035
2	-0.16666667	-0.16647425	0.115
3	-0.16666667	-0.16651536	0.091
4	-0.16666667	-0.16614634	0.312
5	-0.16666667	-0.16672751	0.037

Table 6. Partial derivative of ocean bottom depth with respect to down range for reflections off a planar ocean bottom sloping upward in the z direction only, with no variation in the x direction, with unevenly spaced bathymetric data.

Figure 30 shows a ray propagating and reflecting off a rolling or oscillating bottom with evenly spaced bathymetric data, as presented in Figure 19. Although the ocean bottom surface fit is 7^{th} -order, the ocean bottom model closely approximates the discrete bathymetric data generated by Equation (2.32), which is 3^{rd} -order. Table 7 shows that the reflection angles produced by the RRA algorithm are accurate estimates of the theoretical values. Table 8 compares the estimated partial derivatives produced by the RRA algorithm and the partial derivatives obtained by differentiating Equation (2.32).

The test cases shown in Figures 28 and 30 are good examples of the insight into ray propagation provided by using a two-dimensional ocean bottom model in the RRA ray tracing program. Reflections that turn the ray causing a cross-range displacement can be easily computed and plotted. It is important to note that the modeling of ray

RECURSIVE RAY ACOUSTICS



CASE: SX6 OSCILLATING OCEAN BOTTOM
 YO: 800.0M DLTS: 4.0M
 BETAO: 75.0DEG PHIO: 70.0DEG

Figure 30. A sound ray propagating and reflecting off a rolling or oscillating ocean bottom with evenly spaced bathymetric data.

BOUNCE	β_i	$\hat{\beta}_i$	% Error	ϕ_i	$\hat{\phi}_i$	% Error
1	115.278	115.278	0.000	71.836	71.836	0.000
2	108.991	108.991	0.000	70.577	70.577	0.000
3	145.242	145.255	0.009	90.770	90.747	0.025
4	145.067	145.106	0.027	179.529	179.473	0.031
5	108.882	108.889	0.007	-160.551	-160.560	0.005

Table 7. Angles of reflection off a rolling ocean bottom with unevenly spaced bathymetric data.

BOUNCE	$\frac{\partial b(x,z)}{\partial x}$	$\hat{\frac{\partial b(x,z)}{\partial x}}$	% Error	$\frac{\partial b(x,z)}{\partial z}$	$\hat{\frac{\partial b(x,z)}{\partial z}}$	% Error
1	-0.07069	-0.07069	0.001	-0.07069	-0.07069	0.001
2	0.04327	0.04327	0.000	0.04327	0.04327	0.000
3	-0.28082	-0.28059	0.082	-0.28082	-0.28059	0.082
4	-0.34430	-0.34388	0.345	-0.34430	-0.34388	0.345
5	-0.28010	-0.27988	0.079	-0.28010	-0.27988	0.079

Table 8. Partial derivatives of ocean bottom depth with respect to cross range and down range for reflections off a rolling ocean bottom with unevenly spaced bathymetric data.

propagation is intended to be an exact representation of ray propagation in the ocean. However, the implementation of mathematical algorithms in a computer simulation requires approximations to be made. The effort is to model the ocean as accurately as possible in order to simulate the ocean. The algorithms used in a computer model designed for real-time ray tracing must be accurate and as fast and as simple as possible to provide fast calculations. The two-dimensional ocean bottom model produced by the orthogonal function expansion provides these features.

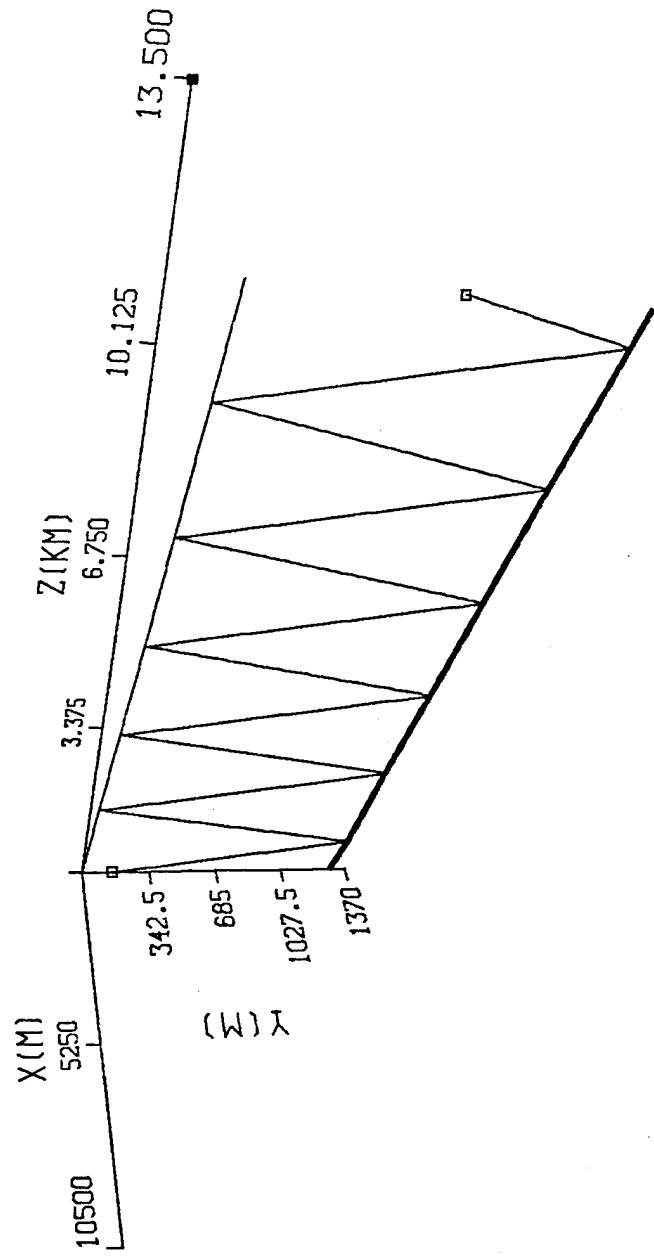
Finally, Figure 31 demonstrates the ability of the orthogonal function expansion to smooth through ocean bottom roughness or noisy input bathymetric data. Figure 31 shows a ray propagating and reflecting off a flat ocean bottom with a zero-mean random gaussian noise added to the discrete bathymetric data as depicted in Figure 16. With a standard deviation of the noise at 1% of the ocean bottom depth, the ocean bottom model provides a smooth fit through the noise. The data in Table 9 is provided only to illustrate the smoothing effect of the orthogonal function expansion, and not to validate the reflection angle calculations. Table 9 presents data that compares the theoretical angles of reflection of the propagating ray reflecting off the ocean bottom for the case presented in Figure 25 (no noise) versus the estimated angles of reflection produced by the smooth fit in Figure 31 (with noise). Table 9 reports the discrepancies as a ‘% difference’ since

BOUNCE	β_r Fig. 25	$\hat{\beta}_r$ Fig. 31	% Difference	ϕ_r Fig. 25	$\hat{\phi}_r$ Fig. 31	% Difference
1	135.000	134.568	0.32	65.000	64.845	0.24
2	135.000	134.786	0.16	65.000	64.922	0.12
3	135.000	134.790	0.16	65.000	64.924	0.12
4	135.000	134.854	0.11	65.000	64.947	0.08
5	135.000	134.550	0.33	65.000	64.838	0.25
6	135.000	134.295	0.52	65.000	64.748	0.39

Table 9. Angles of reflection off a flat ocean bottom with rough or noisy bathymetric data (Fig.25) versus a flat ocean bottom with no irregularities (Fig.31).

the difference is due to ocean bottom roughness or noisy data. The average ‘% difference’ between β_r and $\hat{\beta}_r$ is 0.27%, and the average ‘% difference’ between ϕ_r and $\hat{\phi}_r$ is 0.20%. The error produced by successive reflections is cumulative. After propagating the ray over 14 kilometers, the largest difference introduced by the ocean

RECURSIVE RAY ACOUSTICS



CASE: 8X10 FLAT OCEAN BOTTOM WITH NOISE
 Y0: 150.0M DLTS: 4.0M
 BETAO: 45.0DEG PHIO: 65.0DEG

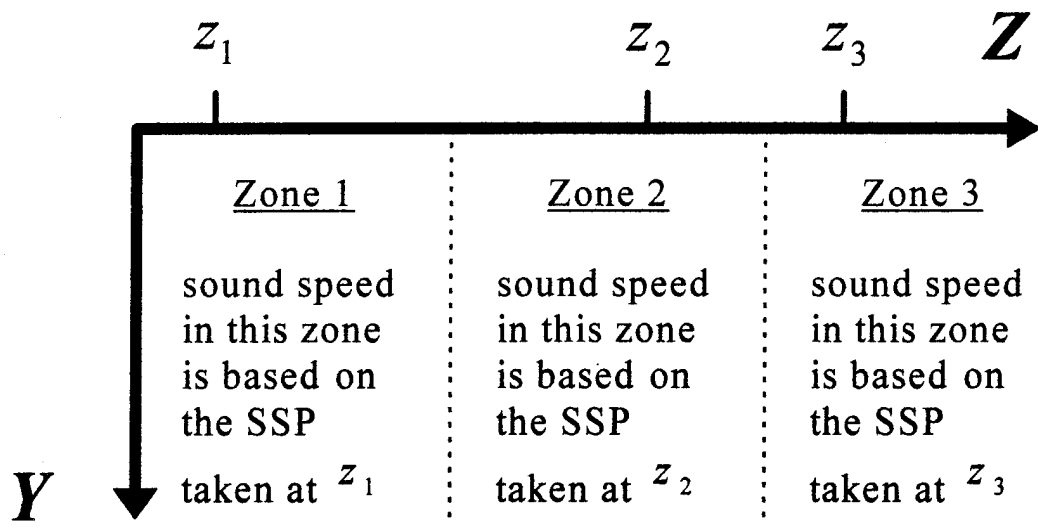
Figure 31. A sound ray propagating and reflecting off a flat ocean bottom with evenly spaced bathymetric data corrupted by a zero-mean random gaussian noise added to the depth of each data point.

bottom roughness or noise is a 0.52% difference for the angle of reflection, $\hat{\beta}_r$, off the rough ocean bottom of Figure 31 as compared to the flat ocean bottom of Figure 25. The roughness or noise is effectively smoothed by the orthogonal function expansion.

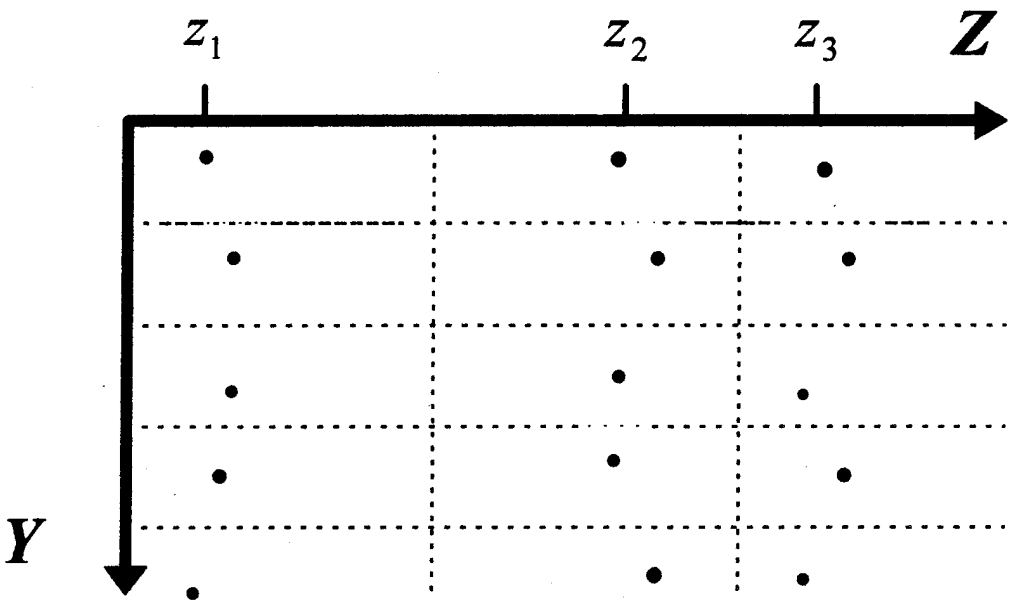
IV. TWO-DIMENSIONAL ORTHOGONAL FUNCTION EXPANSIONS OF SOUND-SPEED DATA

A. ORTHOGONAL FUNCTION EXPANSION AND THE BASIS FUNCTIONS

Sound speed data in the ocean is typically measured as a function of depth at a particular geographic location. In terms of the Cartesian coordinate system presented in Chapters II and III, sound speed is typically measured at a fixed cross-range and down-range location (x,z) , and the sound speed is a function of depth (y) only. This type of sound-speed measurement is called a sound-speed profile (SSP). The sound-speed measurements used in this research as test cases are discrete, and the discrete measurements may be taken at unevenly spaced depths. The one-dimensional orthogonal function expansion discussed in [Ref. 2] was demonstrated to be an effective method to model sound speed when it is a function of one variable, that is, depth. For a ray propagated down-range using the RRA algorithm, the sound-speed model developed with the one-dimensional orthogonal function expansion does not vary as a function of down-range. The one-dimensional orthogonal function expansion models sound speed as a function of depth only. Multiple sound-speed profiles can be used to model the speed of sound as a function of depth in areas (or zones) of the ocean. As the sound ray passes from one zone to another zone, the orthogonal function expansion of the next set of discrete sound-speed profile data is computed. The technique of zones is presented in [Ref. 2], and is illustrated in Figure 32(a). A technique is needed that will use multiple sound-speed profiles taken at different down-range locations to compute the speed of sound as a function of both depth and down-range. The two-dimensional orthogonal function expansion technique can be used to compute sound speed as a function of both depth and down-range given a rectangular matrix of discrete sound-speed data. The rectangular matrix of data is made up of multiple discrete sound-speed profiles taken at different down-range locations. The rectangular matrix of discrete sound-speed data is illustrated in Figure 32(b).



(a)



(b)

Figure 32. (a) Speed of sound as a function of depth (y) only, employed in areas (zones) of the ocean. (b) Rectangular matrix of discrete sound-speed data from multiple sound-speed profiles.

1. Definition of the Two-Dimensional Orthogonal Function Expansion

The technique being employed in this chapter to model sound speed as a function of depth and down-range is the same mathematical technique that was presented in Chapter II to model ocean bathymetry as a function of cross-range and down-range. The two-dimensional orthogonal function expansion used to fit a smooth surface to a rectangular matrix of sound-speed data as a function of depth and down-range is given by

$$\hat{c}(y,z) = \sum_{n=0}^{N_c} c_n \varphi_{c_n}(y,z), \quad (4.1)$$

where the coefficient

$$\begin{aligned} c_n &= \left\langle c_m(y_{ij}, z_{ij}), \varphi_{c_n}(y_{ij}, z_{ij}) \right\rangle, \\ &= \sum_{i=1}^{M_{c_y}} \sum_{j=1}^{M_{c_x}} c_m(y_{ij}, z_{ij}) \varphi_{c_n}^*(y_{ij}, z_{ij}), \quad n = 0, 1, \dots, N_c, \end{aligned} \quad (4.2)$$

represents the inner product of the measured discrete sound-speed data $c_m(y_{ij}, z_{ij})$, for $i = 1, 2, \dots, M_{c_y}$ and $j = 1, 2, \dots, M_{c_x}$, with the set of orthonormal basis functions $\varphi_{c_n}(y, z)$, $n = 0, 1, \dots, N_c$, evaluated at the discrete depth (y_{ij}) and down-range (z_{ij}) values corresponding to the discrete sound-speed data. The order of the expansion is represented by N_c . The discrete data must be entered in a matrix, where M_{c_y} is the total number of depth rows and M_{c_x} is the total number of down-range columns. The matrix is, in general, rectangular, not square, and the data is, in general, *unevenly spaced* in both the y and z directions.

2. The Basis Functions from the Generating Functions

As in Chapter II, the set of orthonormal basis functions $\varphi_{c_n}(y, z)$, $n = 0, 1, \dots, N_c$, were determined by using the Gram-Schmidt procedure [Ref. 3] on the set of generating

functions $f_n(y,z) = (y+z)^n$, $n = 0,1,\dots,N_c$. The generating function chosen is of the same form as in Chapter II. The general equation of the *Gram-Schmidt Orthogonalization Procedure* is given by

$$\begin{aligned} \varphi_{c_n}(y,z) = f_n(y,z) - \frac{\langle f_n(y,z), \varphi_{c_0}(y,z) \rangle}{\langle \varphi_{c_0}(y,z), \varphi_{c_0}(y,z) \rangle} \varphi_{c_0}(y,z) - \dots \\ \dots - \frac{\langle f_n(y,z), \varphi_{c_{n-1}}(y,z) \rangle}{\langle \varphi_{c_{n-1}}(y,z), \varphi_{c_{n-1}}(y,z) \rangle} \varphi_{c_{n-1}}(y,z), \quad n = 0,1,2,\dots \end{aligned} \quad (4.3)$$

The Gram-Schmidt procedure to find the basis functions, φ_{c_n} , for $n = 0,1,\dots,N_c$, is the same as the procedure detailed in Section A of Chapter II, and it will not be repeated here. As a means of comparison to the derivation shown in Chapter II, the final equations for the first three basis functions are listed below:

The *0th*-order basis function is given by

$$\varphi_{c_0}(y,z) = 1 . \quad (4.4)$$

The *1st*-order basis function is given by

$$\varphi_{c_1}(y,z) = y + z - W_{10} . \quad (4.5)$$

The *2nd*-order basis function is given by

$$\varphi_{c_2}(y,z) = (y+z)^2 - W_{20} - W_{21}[y+z - W_{10}] . \quad (4.6)$$

The use of the two-dimensional orthogonal function expansion to model sound speed as a function of depth and down-range gives similar results as the model of

bathymetric data presented in Chapter II. The data may be unevenly spaced. As in Chapter II, where $N_b = 7$ is the maximum order fit, the maximum order sound-speed fit is $N_c = 7$. Noise in the input discrete sound-speed data does not affect the overall fit. Also, the mean-squared error (*MSE*) is computed for $N_c = 0, 1, \dots, 7$. The value of N_c that produces the lowest mean-squared error is used to reconstruct the sound-speed data.

B. COMPUTER SIMULATION RESULTS OF SOUND-SPEED FITS

The two-dimensional orthogonal function expansion technique to model sound-speed data was implemented in the RRA Algorithm FORTRAN ray tracing program. The results of various test cases are presented graphically to demonstrate both the successes and the shortcomings of this method of modeling discrete sound-speed data. The discrete sound-speed data is made up from three sound-speed profiles (sound-speed versus depth) taken at three different down-range locations. The graphs, presented in Figures 33 to 41, show the discrete sound-speed data points as large black dots (\bullet). The estimated fit to the discrete data computed by the orthogonal function expansion is presented as a mesh of lines to represent the two-dimensional, continuous surface.

The technique of using a two-dimensional orthogonal function expansion to provide a continuous surface fit to discrete data is the same technique that was tested in Chapter II. The general conclusions and shortcomings presented in Chapter II apply in this chapter. Even with the shortcomings discussed in Chapter II, the testing of this technique to fit sound-speed data will validate the FORTRAN subroutines that compute the two-dimensional orthogonal function expansion of sound-speed data in the RRA algorithm computer program. The test cases will also provide specific conclusions and shortcomings of this technique when it is applied to fit discrete sound-speed data.

Each plot contains a legend with the following information:

- (1) 'CASE:', a description of the test case
- (2) 'SIGMAC:', the value of the standard deviation, σ_c , of a randomly

- generated zero-mean gaussian noise added to each sound-speed data point
- (3) the order of the fit, N_c , based on the minimum mean-squared error criterion
 - (4) 'MSE0:' to 'MSE7:', the mean-squared error for $N_c = 0,1,2,\dots,7$

Figures 33 and 34 demonstrate the fit of the most basic test case, a constant speed of sound. The exact equation used to generate the 6×3 rectangular matrix of data for Figures 33 and 34 is given by

$$c(y,z) = 1500. \quad (4.7)$$

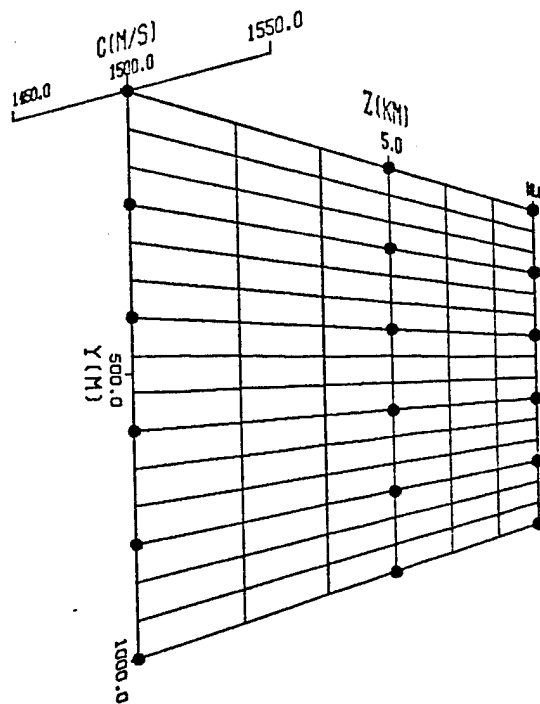
In both test cases, the fit is an exact $0th$ -order fit with the orthogonal function expansion returning a value of 1500 m/s for any combination of depth and down-range. Figure 34 shows that the data may be entered at unevenly spaced coordinates without affecting the fit.

Figures 35, 36, and 37 demonstrate exact $1st$ -order fits. The exact equation used to generate the 6×3 rectangular matrices of data for Figures 35, 36, and 37 is given by

$$c(y,z) = 1490 + 0.02y, \quad (4.8)$$

which represents sound speed that is linearly increasing as a function of depth. Figure 35 reveals the same shortcoming that was found with the $1st$ -order bathymetric fits presented in Chapter II. The corner of the surface fit at the maximum depth and minimum down-range location ($y = 1000$ m, $z = 0.0$ km) is below the discrete sound-speed data points; the corner of the surface fit at the minimum depth and maximum down-range location ($y = 0.0$ m, $z = 1.0$ km) is above the discrete sound-speed data points. The fitted surface approximates a $1st$ -order planar surface that slopes upward equally in both the y and z directions. Therefore, the fitted plane is below half of the discrete sound-speed data

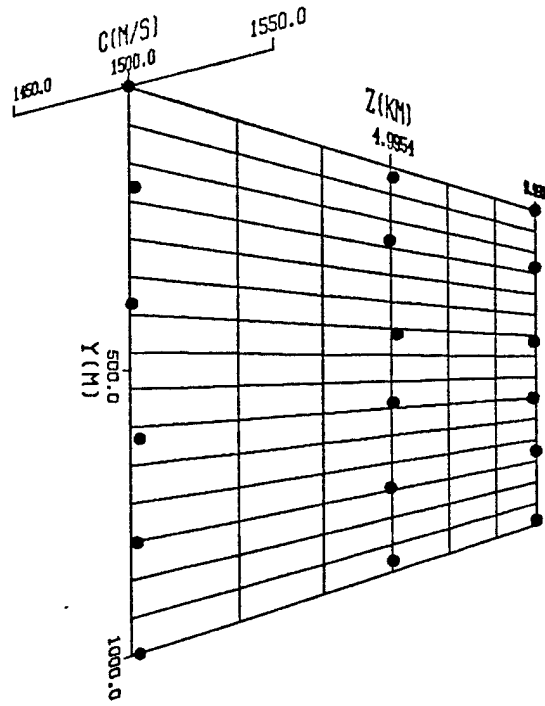
SOUND SPEED



CASE: CONSTANT SOUND SPEED WITH EVENLY SPACED DATA
SIGMAC: 0.0M 0TH-ORDER MMSE SURFACE FIT
MSE0: 4.098×10^{-8} MSE2: 4.098×10^{-8} MSE4: 4.098×10^{-8} MSE6: 4.098×10^{-8}
MSE1: 4.098×10^{-8} MSE3: 4.098×10^{-8} MSE5: 4.098×10^{-8} MSE7: 4.098×10^{-8}

Figure 33. Constant sound-speed with evenly spaced data.

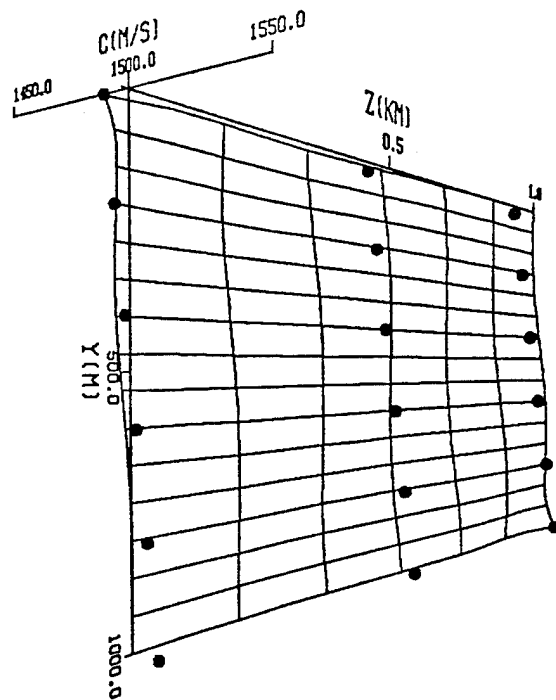
SOUND SPEED



CASE: CONSTANT SOUND SPEED WITH UNEVENLY SPACED DATA
SIGMAC: 0.0M OTH-ORDER MMSE SURFACE FIT
MSE0: 4.098×10^{-8} MSE2: 4.098×10^{-8} MSE4: 4.098×10^{-8} MSE6: 4.098×10^{-8}
MSE1: 4.098×10^{-8} MSE3: 4.098×10^{-8} MSE5: 4.098×10^{-8} MSE7: 4.098×10^{-8}

Figure 34. Constant sound-speed with unevenly spaced data.

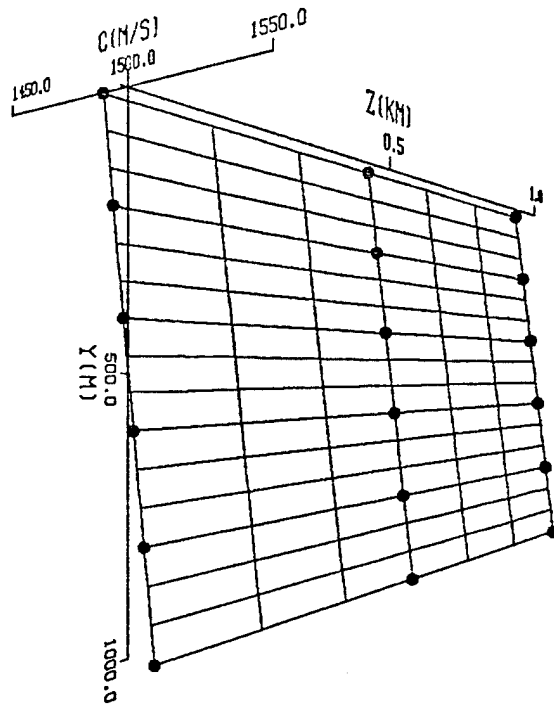
SOUND SPEED



CASE: SS LINEARLY INCREASING, EVENLY SPACED DATA NO WT
 SIGMAC: 0.0M 7TH-ORDER MMSE SURFACE FIT
 MSE0: 8.400×10^2 MSE2: 4.941×10^2 MSE4: 4.827×10^2 MSE6: 4.825×10^2
 MSE1: 4.941×10^2 MSE3: 4.827×10^2 MSE5: 4.825×10^2 MSE7: 4.663×10^2

Figure 35. Sound-speed that is linearly increasing as a function of depth,
 with no variation in the down-range direction, modeled without
 weighting x and z separately, with evenly spaced data.

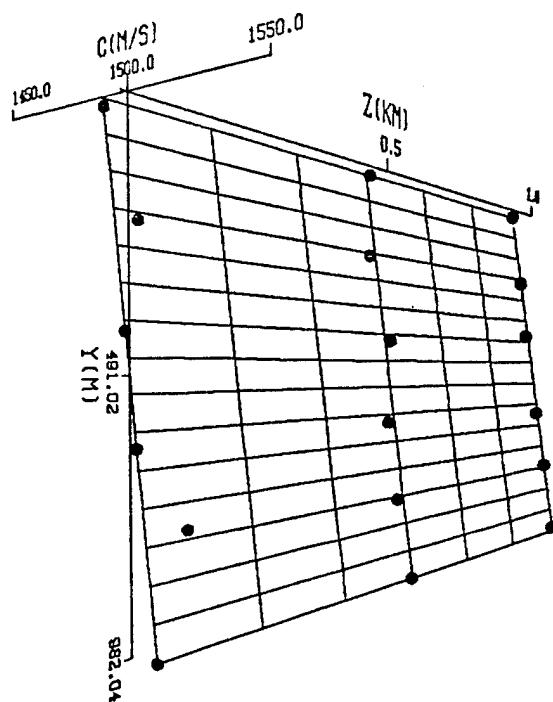
SOUND SPEED



CASE: SS LINEARLY INCREASING, EVENLY SPACED DATA WITH WT
 SIGMAC: 0.0M 1ST-ORDER MMSE SURFACE FIT
 MSE0: 8.400×10^2 MSE2: 5.215×10^{-8} MSE4: 5.215×10^{-8} MSE6: 5.215×10^{-8}
 MSE1: 5.215×10^{-8} MSE3: 5.215×10^{-8} MSE5: 5.215×10^{-8} MSE7: 5.215×10^{-8}

Figure 36. Sound-speed that is linearly increasing as a function of depth,
 with no variation in the down-range direction, using $W_y = 1$ and $W_z = 0$,
 with evenly spaced data.

SOUND SPEED



CASE: SS LINEARLY INCREASING, WITH UNEVENLY SPACED DATA
 SIGMAC: 0.0M 7TH-ORDER MMSE SURFACE FIT
 MSE0: 7.895×10^2 MSE2: 1.321×10^{-2} MSE4: 1.311×10^{-2} MSE6: 1.275×10^{-2}
 MSE1: 1.370×10^{-2} MSE3: 1.317×10^{-2} MSE5: 1.290×10^{-2} MSE7: 1.157×10^{-2}

Figure 37. Sound-speed that is linearly increasing as a function of depth,
 with no variation in the down-range direction, using $W_y = 1$ and $W_z = 0$,
 with unevenly spaced data.

points in the lower half of Figure 35, and above half of the discrete sound-speed data points in the upper half of Figure 35. The best fit is limited in its accuracy due to the fact that y and z are summed in every term of the orthogonal function expansion. As in Chapter II, an independent weighting with respect to y and an independent weighting with respect to z need to be added to the orthogonal function expansion to correct this shortcoming. With the addition of weighting factors, the orthogonal function expansion becomes

$$\hat{c}(y,z) = \sum_{n=0}^{N_c} c_n \varphi_n(W_y y, W_z z), \quad (4.9)$$

where W_y and W_z are weighting factors to introduce independence in y and z .

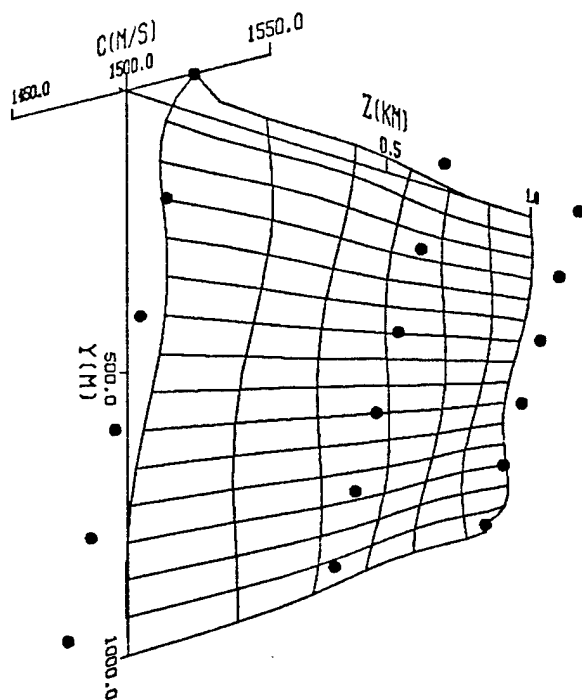
Figure 36 presents the same test case presented in Figure 35, except that the weighting factors, W_y and W_z , were added as shown in Equation (4.9) with $W_y = 1$ and $W_z = 0$. The result is an exact *1st*-order fit. Figure 37 presents the same test case with the discrete sound-speed data entered at unevenly spaced locations. The fit determined by the orthogonal function expansion is *7th*-order due to using only five significant digits for the discrete sound-speed data. The overall fit is *1st*-order; the higher order terms of the orthogonal function expansion only affect the lower significant digits of the estimated value of sound speed.

Figures 38, 39, and 40 present a test case with discrete sound-speed data generated by the exact equation given by

$$c(y,z) = 1525 - 0.05y, \quad (4.10)$$

which represents sound-speed that is linearly decreasing as a function of depth. In Figure 38, no weighting is applied, and the orthogonal function expansion produces a poor fit. In Figures 39 and 40, the weighting factors, W_y and W_z , were added as shown in

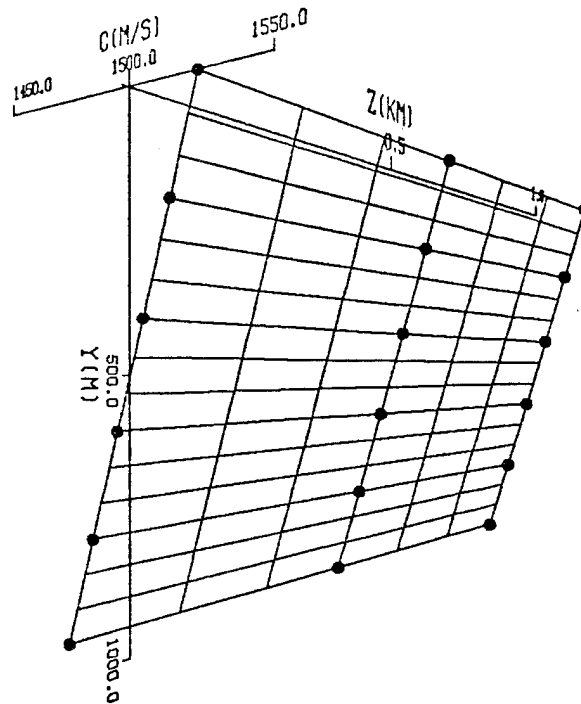
SOUND SPEED



CASE: SS LINEARLY DECREASING, EVENLY SPACED DATA NO WT
SIGMAC: 0.0M 7TH-ORDER MMSE SURFACE FIT
MSE0: 5.250×10^3 MSE2: 3.088×10^3 MSE4: 3.017×10^3 MSE6: 3.016×10^3
MSE1: 3.088×10^3 MSE3: 3.017×10^3 MSE5: 3.016×10^3 MSE7: 2.914×10^3

Figure 38. Sound-speed that is linearly decreasing as a function of depth, with no variation in the down-range direction, modeled without weighting x and z separately, with evenly spaced data.

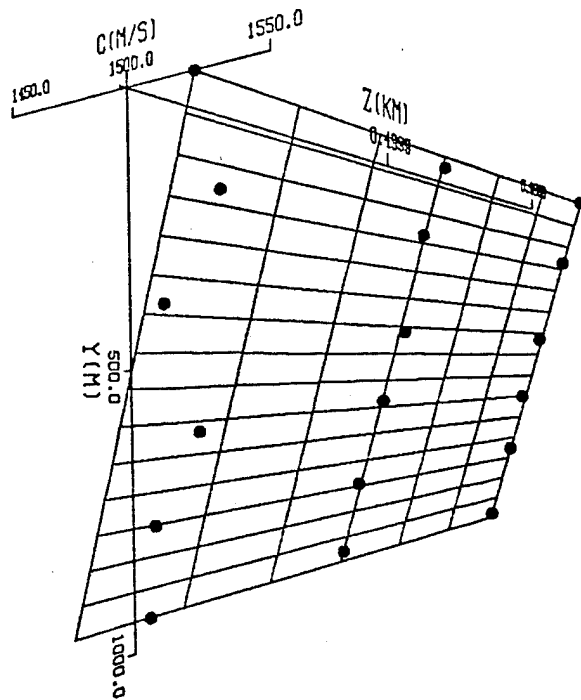
SOUND SPEED



CASE: SS LINEARLY DECREASING, EVENLY SPACED DATA WITH WT
SIGMAC: 0.0M 1ST-ORDER MMSE SURFACE FIT
MSE0: 5.250×10^3 MSE2: 7.078×10^{-8} MSE4: 7.078×10^{-8} MSE6: 7.078×10^{-8}
MSE1: 7.078×10^{-8} MSE3: 7.078×10^{-8} MSE5: 7.078×10^{-8} MSE7: 7.078×10^{-8}

Figure 39. Sound-speed that is linearly decreasing as a function of depth,
with no variation in the down-range direction, using $W_y = 1$ and $W_z = 0$,
with evenly spaced data.

SOUND SPEED



CASE: SS LINEARLY DECREASING, WITH UNEVENLY SPACED DATA
 SIGMAC: 0.0M 7TH-ORDER MMSE SURFACE FIT
 MSE0: 5.120×10^{-3} MSE2: 7.723×10^{-3} MSE4: 6.346×10^{-3} MSE6: 6.023×10^{-3}
 MSE1: 8.196×10^{-3} MSE3: 7.668×10^{-3} MSE5: 6.024×10^{-3} MSE7: 6.013×10^{-3}

Figure 40. Sound-speed that is linearly decreasing as a function of depth,
 with no variation in the down-range direction, using $W_y = 1$ and $W_z = 0$,
 with unevenly spaced data.

Equation (4.9) with $W_y = 1$ and $W_z = 0$. An exact 1st-order fit results in Figure 39. Figure 40 demonstrates that the discrete sound-speed data may be unevenly spaced without affecting the overall fit.

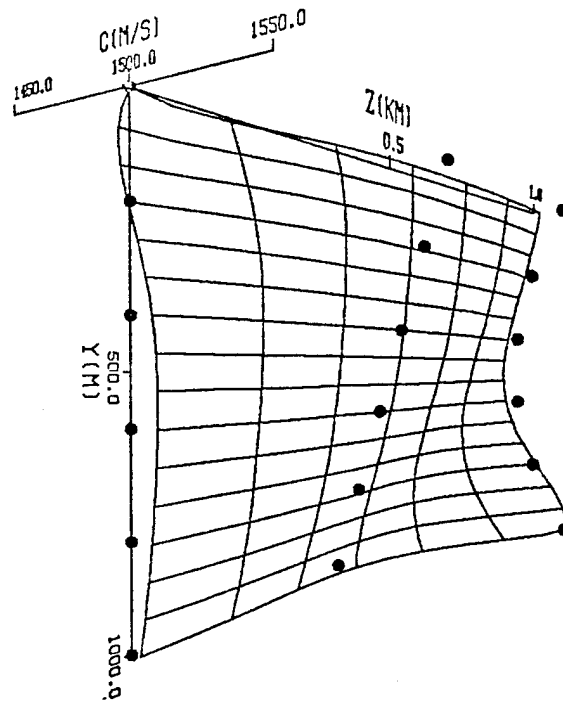
Figure 41 demonstrates a more complicated test case. The discrete sound-speed data used in this test case represents three different sound-speed profiles taken at three different down-range locations. The discrete data for the constant sound-speed profile at $z = 0.0$ km is generated by Equation (4.7). The discrete data for the linearly decreasing sound-speed profile at $z = 0.5$ km is generated by Equation (4.10). The discrete data for the parabolic sound-speed profile at $z = 1.0$ km is generated by the exact equation given by

$$c(y, z) = 1490 + 0.0001(y - 500)^2. \quad (4.11)$$

The three sound-speed profiles form a 6×3 rectangular matrix of discrete sound-speed data. The result from the orthogonal function expansion is a smooth surface fit that attempts to transition from the constant sound-speed profile to the linearly decreasing sound-speed profile to the parabolic sound-speed profile. The smooth transition is obtained. However, at the down-range locations where the sound-speed profiles were taken, the characteristics of the speed of sound as a function of depth have been distorted. The distortion can be seen more clearly by examining a two-dimensional plot of the fitted speed of sound versus depth taken at the fixed down-range locations of the three sound-speed profiles.

Figures 42, 43, and 44 show two-dimensional plots of the speed of sound versus depth for the test case presented in Figure 41. The plots show the discrete sound-speed data points as large black dots (\bullet). The estimated fit to the discrete data computed by the two-dimensional orthogonal function expansion is presented as a continuous curve. Significant distortion resulted.

SOUND SPEED



CASE: VARYING SOUND SPEED, CONSTANT-LINEAR-PARABOLIC

SIGMAC: 0.0M 7TH-ORDER MMSE SURFACE FIT

MSE0: 2.358×10^3 MSE2: 2.157×10^3 MSE4: 9.409×10^2 MSE6: 8.813×10^2

MSE1: 2.182×10^3 MSE3: 1.109×10^3 MSE5: 8.929×10^2 MSE7: 8.457×10^2

Figure 41. Sound-speed that varies in the down-range direction, with the discrete sound-speed data constant as a function of depth at $z = 0.0$ km, linearly decreasing as a function of depth at $z = 0.5$ km, and parabolic as a function of depth at $z = 1.0$ km, modeled without weighting x and z separately, with evenly spaced data.

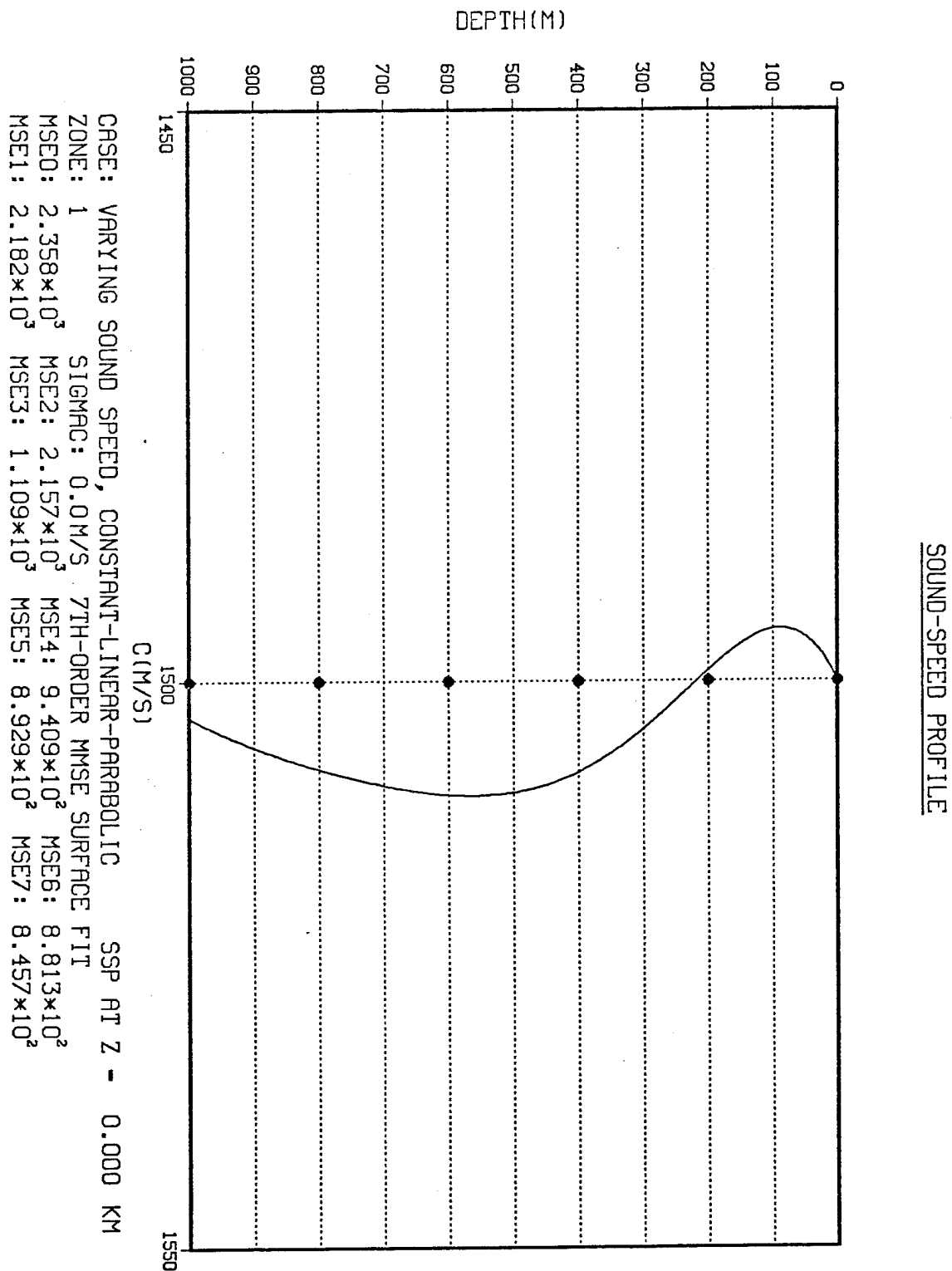


Figure 42. Sound-speed versus depth at $z = 0.0$ km for the test case shown in Figure 41, with the discrete sound-speed data constant as a function of depth at $z = 0.0$ km, modeled without weighting x and z separately, with evenly spaced data.

SOUND-SPEED PROFILE

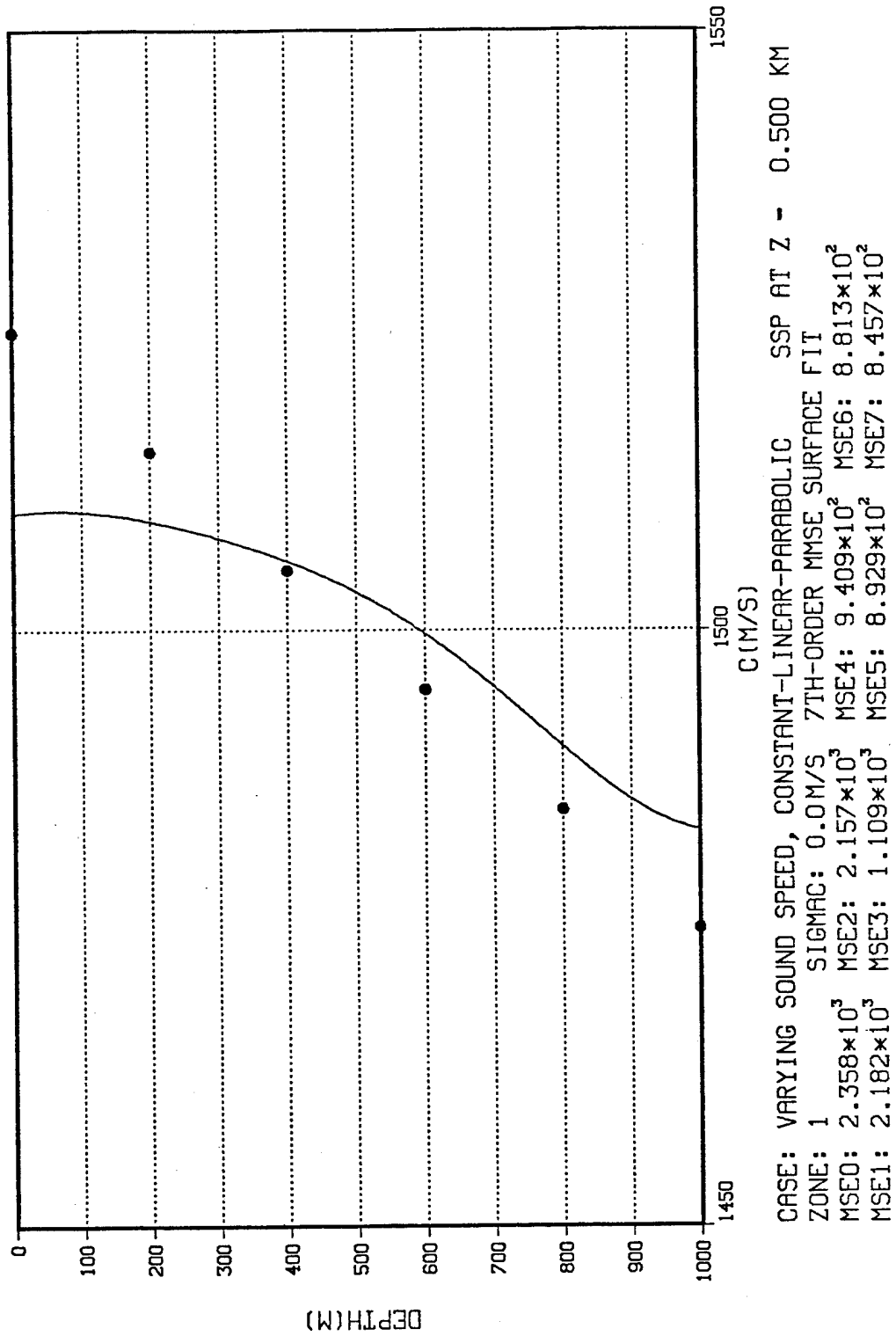


Figure 43. Sound-speed versus depth at $z = 0.5$ km for the test case shown in Figure 41, with the discrete sound-speed data linearly decreasing as a function of depth at $z = 0.5$ km, modeled without weighting x and z separately, with evenly spaced data.

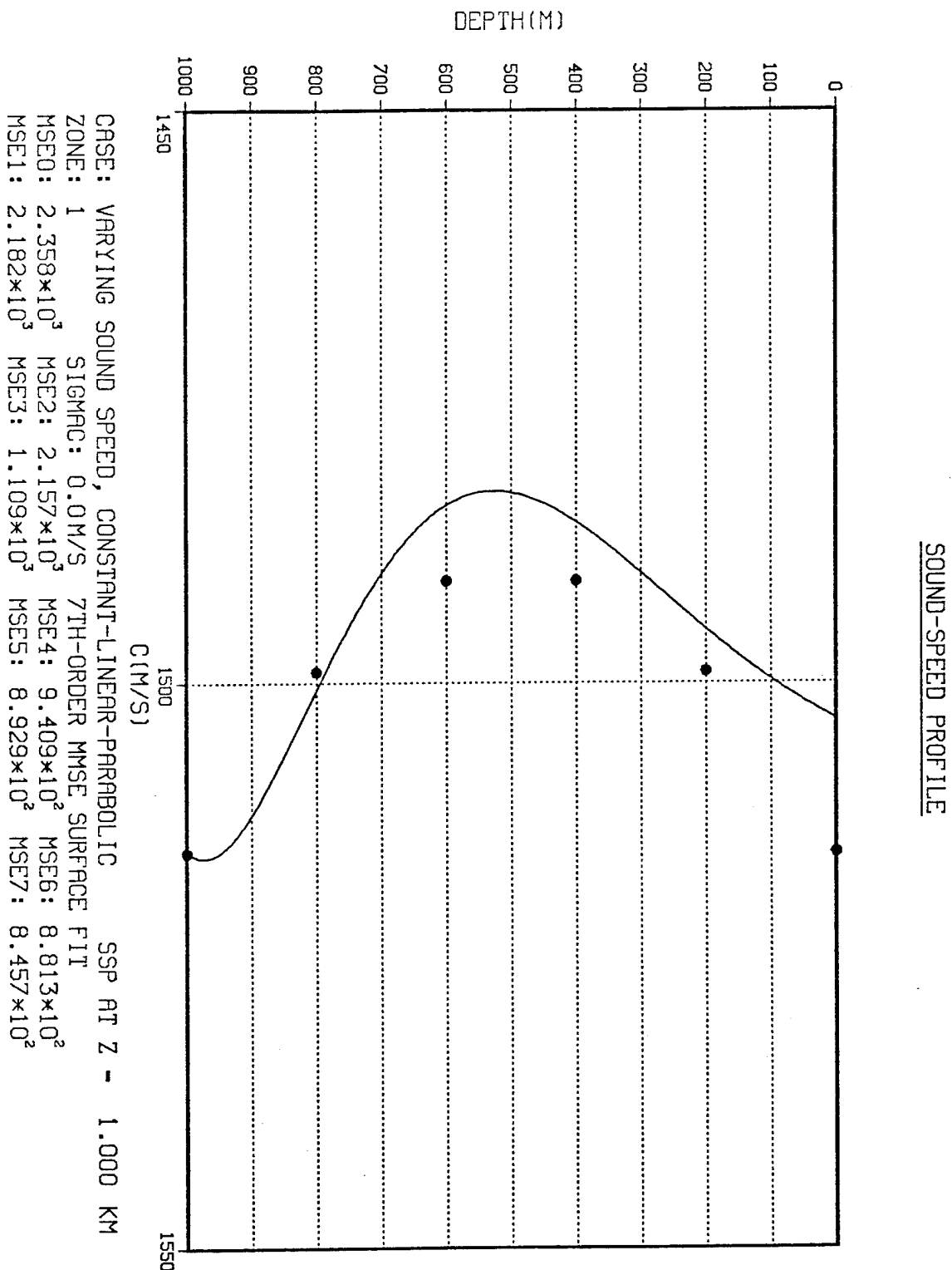


Figure 44. Sound-speed versus depth at $z = 1.0$ km for the test case shown in Figure 41, with the discrete sound-speed data parabolic as a function of depth at $z = 1.0$ km, modeled without weighting x and z separately, with evenly spaced data.

The distortion of the fitted sound-speed as compared to the discrete sound-speed profiles is due to the smoothing effect of the orthogonal function expansion. If the orthogonal function expansion was computed to a higher order using $N_c > 7$, then the sound-speed surface fit would more closely match the changes in the discrete sound-speed profiles. The distortion is also a result of the set of generating functions used. As discussed in Chapter II, the surface fits have a constant value for the estimated sound speed across lines of contour given by

$$y + z = C, \quad (4.12)$$

where C is a positive constant. Therefore, the surface fits have no curvature along these contours. The amount of distortion for different sound-speed profiles will depend on how well the rectangular matrix of discrete sound-speed data matches the form of the generating functions. For a given set of data, the fit that is obtained may be acceptable, but the technique is not versatile enough to provide acceptable fits in all cases.

As in Chapter II, the method of orthogonal function expansion to fit two-dimensional, discrete data provides a starting point for the use of this technique to compute a continuous model of the speed of sound as a function of depth and down-range. The orthogonal function expansion needs more variability in the maximum order fit that is selected, N_c . The technique could be improved by using a different set of generating functions that will not return constant values for the speed of sound across lines of contour given by Equation (4.12). For two-dimensional sound-speed fits, the use of this technique has an additional shortcoming. For the sound-speed profiles used as input data, their basic shape as a function of depth may be distorted. A better and simpler technique may be to use a one-dimensional orthogonal function expansion to fit each sound-speed profile separately, and then average or interpolate between the nearest one-dimensional sound-speed fits.

V. CONCLUSIONS AND RECOMMENDATIONS

This thesis had two primary goals. First, to derive and test the two-dimensional orthogonal function expansions of ocean bathymetric and sound-speed data. This technique provides a continuous mathematical model, from unevenly spaced discrete input data, of bathymetry as a function of cross-range and down-range, and the speed of sound as a function of depth and down-range. The second goal was to implement the expansions in the Recursive Ray Acoustics (RRA) Algorithm FORTRAN program to evaluate the successes and shortcomings of this technique to model the ocean bottom and the speed of sound. In order to implement the technique as the ocean bottom model in the RRA Algorithm, a method of computing accurate angles of reflection also had to be developed. The orthogonal function expansion has many positive features. It takes discrete input data that may be unevenly spaced, and provides a fit to the discrete data that smoothes through noise or rapid variations in the data. The result is a continuous two-dimensional model of the discrete data. The major shortcoming is that the technique is limited by the choice of the set of generating functions used. Also, the maximum order fit that is implemented has been limited to seventh order. The choices for the set of generating functions and the maximum order fit were based upon previous research with the one-dimensional orthogonal function expansion [Ref. 2].

The effort to provide a more sophisticated one-dimensional ocean bottom model for the RRA Algorithm, other than a flat ocean bottom, began in 1991 with the use of Spatial Fourier Series [Ref. 4]. The technique met with limited success. The one-dimensional orthogonal function expansion was developed and presented in 1994 [Ref. 2]. The one-dimensional orthogonal function expansion was successful, and the technique was used to model both bathymetric and sound-speed data in the RRA Algorithm. The two-dimensional orthogonal function expansion may yet prove to be a viable tool in modeling both ocean bathymetric data and sound-speed data, but its immediate utility, based on the analysis conducted, is limited.

It is recommended that future research apply higher-order fits and test generating functions that will correct the shortcomings produced by the set of generating functions used in this analysis. A possible alternative technique could be a two-dimensional orthogonal function expansion that is based on the generating functions of the one-dimensional case [Ref. 9]. The form of the orthogonal function expansion used to fit a rectangular matrix of discrete ocean bathymetric data as a function of cross-range and down-range would then be given by

$$\hat{y}_b(x, z) = \sum_{n=0}^{N_b} \sum_{m=0}^{N_b} b_{n,m} \varphi_{b_n}(x) \psi_{b_m}(z), \quad (5.1)$$

where $\varphi_{b_n}(x)$, $n = 0, 1, \dots, N_b$, and $\psi_{b_m}(z)$, $m = 0, 1, \dots, N_b$, are the orthogonal functions obtained by applying the *Gram-Schmidt Orthogonalization Procedure* to the generating functions given by

$$f_n(x) = x^n, \quad n = 0, 1, \dots, N_b, \quad (5.2)$$

to find $\varphi_{b_n}(x)$, and

$$g_m(z) = z^m, \quad m = 0, 1, \dots, N_b, \quad (5.3)$$

to find $\psi_{b_m}(z)$. The coefficients $b_{n,m}$, $n = 0, 1, \dots, N_b$ and $m = 0, 1, \dots, N_b$, would be obtained by computing the inner product of the measured discrete ocean bathymetric data with the orthonormal basis functions $\varphi_{b_n}(x) \psi_{b_m}(z)$. This technique would provide a greater degree of freedom to fit the surfaces with more independence in x and z . For a seventh-order fit, $N_b = 7$, this technique would produce 64 coefficients

$(b_{0,0}, b_{0,1}, \dots, b_{7,6}, b_{7,7})$ as opposed to the eight coefficients developed in the technique presented in Chapter II.

The ray trace plots presented in Chapter III provide insight into the complexity of ray propagation in the ocean. The study of sound propagation involving multiple ocean bottom reflections requires a good two-dimensional ocean bottom model. With the continued interest of the United States Navy in understanding the acoustic environment in the littorals, more advanced study in this technique of mathematical modeling is warranted.

LIST OF REFERENCES

1. Ziomek, L. J., and Polnicky, F. W., "The RRA algorithm: Recursive ray acoustics for three-dimensional speeds of sound," *IEEE J. Oceanic Eng.*, vol. 18, pp. 25-30, 1993.
2. Ziomek, L. J., "Sound-pressure level calculations using the RRA algorithm for depth-dependent speeds of sound valid at turning points and focal points," *IEEE J. Oceanic Eng.*, vol. 19, pp. 242-248, 1994.
3. Kaplan, W., *Advanced Mathematics for Engineers*, Addison-Wesley, Reading, MA, 1981, pp. 165-166.
4. Jones, T. N., *Ocean Bottom Modeling for Ray Acoustics*, MSEA Thesis, Naval Postgraduate School, Monterey, CA, December, 1991.
5. Ziomek, L. J., *Fundamentals of Acoustic Field Theory and Space-Time Signal Processing*, CRC Press, Inc., Boca Raton, Florida, 1995.
6. Davis, H. F., and Snyder, A. D., *Introduction to Vector Analysis*, WCB Publishers, Dubuque, IA, 1991, pp. 33-34.
7. Gerald, C. F., & Wheatley, P. O., *Applied Numerical Analysis*, 4th edition, Addison-Wesley Publishing Company, New York, 1989.
8. Goodman, A. W., *Analytic Geometry and the Calculus*, The Macmillan Company, New York, 1963, pp. 547-549.
9. Scandrett, C., Prof., personal meeting, Naval Postgraduate School, Department of Mathematics, Monterey, CA, May, 1995.

INITIAL DISTRIBUTION LIST

1. Defense Technical Information Center 2
Cameron Station
Alexandria, Virginia 22304-6145
2. Library, Code 52 2
Naval Postgraduate School
Monterey, California 93943-5101
3. Chairman, Code EC 1
Electrical and Computer Engineering Department
Naval Postgraduate School
Monterey, California 93943-5121
4. Lawrence J. Ziomek, Code EC/Zm 3
Electrical and Computer Engineering Department
Naval Postgraduate School
Monterey, California 93943-5121
5. Clyde Scandrett, Code MA/Sd 1
Mathematics Department
Naval Postgraduate School
Monterey, California 93943-5216
6. Rodney Luck 1
215 McIntosh Road
Cherry Hill, New Jersey 08003